Technische Universität München
Physik-Department
Lehrstuhl für Physik E14

Spectral Color Effects in Biomolecular Interactions – Persistent Spectral Hole Burning Studies

Christoph Hecht

Vollständiger Abdruck der von der Fakultät für Physik der Technischen Universität München zur Erlangung des akademischen Grades eines

Doktors der Naturwissenschaften (Dr. rer. nat.)

genehmigten Dissertation.

Vorsitzender:		Univ.-Prof. Dr. J. Leo van Hemmen
Prüfer der Dissertation:	1.	Univ.-Prof. Dr. Josef Friedrich
	2.	Univ.-Prof. Dr. Fritz G. Parak

Die Dissertation wurde am 7.11.2006 bei der Technischen Universität München eingereicht und durch die Fakultät für Physik am 4.12.2006 angenommen.

PHYSIK-DEPARTMENT

Spectral Color Effects in Biomolecular Interactions – Persistent Spectral Hole Burning Studies

PhD Thesis
of

Christoph Hecht

Contents

You can't wait for inspiration. You have to go after it with a club.

Jack London

Chapter 1

Introduction

The functionality of molecules, especially in biology, biophysics and biochemistry, heavily depends on their interaction with other molecules [1, 2]. However, as biochemical tasks in living systems are complex and require a high degree of specificity most molecules have an equally complex and specific chemical structure. Together with the large number of different molecules that interact with each other in living systems it is quite obvious that a multitude of electrostatic, thermodynamic and statistic effects must be evaluated when trying to assess properties of a single biophysically relevant molecule [3–6]. When trying to use optical spectroscopy to investigate biomolecular systems, one has to rely in most cases on a probe within the system that can be used to map out the surrounding environment and its impact on the optical behavior via its changing optical properties during biomolecular processes [7–9]. For this approach to be successful the probe itself must be characterized very carefully to allow for a good estimation of its influence on the system and its behavior upon certain events. Even for a single probe molecule in a solvent the molecular interactions are still manifold. Those interactions usually lead to solvent shifts of various magnitudes and directions. In a conventional absorption spectrum every single molecule in the sample will contribute with a different solvent shift leading to broad absorption bands in bulk spectra [10–13].

A very helpful technique to disentangle the contributions is the **Persistent Hole Burning Spectroscopy** [14–18]. Its main advantage is the high resolution which allows to pick subensembles within a very narrow spectral margin and to investigate them independently of the rest of the molecules. The main idea of hole burning is to apply light of a well defined wavelength to the molecules and excite them to a higher electronic state. Under certain circumstances some of the molecules will not return to their initial ground state but to some other photochemically or photophysically populated state [19, 20], thus leaving a spectral hole in the original absorption spectrum. Such a hole is a small dip in the spectrum that can be recorded by detuning a scanning laser around the burning wavelength. The molecules constituting this hole have similar spectral properties because their solvent shift was similar. By lowering the temperature enough the holes can be conserved over hours or even weeks allowing a detailed analysis of their shape. Controlled altering of outer parameters such as an electric field, isotropic pressure, temperature or aging time invokes changes in the natural shape of such a hole that correspond with the nature of the interaction of the

molecules in the subensemble with their environment. Depending on the type of interaction some parameters may or may not influence their solvent shift. The sensitivity of a spectral hole to changes applied from outside will be enhanced by orders of magnitude in contrast to the whole inhomogeneously broadened absorption band. For molecules in glassy solvents with large inhomogeneous broadening the width of a spectral hole can be up to five orders of magnitude smaller than the inhomogeneous bandwidth, thus increasing the resolution dramatically.

Besides the high resolution spectral hole burning offers another unique feature. While crystalline or matrixlike structures around chromophores only allow for the investigation of special solvent defined interaction setups and glassy structures are too ill-resolved for conventional absorption spectroscopy, hole burning in amorphous or glassy materials can bridge this gap. The variety of molecular interaction types and binding geometries present in glasses can be selectively investigated by spectrally separating the subensembles in question in persistent holes. Furthermore, within the same sample different subensembles can be labeled and their properties directly compared to each other. This possibility gives rise to so-called **Spectral Color Effects**. As the inhomogeneous absorption band is scanned along the interactions between chromophore and the solvent may change. Depending on the nature of these changes various techniques in combination with spectral hole burning can reveal details about the types of interactions. Color effects have been reported and explained in different systems [21–25].

The aim of this work is to highlight miscellaneous aspects of the sources of color effects and to evaluate their usefulness in the investigation of probe–solvent interactions. The model chromophore thionin has been studied with various hole burning techniques in context with diverse biologically relevant molecules. Finally, the protein phycocyanin as an example for naturally appearing chromophores has been investigated with respect to color effects in its electrostatic properties.

Thionin is a synthetically designed chromophore of the phenothiazine family. Phenothiazinium derivatives have become popular in the second half of the 19th century because of their staining abilities in living organisms. Especially microscopy techniques of tissues and cells benefitted strongly from those dyes that could selectively stain different types of cells depending on their slightly varying chemical structure. This selectivity made scientists think about actively deploying various phenothianzinium dyes to target specific parts of living organisms in a concerted manner. Guttmann and Ehrlich were in 1891 the first to provide evidence for successful chemotherapy when they treated malaria with methylene blue, a similar compound to thionin [26]. As dye science evolved, a lot of fields of application for phenothiazines were uncovered. Of course, with growing knowledge about the detailed molecular interactions present in living organisms it is important to know, in which way selectively operating dyes interact with given systems and what mechanisms cause them to fulfill their

special medicinal role.

First, the dye in question has to be characterized by subjecting it to the different hole-burning techniques assessing its thermodynamical and electrostatical behavior in a glassy environment. The results of those experiments are shown in chapter 4. All experiments are conducted in a mixture of glycerol and water which forms an amorphous solid at low temperatures, so the normalization of parameters has to be done in that particular solvent. There are four main hole-burning techniques used in this work that supply – in conjunction with each other – the necessary information to evaluate color effects in the interaction of thionin with other molecules:

- **Homogeneous Linewidth Measurements**: Burning a hole always entails artificial broadening of the hole. Within certain conditions the hole width can be extrapolated to hole burning without any artificial and systematic broadening. The parameter gained with this technique, the quasi-homogeneous linewidth, discloses information about the lifetime of the excited electronic states used in the hole-burning process and consequentially the coupling strength of the chromophore to its surrounding molecules.

- **Satellite Hole Burning**: Any spectral range within an inhomogeneously broadened absorption band consists of different contributions from chromophores with separate electronic transition energies. Hence, hole-burning at a certain spectral position not only yields a hole at the spectral burning position but several red or blue shifted holes in different spectral ranges. Those holes can mainly be attributed to vibrational modes of the chromophore. The evaluation of the vibration energies can help in distinguishing deformed or geometrically or chemically altered chromophores.

- **Stark Spectroscopy**: Depending on the electric field the chromophore experiences, its excitation energy will change. Therefore, varying an outer electric field will cause a previously burnt hole to change in shape. These changes can be traced back to reveal different electrostatic parameters such as the changes in dipole moment of the chromophore upon excitation.

- **Pressure Tuning Spectroscopy**: Similar to the Stark spectroscopy changes in pressure can cause holes to change their shape. The values of the local isothermic compressibility and the vaccuum frequency can unveil details about the immediate environment of the chromophore and its stability.

Thionin by itself offers some peculiarities. Chapter 5 focuses on the color effects found in the homogeneous linewidth measurements of thionin and BODIPY, a different stain investigated in the PhD thesis of M. Stübner [27]. Quite surprisingly at first glance, the color effects for each of the dyes are in stark contrast to each other. The different mechanisms of the interactions between those molecules and their environment give insight to effects that can not be revealed by conventional broadband absorption spectroscopy.

The chapters 6 and 7 deal with thionin bound to oligonucleotide systems and its cage complexes with cyclodextrines. The oligonucleotides used in this work were various forms of short DNA strands rich in guanine, often found in telomeric DNA. Chromosomes of eukaryotic cells have termini that build up structures of DNA sequences that carry little or no genetic information. Those structures, called telomeres, prevent the actual chromosome from being damaged or coagulating with other chromosomes. They also play an important role in DNA replication [28, 29]. Thionin as well as other phenothiazine dyes are known to specifically bind to the telomeric structures [30] and carry out medically vital functions such as inhibiting telomerase activity or influencing DNA replication speed. Malfunctioning telomerase activity is associated with cancer and tumor growth [31] as well as the aging of cells [32, 33]. Several special types of oligonucleotides have been investigated in terms of their binding properties to thionin. Based on pressure tuning experiments different modes of interaction can be characterized leading to a deeper understanding of how to synthetically optimize molecules for specific biochemical behavior.

Cyclodextrines – cyclic oligosaccharides of various size – have been a subject of research since their first discovery in the end of the 19th century [34]. Their most intriguing feature, however, is the ability to form non-covalently bound supramolecular complexes with smaller guest molecules. Shaped like a truncated cone they allow the hosting of hydrophobic molecules in their more hydrophobic inside. The complex formation is reversible, making cyclodextrines potentially very useful to carry drugs or micro-manipulate certain properties of the encapsulated molecules. Depending on size, geometry, hydrophilicity, charge and outer conditions in the bulk the exact shape of the supramolecular complex can change drastically. In this work, cyclodextrines of various length have been analyzed with regard to their complexation behavior with thionin. The color effects in the homogeneous linewidths and the compressibility allow to draw conclusions on the complex geometry and the role of the solvent.

Finally, chapter 8 outlines color effects in phycocyanine and its constituting parts. Usually an external chromophore like thionin has to be used as molecular probe to monitor its interaction with biomolecules in question. However, the usage of an externally applied dye always interferes with the system itself. In special cases biomolecules provide their own naturally occurring chromophore. For example, hemeproteins have always been a subject of spectroscopic studies because of their heme unit that absorbs in the spectral range of visible light [35]. Other experiments have been conducted with amino acids themselves as spectroscopic markers [36–39]. Proteins of the phycobilisome, such as phycocyanine, display a variety of slightly different chromophores [40, 41]. Thorough investigation of the homogeneous linewidths and the dipole moments of the chromophore of phycocyanine reveals novel insights in the electrostatics of the protein environment. By means of a protein internal probe it should be possible to evaluate the static dielectric constant within a protein, a parameter, that is experimentally hitherto very difficult to obtain.

In physics, you don't have to go around making trouble for yourself – nature does it for you.

Frank Wilczek

Chapter 2

Hole Burning Spectroscopy

2.1 Optical Spectroscopy

2.1.1 Optical Transitions in Molecules

Whenever electromagnetic radiation encounters molecules there is a certain probability that the molecules will absorb the energy of the radiation. In this case the radiation field will couple to the energy transitions of a molecule, transferring it from its original state to a state of higher energy. The quantum mechanical probability for this to happen can be estimated by applying time-dependent perturbation theory leading to a term known as Fermis Golden Rule:

$$P_{i\to f}(\omega) = \frac{2\pi}{\hbar}|M_{if}|^2\rho \cdot \delta(\omega_{if} \pm \omega). \tag{2.1}$$

The probability $P_{i\to f}(\omega)$ for a molecule to be transferred from its initial state i to a final state f depends on the transition matrix element M_{if}, the density of the final states ρ and the frequency ω of the electromagnetic radiation. While ρ can be understood as the number of different ways leading from the initial state to the final state, M_{if} describes the coupling strength between the radiation field and the molecules:

$$M_{if} =< \Psi_f|H_{em}|\Psi_i >= \int \Psi_f^* H_{em}\Psi_i d\nu. \tag{2.2}$$

Here Ψ_f and Ψ_i are the wave functions of the initial and the final state. $H_{em} = -\vec{\mu}\cdot\vec{E}$ is the Hamiltonian of the perturbation caused by the interaction of the radiation field with the dipole moment μ of the the molecule. Obviously the transition probability is proportional to the square of the electric field $\vec{E}$ and therefore proportional to the frequency dependent intensity $I(\omega)$ of the incident radiation field. This means that over time the intensity of the radiation field drops as energy is absorbed at a constant rate. Formally this can be written as a differential equation:

$$-\frac{\partial I(\omega)}{\partial t} = \varepsilon(\omega)\cdot I(\omega) = \sum_f \hbar\omega P_{i\to f}(\omega). \tag{2.3}$$

Using the integral form for the Dirac delta function $2\pi\delta(\omega) = \int_{-\infty}^{\infty} \exp(i\omega t)dt$ and averaging the electric field over all possible initial states for an ensemble of homogeneously distributed molecules one can obtain the intensity profile dependent on the evolution of the dipole moment of the ensemble molecules:

$$I(\omega) = \frac{1}{2\pi} \int_{\infty}^{\infty} \exp(i\omega t) \cdot \overline{\vec{\mu} \cdot \vec{\mu}(t)} dt. \tag{2.4}$$

$\overline{\vec{\mu} \cdot \vec{\mu}(t)} = C(t)$ is the so-called dipole correlation function which relates the dipole moment of the molecule after transition to the initial dipole moment. Any transition induced by an electromagnetic field causes the dipole moment of the system to oscillate coherently with the same frequency ω_0 as the dipole moment of the inducing field. However, since every (excited) state is subject to relaxation processes the time-dependent dipole moment function will resemble that of a dampened harmonic oscillator:

$$\mu(t) = \mu \cdot \cos(\omega_0 t) \cdot \exp\left(-\frac{\Gamma}{2}t\right), \tag{2.5}$$

where Γ is the dephasing rate of the excited state. Evaluating the intensity profile for this dipole moment function will yield the line shape $g(\omega)$ as the real part of the complex intensity function:

$$\begin{aligned} g(\omega) &= Re\left(\frac{1}{2\pi} \cdot \int_0^{\infty} \exp(i(\omega \pm \omega_0)t)\mu \cdot \cos(\omega_0 t) \cdot \exp\left(-\frac{\Gamma}{2}t\right) dt\right) \\ &= \frac{\mu^2}{4\sqrt{2\pi}} \frac{\Gamma}{(\omega_0 - \omega)^2 + \frac{\Gamma^2}{4}} \end{aligned} \tag{2.6}$$

This is a so-called *Lorentzian* line shape with a full width at half maximum (FWHM) of Γ. Lorentzian absorption profiles always emerge from homogeneous line broadenings, such as spontaneous emission or phase coherency decay.

2.1.2 Optical Transitions in Ideal Matrices

The simple Lorentzian line profile is only valid for two state systems. While often transitions to higher electronic states can be neglected in optical spectroscopy, vibronic transitions can not be disregarded. In ideal matrices where all guest molecules are embedded in exactly the same way there are two contributions to consider:

- *Molecular Vibrations:* Molecules can be excited to a higher vibrational state of the first excited electronic state. Following the rule of Kasha higher vibrational states will relax very fast to the vibrational ground state by non-radiative processes.

- *Phonons:* Depending on the electron-phonon coupling strength part of the transition energy can be transferred to vibrations of the host molecules.

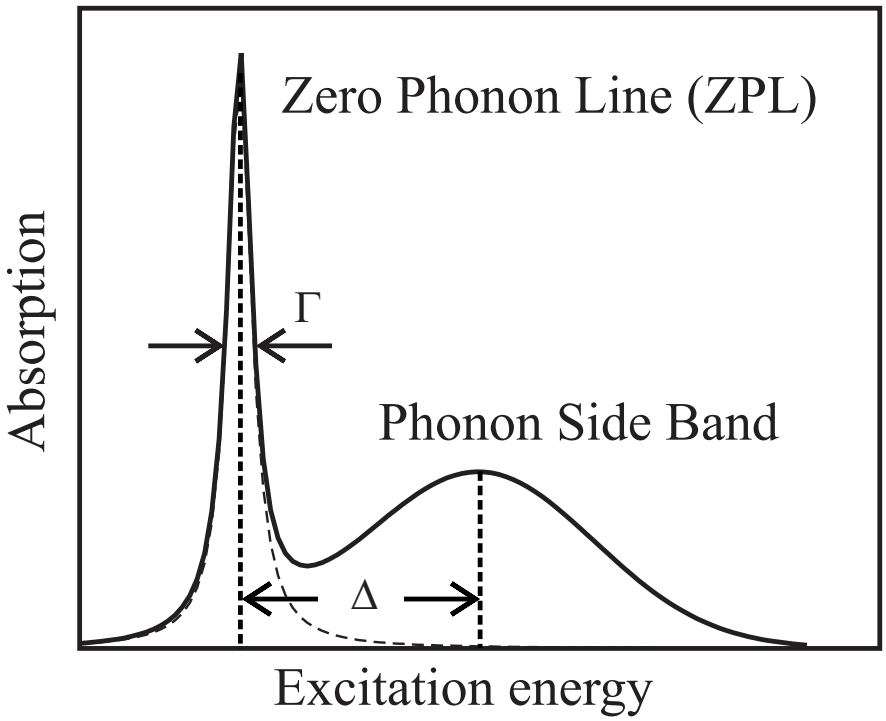

Figure 2.1: *The low temperature absorption spectrum of a molecule in an ideal matrix. Besides the Zero Phonon Line (ZPL) with full width at half maximum of* Γ *there is a blue shifted Phonon Side Band (PSB) whose relative intensity depends on the strength of electron-phonon coupling.*

Phonons have less energy than vibrational modes of the excited state, so in the spectral vicinity of the pure electronic transition there will mainly be found additional phonon modes. While the pure electronic transition still resembles a Lorentzian, the phonons will be distributed according to the Franck-Condon principle. In case of a linear electron–phonon coupling the probability distribution of excited phonons can be described by a Poisson distribution function. The electronic transition is often referred to as Zero Phonon Line (ZPL), whereas the phonons make up the Phonon Side Band (PSB) (*cf.* Fig 2.1) which is shifted to higher frequencies by the Stokes shift Δ. If the overall intensity of both bands is normalized to unity, the fraction of absorption covered by the ZPL is given by the Debye-Waller factor α.

The factor α can be influenced by controlling the temperature. At low temperatures the phonon density will be lowered as well so that α will increase.

2.1.3 Optical Transitions in Disordered Matrices

Unlike an ideally ordered matrix disordered materials will provide different microenvironments for each individual guest molecule. If the number of guest molecules is sufficiently low to prevent chromophores to interact with each other this will result in a distribution of transition energies which can be described by a Gaussian using the central limit theorem due to the large number of

microenvironments.

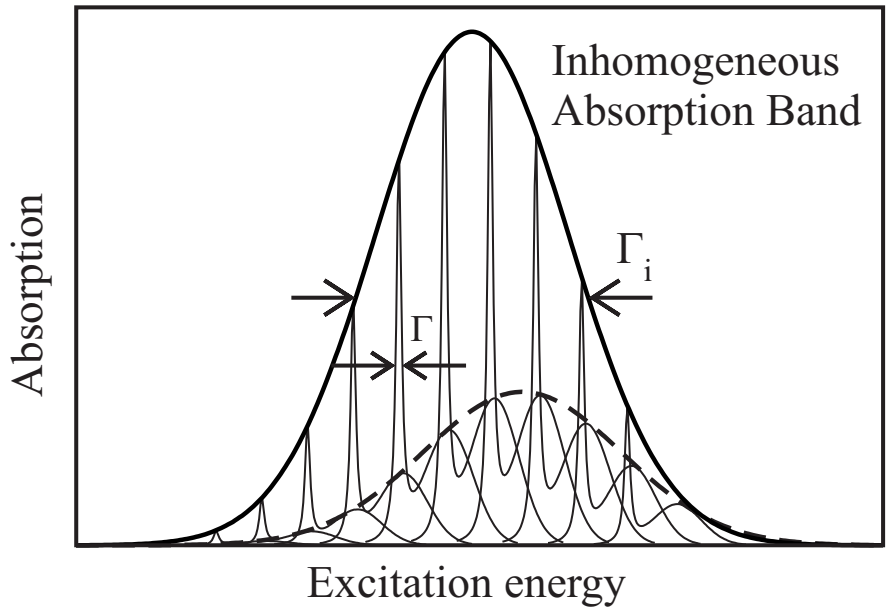

Figure 2.2: *The absorption spectrum of a molecule in a disordered matrix. Zero Phonon Lines of width* Γ *and their corresponding Phonon Side Bands are distributed around some central frequency yielding an overall absorption band of width* Γ_i*. Usually this band can be well approximated by a Gaussian.*

The resulting inhomogeneous width Γ_i may be orders of magnitude larger than the respective Lorentzian width Γ. This is the main problem in conventional optical spectroscopy of biological relevant molecules: With water being the main solvent for biomolecules, the microenvironments for each individual molecule may vary greatly. Details in the interaction between guest and host molecules are therefore hard to evaluate because of overlaying effects from different environments when studying biomolecules in bulk. Important techniques to overcome this problem include for example Single Molecule Spectroscopy (SMS) or Fluorescence Line Narrowing (FLN).

2.2 Persistent Spectral Hole Burning

Yet one of the most high-resolution spectroscopical techniques is Persistent Spectral Hole Burning (PSHB) [16, 18, 42]. Spectral holes can only be produced in an inhomogeneously broadened absorption band, where chemically identical molecules display a distribution of absorption frequencies due to different micro-environments around each chromophore. If laser light of a well-defined frequency illuminates a sample of chromophores in such a inhomogeneous host matrix, a fraction of the molecules can be excited to a higher electronic state.

Eventually those molecules will relax back to the ground state, which will usually take place within a timeframe of parts of nanoseconds to picoseconds, so that the decrease in absorption at the laser frequency will only be visible while

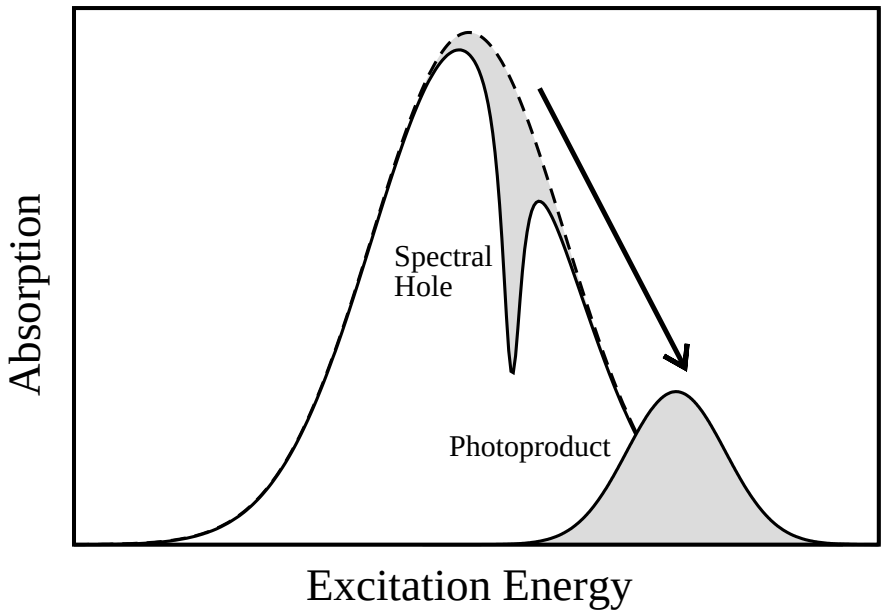

Figure 2.3: *Upon photoexcitation chromophores might relax to a different state than the original ground state, the so-called product state. If this product state is stable, illuminating a subensemble of chromophores within the absorption band will transfer molecules from one spectral absorption position to another. The resulting dip in the absorption band at the illumination frequency is called a hole, the arising spectrally shifted absorption structure is called anti-hole.*

illuminating the sample. This effect is used in various pump–probe spectroscopy techniques [43–45] where a high intensity laser beam upholds the absorption decrease which can in turn be observed with a probing laser beam or be returned to the ground state by stimulated emission. In order to create a persistent decrease in absorption some excited molecules must be able to relax to a third state different from the initial ground state[16, 18]. If this product state is stable with respect to relaxation to the ground state, a spectral inequilibrium of absorption frequencies can be realized resulting in a persistent absorption decrease at the laser frequency, often referred to as *spectral hole* [16, 18, 42] and a concomitant increase at a spectrally shifted frequency, the so-called *anti-hole* (*cf.* Fig. 2.3). The longevity of the product states depends on the temperature [46], so effective PSHB will take place at low temperatures around liquid helium temperature. The existence of those product states, however, varies from system to system and can be guaranteed by one of the following processes.

2.2.1 Photochemistry

Upon excitation the chromophore might undergo a change of chemical properties more easily. These changes may consist of proton transfers [47, 48], tautomerisations [49, 50] or rearrangements of bonding geometry [51]. When the electronic excitation subsides again, the molecule in question displays a different chemical appearance shifting its absorption frequency. In terms of energy requirement changes of chemical properties are expensive, which usually leads to a spectral anti-hole far away from the absorption frequency. Photochemistry often leads

to an increase in phonon coupling strength which in turn leads to a broadening of the spectral hole rendering some product states useless for high-resolution experiments. Some applications of photochemical hole burning spectroscopy are described by Moerner[14], including the investigation of spectral dynamics in fluorescent proteins [52, 53] or the use in holographic data storages [54, 55].

2.2.2 Photophysics

Secondly, while the chromophore itself may stay chemically unchanged, the orientation of solvent molecules can be altered when a chromophore is in the excited state [20, 56] causing the interaction between solvent and solute to change. Such changes are usually much smaller than photochemically induced changes leading only to small shifts in the absorption frequency. Often the corresponding anti-holes can be found within a range of several hundred GHz. Examples for photophysical processes comprise local relaxation of organic glasses [57, 58] or proton tunneling in low-temperature organic [59] or non-organic crystal systems [60].

2.3 Spectral Linewidths

Ideally the shape of a spectral hole would only depend on the spectral shape of the incident laser light. Modern cw-lasers can reach a spectral resolution in the order of 10 kHz, so an ideal spectral hole would only have a full width (FWHM) on the same order of magnitude. However, several processes prevent the formation of such highly resolved holes.

2.3.1 Homogeneous Linewidth

The upper boundary of spectral resolution is given by the homogeneous linewidth which results from the finite lifetime of the photoinduced excited states and the concomitant uncertainty in state energy according to Heisenbergs uncertainty principle. An excited state with an average lifetime of τ_h will yield a contribution to the hole width of $\frac{1}{\tau_\mathrm{h}}$. Furthermore there will be temperature dependent fluctuations of the solvent environment around chromophores which cause the simultaneously excited molecules to dephase with a typical time constant τ_d. Since those fluctuations affect the excited state as well as the ground state the dephasing contributes twice to the width of the hole, yielding an overall linewidth mostly referred to as the homogenous linewidth Γ_hom:

$$\Gamma_\mathrm{hom} = \frac{1}{2\pi \cdot \tau_\mathrm{h}} + \frac{1}{\pi \cdot \tau_\mathrm{d}}. \tag{2.7}$$

While at room temperature the dephasing time is in the order of 10^{-15} s, cooling the sample with liquid helium to or below a temperature of 4 K can lower τ_d by up to nine orders of magnitude leaving the finite lifetime of the excited state τ_h as determing factor for the homogeneous linewidth. Higher electronic states than the first couple to an exponentially increasing level density leading to fast relaxation [61]. Typical lifetimes for the first excited electronic state are on the order of 10^{-8} s so that the linewidth of spectral holes can be as low as

$10^{-3}\,\mathrm{cm}^{-1}$. Compared to the inhomogenous linewidth of the overall absorption band of $10^{2}\,\mathrm{cm}^{-1}$ to $10^{3}\,\mathrm{cm}^{-1}$ hole burning spectroscopy can increase the spectral resolution by up to a factor 10^{6}.

Since PSHB is such a highly resolving optical techniques, it is sensitive to some line broadening mechanisms which have to be taken into account when observing hole spectra.

2.3.2 Power Saturation Broadening

The probability of stimulated emission from the excited state to the ground state increases with the photon flux density Φ. For a certain photon flux density Φ_{Sat} the transition saturates so that additional photons will have a relatively higher chance be absorbed by molecules in the spectral vicinity. This results in a power broadened spectral hole with the increased width Γ_{P}, which can be estimated by

$$\Gamma_{\mathrm{P}} = \Gamma_0 \cdot \sqrt{1 + \frac{\Phi}{\Phi_{\mathrm{Sat}}}}. \tag{2.8}$$

Here the initial unbroadened hole width Γ_0 increases with the square root of the saturation parameter $s = \frac{\Phi}{\Phi_{\mathrm{Sat}}}$. Thus in experiments the laser intensities have to be kept at a sufficiently low level – usual hole depths in this work do not exceed more than 10% of the overall absorption at any given wavelength, so that power broadening can be disregarded.

2.3.3 Energy Saturation Broadening

As soon as the first molecule is excited to a higher electronic state the system is no longer in equilibrium. Therefore, any following incident photon will have a lower probability to excite a molecule of the same excitation frequency than the first one. With increasing hole depth the disparity in absorption between the hole center and the hole shoulders increases as well, so that more molecules from the hole shoulders will be excited than from the hole center the more photons will be absorbed. Breinl *et al.* [62] showed that for low energy deposition the increase in hole width scales linearly with the increase in hole area. To extract the quasi-homogenous linewidth from the experiments hole spectra will be recorded while increasing the time of radiation exposure. Extrapolation of the hole width to a hole area of zero then leads to the hole width which would be observable in the absorption equilibrium yielding twice the quasi-homogeneous linewidth.

2.3.4 Spectral Diffusion

Apart from increased shoulder bleaching by the laser beam the system itself tries to balance the inequilibrium. Even at low temperatures molecules in the spectral surrounding of a hole tend to relax to the spectral position of the hole rebalancing the spectral distribution. These processes are called spectral diffusion [63, 64]. At liquid helium temperature, however, the relaxation timescale is slowed to hours or even days or weeks, so that within the timeframe of a normal experiment as described in this work, spectral diffusion processes do not contribute to a

broadening during a hole scan. For checking purposes initially burnt holes were compared to holes recorded at the end of an experiment for every experiment to rule out spectral diffusion effects. While spectral diffusion may be disregarded for a single hole scan it can have a severe impact on holes at different spectral positions.

The main aim in PSHB is to artificially influence the hole shape and spectral position by altering the external parameters affecting the molecules like pressure, electric fields or temperature. Due to the high resolution achievable the holes are very sensitive to even minute changes in those parameters allowing detailed descriptions of the interactions between the chromophores and their surroundings on a molecular basis. Several of those special techniques employed in this work are highlighted in the following.

2.4 Satellite Hole Burning Spectroscopy

Originally described by Gorokhovskiĭ et. al. [65] and Kharlamov et. al. [17] satellite holes appear in the absorption spectrum when Frank-Condon active vibrational modes cause non-resonant shifts. The determination of the spectral distance between the zero-phonon line and the relevant non-resonant holes allows the calculation of the vibronic energy levels of the excited and the ground state [66] and the overall distribution of satellite holes allows the assessment of Franck-Condon factors.

Apart from the resonantly excited zero phonon line and the corresponding phonon side band there are several ways to produce non-resonant holes:

- *Pseudo-Phonon Side Band*
  For sufficiently low temperatures the direct phonon side band is always blue (hypsochromically) shifted with respect to the excitation frequency of the laser. On the other hand, the pseudo-phonon side band is produced by molecules that are excited together with the creation of a phonon. Their pure electronic excitation frequency is slightly lower than the laser frequency, so the respective phonon hole will appear on the red (bathochromic) side of the zero phonon line.

- *Blue Shifted Non-Resonant Holes*
  Blue shifted non-resonant holes always appear when a molecule is excited from a higher vibronic level in the ground state to the first electronic state. Upon equilibration of vibronic levels in the ground state hypsochromically shifted non-resonant holes will be created reflecting the distribution of vibrational levels of the ground state. Those holes, however, are strongly temperature dependent since at sufficiently low temperatures the vibronic levels of the ground state will not be occupied any more. In our experiments below 4 K blue shifted non-resonant holes will thus be disregarded.

- *Red Shifted Non-Resonant Holes*
  When a molecule is excited directly to a higher vibronic level of the first electronic state, the associated vibronic ground state transition is bleached

out as well, leaving a bathochromically shifted non-resonant hole. In contrast to their blue shifted equivalents their appearance at low temperatures can even be enhanced by the inverse Franck-Condon factor because red shifted non-resonant holes are zero phonon lines with respect to the corresponding vibronic transition [67]. Satellite hole burning spectroscopy is therefore mostly employed to plot the vibrational levels of the first excited electronic state.

The basic method in satellite hole burning is to take a broadband absorption spectrum, burn a hole at a given frequency and record another absorption spectrum. With sufficiently high resolution the difference spectrum between preburn and postburn absorption spectra will yield a zero baseline with one resonant and several non-resonant satellite holes. Determination of the spectral distance of the satellite holes with regard to the burning frequency will give the vibrational frequencies of the first excited state, which can in turn be used to assign vibrational modes to theoretically calculated molecular models. Satellite hole burning excels at low frequency vibrations less than $500\,\mathrm{cm}^{-1}$, where other related vibrational spectroscopy methods like Raman spectroscopy have problems in separating the vibrational lines from the much more intensive elasticly scattered line. Furthermore, satellite hole burning is a non-destructive technique since holes will recover upon reheating the sample, enhancing its usefulness on biologically relevant chromophores.

2.5 Stark Spectroscopy

2.5.1 Interaction of Holes with Electric Fields

Naturally, electromagnetic interactions of light with matter will lead to changes in the absorption frequencies of electronic transitions. Those changes were first experimentally found by the 1919 nobel prize winner Johannes Stark and are referred to as Stark effect. The reason for the existence of shifts in electronic transition frequencies is a different behavior of the ground state and the excited state of a chromophore with respect to an external electric field. An electronic transition does not change the overall charge of a molecule, so that the first multipole moment can not contribute anything to the frequency shift. However, the polarizability and the dipole moment of a molecule will change upon excitation mainly due to a different electronic configuration. The second multipole moment will therefore cause a frequency shift of the electronic transition for a changing external field. In very good approximation higher multipole moments can be disregarded considering that sufficiently small molecules will be exposed to a nearly homogeneous field. The frequency change ν thus depends on the interaction energy of the electric field $\vec{E}$ with the difference in dipole moments of the ground and excited state $\Delta\vec{\mu}$:

$$\Delta\nu = -\frac{1}{h} \cdot \left(\vec{E} \cdot \Delta\vec{\mu}\right). \tag{2.9}$$

In this equation h is Planck's constant. In any experiment the electric field will be the sum of the local electric field $\vec{E}_{\text{local}}$ that is already present at the site of the chromophore due to surrounding molecules and the external field $\vec{E}_{\text{ext}}$ which is the only adjustable parameter. The local electric field is often referred to as the *pocket field*. Although the field strength averaged over a macroscopically sized sample volume will be zero for a non-charged solvent, the local field strength can be tremendous. With usual external field strengths of several kV/cm the local electric field is about four to six orders of magnitude larger [68]. The external field will be somehow mitigated by the charges and solvent molecules present around the site of the chromophore so that the molecule will experience a change of $f \cdot \vec{E}_{\text{ext}}$ due to the external field. The mitigation factor f is called Lorentz factor which will be discussed later on.

The dipole moment difference $\Delta\vec{\mu}$ itself can be split into two contributing parts. If a molecule has an intrinsic dipole moment that changes upon electronic excitation the intrinsic dipole moment difference $\Delta\vec{\mu}_{\text{mol}}$ will not be zero. This difference vector is fixed within the coordinate frame of the molecule itself because it does not depend on the pocket field. However, with the additional change in polarizability $\Delta\bar{\bar{\alpha}}$ upon excitation the pocket field will induce a dipole moment change $\Delta\vec{\mu}_{\text{ind}}$ whose direction depends on the direction of the pocket field.

$$\Delta\vec{\mu}_{\text{ind}} = \vec{E}_{\text{local}} \cdot \Delta\bar{\bar{\alpha}} \tag{2.10}$$

Using those contributions in Eq. 2.9 a frequency shift with five different sources can be obtained:

$$\begin{aligned} \Delta\nu \;=\; & -\frac{1}{h} \cdot \left(\vec{E}_{\text{local}} \cdot \Delta\vec{\mu}_{\text{mol}} + f \cdot \vec{E}_{\text{ext}} \cdot \Delta\vec{\mu}_{\text{mol}} + \frac{1}{2} \cdot \vec{E}_{\text{local}} \cdot \Delta\bar{\bar{\alpha}}\vec{E}_{\text{local}} \right. \\ & \left. + \frac{1}{2} f^2 \cdot \vec{E}_{\text{ext}} \cdot \Delta\bar{\bar{\alpha}}\vec{E}_{\text{ext}} + f \cdot \vec{E}_{\text{local}} \cdot \Delta\bar{\bar{\alpha}}\vec{E}_{\text{ext}} \right). \end{aligned} \tag{2.11}$$

Two of the contributions do not depend on the external electric field $\vec{E}_{\text{ext}}$ and are responsible for the so-called solvent shift. Due to the large values of $\vec{E}_{\text{local}}$ the solvent shift can amount up to several hundred wavenumbers, a magnitude comparable to the overall inhomogeneous bandwidth [69]. The other three terms are much smaller and can only be detected with a suitably highly resolving spectroscopic technique such as absorption modulation spectroscopy [20], fluorescence anisotropy spectroscopy [70], single molecule spectroscopy [71] or – as in this work – persistent spectral hole burning [72]. A more detailed overview over different applications is given by Bublitz and Boxer [73].

- *Linear Stark Effect*
  The frequency shift $f \cdot \vec{E}_{\text{ext}} \cdot \Delta\vec{\mu}_{\text{mol}}$ only appears for non-centrosymmetric molecules. The linear Stark effect is usually the strongest of the externally controlled shifts, however, for large molecules with an extended π-electron

system the polarizability change can exceed the fixed dipole moment difference. Also, non-centrosymmetric molecules like the aromatic amino acid phenylalanin can lack a measurable linear Stark effect depending on the electrons contributing to the excitation [36].

- *Quadratic Stark Effect*
  Due to the relatively weak strength of the external electric field the quadratic term $\frac{1}{2}f^2 \cdot \vec{E}_{\text{ext}} \cdot \Delta\bar{\bar{\alpha}}\vec{E}_{\text{ext}}$ will be negligible in most cases where linear contributions are to be observed. However, quadratic Stark effects can be investigated when the permanent dipole moment difference vanishes [74] or if $\Delta\bar{\bar{\alpha}}$ can be enhanced by suitable design of the chromophore system [75, 76].

- *Pseudolinear Stark Effect*
  The pseudolinear Stark shift $f \cdot \vec{E}_{\text{local}} \cdot \Delta\bar{\bar{\alpha}}\vec{E}_{\text{ext}}$ originally is a second order phenomenon as well but can not be disregarded in systems with high local electric fields like proteins [68]. For molecules with rather large polarizability differences in the order of 10^3 Å^3 the frequency shift caused by the pseudolinear Stark effect is comparable with the linear Stark shift. Moreover, the pseudolinear Stark effect allows experimental access to an otherwise difficult to measure quantity, the local electric field. By comparing with quantumchemical model calculations, the determination of the pseudolinear Stark shift may allow for assessment of local electrostatic properties of the investigated host system.

2.5.2 Spectral Holes in External Electric Fields

The main advantage of persistent hole burning spectroscopy is its high spectral resolution near the natural linewidth limit. Even tiny changes in the environmental conditions of a chromophore can be quantitatively monitored. However, since a spectral hole is always comprised of a subensemble of molecules of the overall absorption band, each molecule may react differently on external perturbations especially in glasses and inhomogeneously distributed host matrices. The number of molecules contributing to a spectral hole is sufficiently large to justify the same statistical means of description as for the inhomogeneous ensemble. Any shifts due to an external electric field that would affect the molecules will therefore influence the spectral hole in the same way, so that observation of the spectral behavior of the hole can be seen as an observation of the behavior of the burnt molecules.

The statistical distribution function allows two distinct features to be discerned when applying an electric field to a spectral hole, hole broadening and hole splitting. The appearance of either of those features depends on several factors:

- Type of Stark effect
- Orientation of the external field with respect to the local field
- Local anisotropy of chromophore environments
- Spectral position of the burnt hole

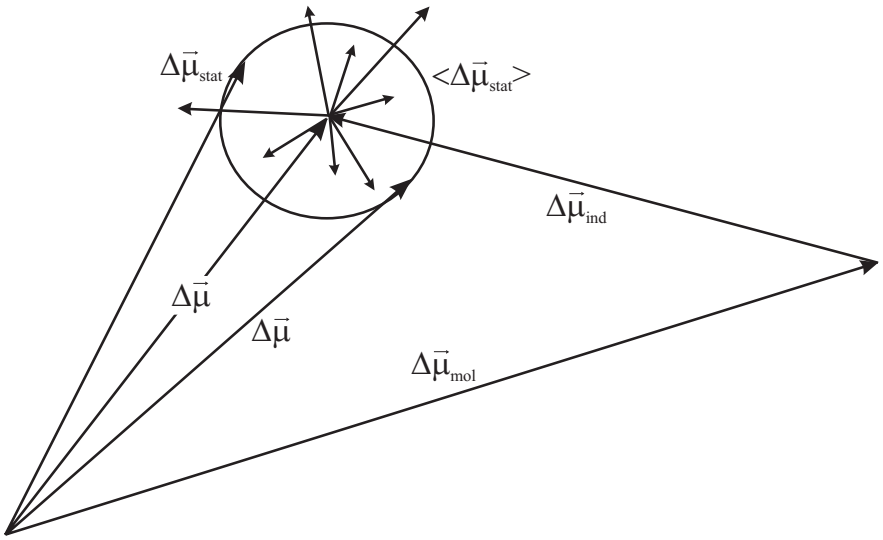

Figure 2.4: *The overall dipole moment difference $\Delta\vec{\mu}$ consists of the permanent intrinsic dipole moment difference $\Delta\vec{\mu}_{\mathrm{mol}}$ and the induced dipole moment difference $\Delta\vec{\mu}_{\mathrm{ind}}$, which can fluctuate with a random contribution $\Delta\vec{\mu}_{\mathrm{stat}}$ depending on the grade of order in the system. The overall dipole moment difference can therefore vary with an average uncertainty of $\langle\Delta\vec{\mu}_{\mathrm{stat}}\rangle$.*

Fig. 2.4 shows the relevant components of the dipole moment difference. While the fixed dipole moment difference $\Delta\vec{\mu}_{\mathrm{mol}}$ is constant within the frame of reference of the molecule and is only affected by the electronic properties of the chromophore itself, the induced dipole moment difference $\Delta\vec{\mu}_{\mathrm{ind}}$ depends on the environment of the chromophore. Ideal crystalline host matrices will incorporate guest molecules in such a way that every single guest molecule experiences the same interactions. The random component $\Delta\vec{\mu}_{\mathrm{stat}}$ will therefore be zero in this case and every induced dipole moment difference will have the same quantity and direction $\Delta\vec{\mu}_{\mathrm{ind}}$. However, in completely disordered host systems quite the opposite is true: With a sufficiently large number of chromophores excited, the distribution of interactions with the environment of the subensemble of molecules making up the spectral hole will be Gaussian-like and the local field will only induce statistically distributed dipole moment differences $\Delta\vec{\mu}_{\mathrm{stat}}$. This effect makes amorphous host systems a valuable tool to distinguish between fixed and induced dipole moment differences. With the intrinsic dipole moment difference being responsible for a constant offset to the overall dipole moment difference, the induced dipole moments will be an indicator for the randomness of the interactions. Experiments with glycerol/water mixtures as a solvent, which forms a glass at low temperatures can therefore reveal details about the local electric field even with a non-centrosymmetric chromophore because the linear Stark effect can be separated from the pseudo-linear Stark effect.

Looking at two extreme hypothetical cases the effects on spectral holes due to the different dipole moment differences can be highlighted. Assuming that there would be no induced dipole moment difference at all, the shape of the spectral hole under the influence of an external electric field is determined by the linear Stark effect. Because of the intrinsic dipole moment difference $\Delta\vec{\mu}_{\mathrm{mol}}$ being

independent of the surrounding solvent molecules the angle θ between $\Delta\vec{\mu}_{\mathrm{mol}}$ and the transition dipole moment $\vec{\mu}_{\mathrm{fi}}$ will be fixed for all molecules contributing to the hole. By using linearly polarized excitation light mainly those molecules with a transition dipole moment parallel or anti-parallel to the direction of the exciting radiation field $\vec{E}_{\mathrm{L}}$ will be selected for the subensemble. The probability of excitation for a molecule whose transition dipole moment displays an angle χ with respect to $\vec{E}_{\mathrm{L}}$ decays with $\cos^2\chi$. Hence, the probability to find a transition dipole moment suitable for excitation in a cone of an aperture angle of about $30\,^\circ$ around the polarization vector of the exciting field is 98%. When the frame of reference is fixed in this way by the choice of excitation polarization the polarization of the external field can be changed to probe the angle θ and the strength of $\Delta\vec{\mu}_{\mathrm{mol}}$.

Again, four extreme cases as depicted in Fig. 2.5 will give an impression of how spectral holes react depending on the molecular properties and the experimental setup. The orientation of the external electric field $\vec{E}_{\mathrm{ext}}$ will always remain the same in the pictures, whereas the orientation of the exciting electric field $\vec{E}_{\mathrm{L}}$ will be either perpendicular or parallel to the latter. $\vec{\mu}_{\mathrm{fi}}$ will always be oriented in the same way as $\vec{E}_{\mathrm{L}}$. $\Delta\vec{\mu}_{\mathrm{mol}}$ is assumed to be either parallel or perpendicular to $\vec{\mu}_{\mathrm{fi}}$ for the sake of the argument. $\vec{\mu}_{\mathrm{fi}}$ and $\Delta\vec{\mu}_{\mathrm{mol}}$ are shown within a cone around the exciting field to show the probability distribution.

a Fig. 2.5 A: $\theta = 0^\circ$ und $\vec{E}_{\mathrm{L}} \parallel \vec{E}_{\mathrm{ext}}$
Molecules that have been excited by $\vec{E}_{\mathrm{L}}$ will mainly have dipole moment differences that are either parallel or antiparallel to $\vec{E}_{\mathrm{L}}$. Since the external electric field $\vec{E}_{\mathrm{ext}}$ is parallel to $\vec{E}_{\mathrm{L}}$ as well, there will be either rather large energy gains or losses $\vec{E}_{\mathrm{ext}} \cdot \Delta\vec{\mu}_{\mathrm{mol}}$. This will result in half of the molecules shifting to the red and half of them shifting to the blue. The center of the hole will deplete because no molecule will have $\Delta\vec{\mu}_{\mathrm{mol}}$ oriented perpendicular to $\vec{E}_{\mathrm{ext}}$. Upon increasing the strength of $\vec{E}_{\mathrm{ext}}$ the hole will be splitting, while broadening only slightly due to the uncertainty of the excitation of $\vec{\mu}_{\mathrm{fi}}$.

b Fig. 2.5 B: $\theta = 0^\circ$ und $\vec{E}_{\mathrm{L}} \perp \vec{E}_{\mathrm{ext}}$
Most of the molecules will have a $\Delta\vec{\mu}_{\mathrm{mol}}$ that is perpendicular to $\vec{E}_{\mathrm{ext}}$ - the frequency shifts are small and equally distributed around zero. The hole will only broaden without splitting at all.

c Fig. 2.5 C: $\theta = 90^\circ$ und $\vec{E}_{\mathrm{L}} \parallel \vec{E}_{\mathrm{ext}}$
Similar to case B the hole will only broaden here.

d Fig. 2.5 D: $\theta = 90^\circ$ und $\vec{E}_{\mathrm{L}} \perp \vec{E}_{\mathrm{ext}}$
Similar to case A the hole will be splitting up, however, the magnitude of splitting will be reduced due to the cone-shaped distribution of $\Delta\vec{\mu}_{\mathrm{mol}}$ around the already cone-shaped distribution of $\vec{\mu}_{\mathrm{fi}}$.

While the orientation of the external electric field can be adjusted precisely to match either of the extreme cases, real chromophores will have an angle θ that is dependent on the electronic configuration of the molecule. Any hole spectra will therefore display mixtures of the phenomena described above. By evaluating two series of hole spectra with parallel or perpendicular orientation of the involved

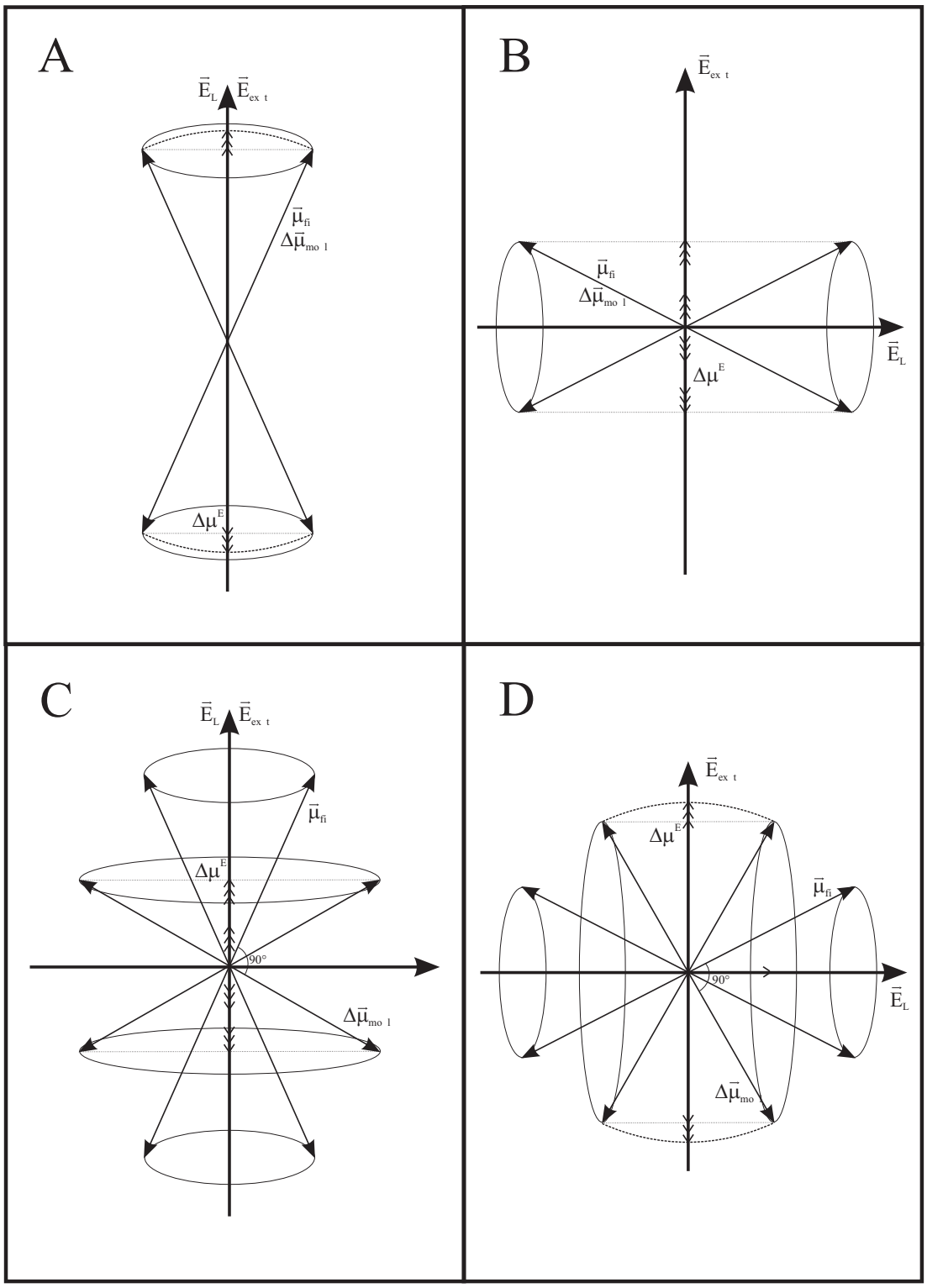

Figure 2.5: *Four geometries for probing the linear Stark effect by modifying the polarization of the external electric field $\vec{E}_{\mathrm{ext}}$ with respect to the polarization of the exciting electric field $\vec{E}_{\mathrm{L}}$. Every picture shows the dipole moments $\Delta\vec{\mu}_{\mathrm{mol}}$ and $\vec{\mu}_{\mathrm{fi}}$ as well as the 30° cone around $\vec{E}_{\mathrm{L}}$ where excitation is probable. $\Delta\mu^{\mathrm{E}}$ is the projection of $\Delta\vec{\mu}_{\mathrm{mol}}$ to the axis of $\vec{E}_{\mathrm{ext}}$.*

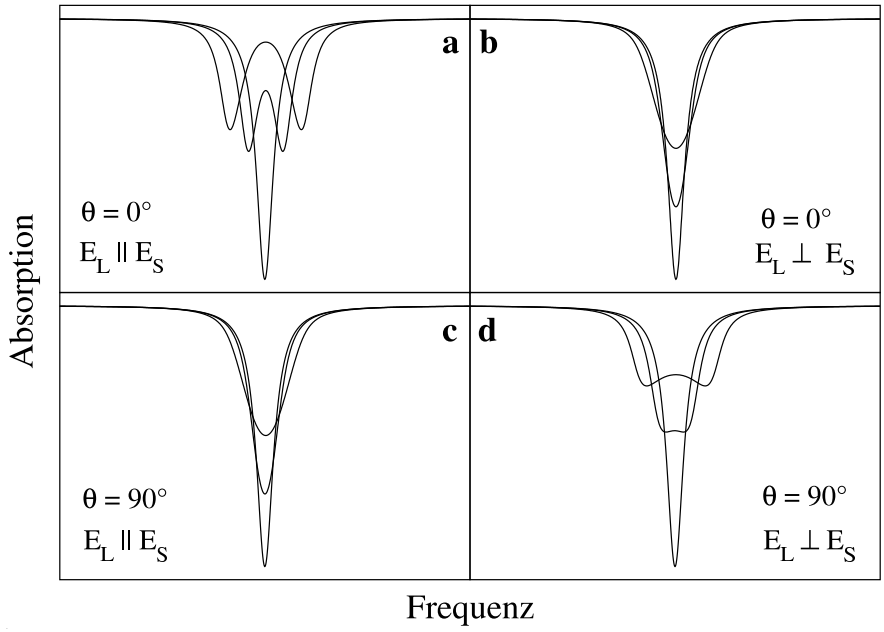

Figure 2.6: *Model spectra according to the theory of Schätz and Maier [77]. The four spectra correspond to the four geometries in Fig. 2.5.*

electric fields simultaneously, the angle θ can be retraced.

Theoretical calculations were done by Schätz and Maier [77]. Four series of simulated Stark spectra with the same geometries as assumed in Fig. 2.5 are shown in Fig. 2.6. Technical difficulties will always arise when the angle θ is in the region of 55°, the so-called *magic angle*. Here, the magnitude of splitting is about the same in both experimental field orientations complicating fitting procedures.

The second extreme case is the one with contributions only due to the pseudo-linear Stark effect. A molecule without a permanent dipole moment difference in an ideal crystalline matrix will display the same properties as in Fig. 2.5 because every induced dipole moment difference will have the same magnitude and direction. It can therefore be regarded as fixed within the frame of reference of the molecule since every molecule is embedded in the same solvent environment. However, the more randomness the matrix contains the larger the statistical fluctuations $\langle \Delta\vec{\mu}_{\mathrm{stat}} \rangle$ of the dipole moment difference will be. Completely disordered matrices will even induce totally random dipole moments so that in an amorphous solvent the average induced dipole moment difference of the whole ensemble of molecules contributing to a spectral hole will be zero. Any external field, regardless of its direction will only be able to produce a broadening of the hole rather than a splitting. This is an advantage when examining the Stark effect of spectral holes in disordered solvents: Any splitting of the hole can be ascribed to the fixed dipole moment difference whereas a broadening is mainly caused by the local electric field and the polarizability of the chromophores. Albeit being largely independent from the fixed dipole moment difference, the hole broadening is much

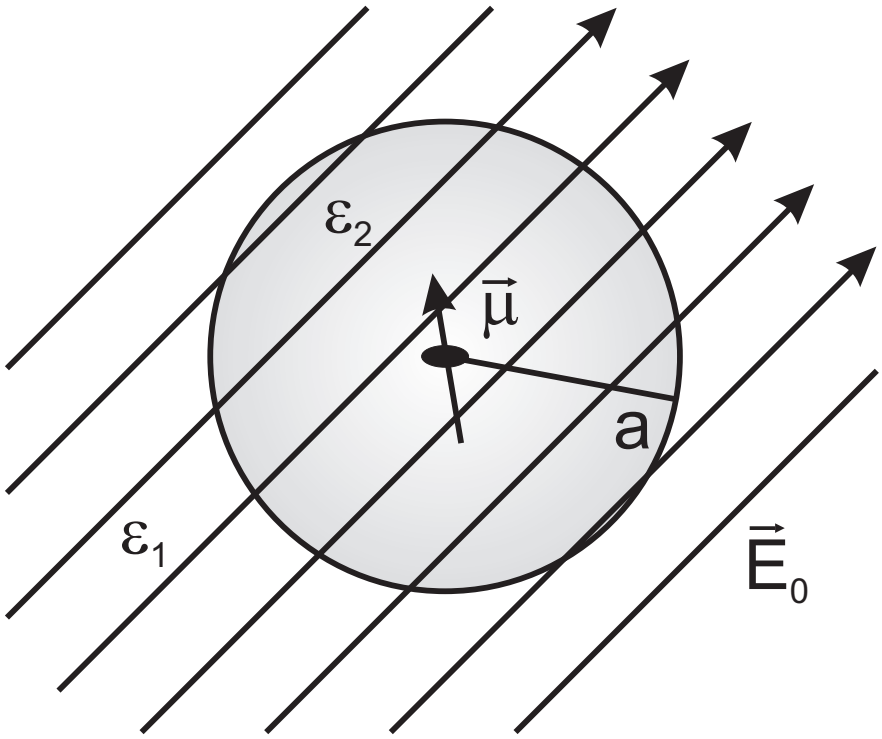

Figure 2.7: *Kirkwood's model [79] assumes a spherical cavity of radius a and homogeneous dielectric constant ϵ_2 within a liquid of dielectric constant ϵ_1. An external electrostatic field E_0 is applied to a pointlike dipole μ at the center of the cavity.*

more complicated to evaluate than the hole splitting because it also depends on the distribution of excited transition dipole moments.

2.5.3 The Lorentz Factor and Kirkwood-Fröhlich theory

As mentioned before, a crucial factor when calculating electrostatic properties of the chromophore like dipole moments and polarizabilities is the mitigation of the external electric field by the surrounding solvent. This correction is given by the so-called Lorentz factor the derivation of which is discussed in detail by Fröhlich [78].

Following the derivation of Onsager [80] and the extended model of Kirkwood [79], the electrostatic potential Ψ of a pointlike dipole μ in a spherical cavity of radius a with a static homogeneous dielectric constant ϵ_2 in a liquid of an also static and homogenous dielectric constant ϵ_1 can be estimated at any point $\vec{r}$ of space as the superposition of the dipole potential and the potential of an homogeneous electrostatic field (*cf.* Fig. 2.7):

$$\Psi\left(\vec{r}\right) = \frac{\vec{A}\cdot\vec{r}}{4\pi\epsilon_0 r^3} + \vec{B}\cdot\vec{r} \tag{2.11}$$

In this equation A is an enhanced dipole moment, consisting of a permanent and an induced dipole moment, and B an enhanced electrostatic field. According

to the separation of regions with different dielectric constants, the electrostatic potential can be divided into two sections Ψ_1 and Ψ_2 – one outside the cavity and one inside with enhanced dipole moments A_1 and A_2 as well as enhanced electrostatic fields B_1 and B_2. There are several boundary conditions that must be met determining those four components:

- Far away the potential must resemble that of a constant electric field.
- In the vicinity of the dipole the potential must resemble that of a dipole.
- The potential must be continuous at the border of the cavity.
- The normal component of the dielectric displacement vector $\vec{D}$ must be continuous at the border of the cavity.
- The tangential component of the electrostatic field $\vec{E}$ must be continuous at the border of the cavity.

The first two criteria directly lead to $\vec{A_2} = \left(\vec{\mu} + \vec{M}\right)$ and $\vec{B_1} = \vec{E_0}$, where $\vec{M}$ is the average dipole moment induced by polarization of molecules within the cavity and $\vec{E_0}$ the externally applied homogeneous electrostatic field. Using the equality of Ψ_1 and Ψ_2 at $|\vec{r}| = a$ and the equality of the spatial derivations of $\epsilon_1\Psi_1$ and $\epsilon_2\Psi_2$ at $|\vec{r}| = a$ the equations can be solved for $A_1 = |\vec{A_1}|$ and $B_2 = |\vec{B_2}|$ respectively. A_1 is the effective dipole moment outside the cavity due to the point dipole and the polarization of the cavity, B_2 is the mitigated electrostatic field acting on μ inside the cavity:

$$\frac{A_1}{a^3} = \frac{\epsilon_1 - \epsilon_2}{2\epsilon_1 + \epsilon_2} E_0 - \frac{3}{2\epsilon_1 + \epsilon_2} \cdot \frac{\mu + M}{4\pi\epsilon_0 a^3} \tag{2.12}$$

$$B_2 = \frac{3\epsilon_1}{2\epsilon_1 + \epsilon_2} E_0 - \frac{3}{2\left(\epsilon_1 - \epsilon_2\right)} \cdot \frac{\mu + M}{4\pi\epsilon_0 a^3} \tag{2.13}$$

Considering the special case of a molecule with negligible fixed dipole moment in an homogeneously polarized cavity, $\vec{M}$ can be ascribed to the overall polarization $\vec{P}$ induced by the external electrostatic field $\vec{E_0}$

$$\frac{\vec{M}}{4\pi\epsilon_0 a^3} = \frac{\left(\epsilon_1 - \epsilon_2\right) E_0}{3}, \tag{2.14}$$

leading to an expression for B_2 in terms of E_0 when inserted in Eq. 2.13:

$$B_2 = \frac{\epsilon_1 + 2\epsilon_2}{3\epsilon_2} E_0. \tag{2.15}$$

The mitigation factor for B_2 is also known as the Lorentz factor [81]. However, a molecule with a strong dipole moment itself will polarize its surrounding causing

the electrostatic field to decrease. Onsager [80] suggested to split the contributions into a cavity field $\vec{G}$ and a reaction field $\vec{R}$ with $\vec{G}$ being the field inside an empty cavity within a polarizable medium and $\vec{R}$ the field induced by polarization of this sphere due to the dipole moment μ of the molecule. This distinction is useful, because only the cavity field can change the orientation of the dipole. The reaction field created by the already aligned dipole does not act back upon itself. Thus the field B_2^{O} present in the cavity will be

$$B_2^{\mathrm{O}} = \frac{3\epsilon_1}{2\epsilon_1 + 1} E_0 + \frac{2\left(\epsilon_1 - \epsilon_2\right)}{4\pi\epsilon_0 a^3 \left(2\epsilon_1 + \epsilon_2\right)} \mu. \tag{2.16}$$

An enhancement in this theory is provided by taking into account the polarizability of the host molecule itself, however, most of the simplifying assumptions can be justified in hole burning spectroscopy of biological molecules. The Lorentz factor allows the determination – or at least a reasonable estimation – of the dielectric constants, if the external field as well as the induced dipole moment difference are known. The latter can be extracted from the broadening of the holes and compared to quantumchemical calculations for a molecule in an unmitigated electrostatic field.

2.6 Pressure Tuning Spectroscopy

While the Stark spectroscopy yields mainly an insight into the molecule's electrostatic properties, pressure tuning spectroscopy unveils details about the structure of the guest matrix and its interactions with the chromophore. Experimentally determined values in pressure tuning are mechanical variables whose usefulness unfolds when comparing to experiments with altered conditions. The isothermic compressibility for example as one of the main properties to be observed is an indicator for the rigidity and general strength of chromophore binding to its environment. The pressure tuning experiments in this work were conducted in the low pressure regime ($p < 10\,\mathrm{MPa}$) where all deformations can be assumed as reversible and elastic. Sufficiently high pressures ($p > 100\,\mathrm{MPa}$) lead to phase transitions and irreversible transformations and have to be evaluated in a completely different way [82]. Laird and Skinner [83] provided a theory to compute the behavior of a spectral hole under low pressure.

2.6.1 Pressure Induced Matrix Changes

When applying pressure to chromophores in a host matrix the intermolecular distances will change. Due to their electrostatic nature, molecular interactions will heavily depend on the distance between the interacting partners, so systematic parameters like isothermic compressibility or solvent shifts can be investigated. Electrostatic interactions mainly comprise of ion-ion-, ion-dipole, dipole-dipole- and dispersion interactions [84] since any interactions due to higher order multipoles can be neglected in most cases. Changes in the absorption behavior of chromophores depend on differences between the ground and the excited state, so interactions involving the first multipole moment, the charge

of a probe molecule, can not be directly observed by hole burning spectroscopy. The charge of a molecule will not change upon electronic excitation leaving the excitation frequency untouched upon change of interactions depending on the ionic strength, hence the shape of a spectral hole would not change with pressure from the ionic interactions. However, if a probe molecule with a changing dipole moment interacts with charges of the environment the ion–dipole coupling will result in hole shifts.

The distance dependence of electrostatic interactions scales with R^{-n} with variable n for different kinds of interactions. For non-polar solvents the dominating interaction type will be that between dipoles and induced dipoles along with dispersion interactions. Both of those interactions scale with R^{-6}. Comparison with experiments in solvents of already known compressibility and solvent shifts shows that in amorphous matrices the main contribution to the pressure induced hole shifts comprises of R^{-6} potentials [85–87]. Depending on the type of interaction spectral holes will either experience bathochromic or hypsochromic shifts. Dispersion interactions mainly result in red shifts because of the higher polarizability of excited states and the concomitant increase in interaction energy between two induced dipoles [88]. Dipole-dipole interactions may result in different shifts considering the different orientations of dipole moments in ground and excited states [13, 89, 90]. Any experimentally observable shifts are superpositions of the various effects. At a certain spectral hole burning position the net shift will be zero though if all effects cancel each other. That particular burning frequency is referred to as *vacuum frequency* ν_{vac}, because similarly to isolated molecules in vacuum there is no frequency shift. The spectral distance between the center of the inhomogeneous absorption band and the vacuum frequency is the solvent shift s, which is an average shift of a molecule in the specific amorphous matrix.

2.6.2 Spectral Holes Under Pressure

A single chromophore interacting with a single solvent molecule will have an absorption frequency ν that is altered by a fraction $\Delta\nu$ if a pressure p is exerted on the system. For sufficiently small pressure changes the shifted absorption frequency ν_{p} can be estimated by using a first order expansion:

$$\nu_{\mathrm{p}} = \nu + \Delta\nu_{\mathrm{p}} = \nu + \frac{\partial\nu}{\partial p} \cdot \Delta p \tag{2.17}$$

with a pressure dependent frequency shift $\frac{\partial\nu}{\partial p}$ of

$$\frac{\partial\nu}{\partial p} = \frac{\partial\nu}{\partial R} \cdot \frac{\partial R}{\partial V} \cdot \frac{\partial V}{\partial p}, \tag{2.18}$$

where R is the distance between the chromophore and the solvent molecule and V the volume of the sphere with radius R around the the probe molecule. Obviously, $\frac{\partial\nu}{\partial p}$ should be independent of the observed volume so the pressure dependent volume change will be normalized using the standard definition of the isothermic compressibility κ

$$\kappa = -\frac{1}{V}\frac{\partial V}{\partial p}\bigg|_{T=T_0}. \tag{2.19}$$

The small and isotropic pressure will only change the size of the volume, not the relative orientation of the molecules to each other, so the volume can be assumed as spherical to match the centrosymmetric potential

$$\begin{aligned} V &= \frac{4}{3} \cdot \pi R^3 \\ \Rightarrow \frac{\partial R}{\partial V} &= \frac{R}{3V}, \end{aligned} \tag{2.20}$$

and the frequency shift under pressure of a single pair of chromophore and solvent molecule will be

$$\Delta\nu_{\mathrm{p}} = -\frac{R \cdot \kappa}{3} \cdot \frac{\partial \nu}{\partial R} \Delta p. \tag{2.21}$$

Assuming a low solute concentration the interactions between different chromophores can be neglected due to the small range of the electrostatic potentials. However, there will be more than one solvent molecule interacting with a given chromophore leading to an expression for the distribution of pressure induced frequency changes for an ensemble of chromophores $f(\nu, p)$ at burning frequency ν interacting with an average number of N solvent molecules each:

$$f(\nu, \Delta\nu_{\mathrm{p}}, p) = \frac{1}{I(\nu) \cdot V^N} \int P(R_1, \ldots, R_N) \cdot \delta(\nu) \cdot \delta(\Delta\nu_{\mathrm{p}})\, dR_1 \cdots dR_N. \tag{2.22}$$

Here the initial inhomogeneous distribution of all chromophores at burning frequency ν is $I(\nu)$:

$$I(\nu) = \frac{1}{V^N} \int P(R_1, \ldots, R_N) \cdot \delta(\nu)\, dR_1 \cdots dR_N. \tag{2.23}$$

The most severe assumption, that has to be made to be able to evaluate these integrals analytically, is to view the solute molecules as independent from each other. Instead of considering $N!$ interactions the N particle distribution function $P(R_1, \ldots, R_N)$ can be disintegrated into a product of two-particle distribution functions $g(R_1) \cdots g(R_N)$. That will simplify the inhomogeneous distribution function [91] as well as the distribution of frequency changes $f(\Delta\nu_{\mathrm{p}}, \nu, p)$. Assuming furthermore a sufficiently high density of solvent molecules in the surrounding of the chromophores $f(\Delta\nu_{\mathrm{p}}, \nu, p)$ can be approximated via the central limit theorem by a Gaussian [92]. Following the derivations of Laird and Skinner [83] the first two moments of this Gaussian reflect the frequency shift of the center of the subensemble distribution $\Delta\nu_{\mathrm{g}}$ and the full width at half maximum of the

distribution $\Delta\sigma_g$:

$$\Delta\nu_g = \frac{N}{V}\left(\int g(R_1)\cdots g(R_N)\cdot\Delta\nu_p\, dR_1\cdots dR_N + \frac{8\ln 2\cdot\int g(R_1)\cdots g(R_N)\cdot\Delta\nu_p\cdot\nu\, dR_1\cdots dR_N\,(\nu-\nu_{vac})}{\Gamma_i}\right)\cdot\Delta p, \tag{2.24}$$

$$\Delta\sigma_g = \left(\frac{N}{V}\right)^{1/2}\left(\int g(R_1)\cdots g(R_N)\cdot(\Delta\nu_p)^2\, dR_1\cdots dR_N + \frac{8\ln 2\cdot N\cdot(\int g(R_1)\cdots g(R_N)\cdot\Delta\nu_p\cdot\nu\, dR_1\cdots dR_N)^2\,(\nu-\nu_{vac})}{V\cdot\Gamma_i}\cdot(\Delta p)^2\right)^{1/2}\Bigg). \tag{2.25}$$

Γ_i is the full width at half maximum of the inhomogenous absorption band, ν_{vac} the afore mentioned vacuum frequency.

Using Eq. 2.21 and R^{-6} potentials the pair distribution integrals can be evaluated yielding a rather simple equation for the pressure dependent frequency shift $\Delta\nu_g$ which will be the main focus of this work:

$$\Delta\nu_g = 2\cdot\kappa\cdot(\nu-\nu_{vac})\cdot\Delta p. \tag{2.26}$$

In a doubly linear plot of the experimentally observable $\Delta\nu_g$ versus the pressure change Δp and the hole burning frequency ν the slope of the graph will be twice the isothermic compressibility κ. The results obtained with this approximation are in line with findings with other techniques [93–95].

This simplification requires the neglection of repulsive potentials such as the R^{-12} part of the Lennard-Jones potential. However, those repulsive potentials concern only the nearest neighbors to the probe. At low temperatures those are generally in a very stable position regarding the interaction with the chromophore. For very small changes in the distance the gradient of a R^{-12} potential will therefore be close to zero. Linear effects would thus contribute nothing to the frequency changes caused by pressure induced distance changes. This allows for the analytical solution of the approximation using only the attractive part of the Lennard-Jones potential.

2.6.3 Justification of the Approximations

Some of the approximations made by Laird and Skinner are rather severe – some justifications about why they are still applicable in the evaluation of the results obtained in this work are to be made here:

- *Scalar Compressibility*
  The isothermic compressibility κ is only scalar for a perfectly isotropic and homogeneous medium. In anisotropic media κ resembles a tensor that accounts for the anisotropy of the solvent; in disordered media it is subject

to a dispersion. However, using a scalar compressibility in glasses only allows the determination of some average local compressibility. In this work, any conclusions drawn from values of this averaged compressibility are of comparative nature, thus proving this simplification as adaequate for the investigated problems.

- *Local Compressibility*
  Furthermore, it must be stressed that the compressibility featured in this work is a locally limited property. With a low concentration of solute molecules and the short range of the dipolar interactions the compressibility can only be measured in the immediate surrounding of a chromophore [96]. When comparing the values measured with spectral hole burning with those of other methods this difference has to be taken into account.

- *Reversible Compression*
  The reversibility of the pressure deformations caused in the used pressure range could be verified by monitoring hole spectra before and after a pressure tuning experiment. Holes under ambient pressure were compared to the respective holes where the pressure was relieved after the experiment again. The shape of the hole was retained for every experiment.

- *Independent Solvent Molecules*
  Along with the assumption of a sufficiently large density of solvent molecules to approximate the distribution of frequency changes as a Gaussian, the notion of statistically independent solvent molecules may appear contradictory. Any distance changes, however, are in the range of fractions of Ångstroms – a pressure change of 1 MPa for example will only result in a relative intermolecular distance change in the order of around 10^{-3} Å. Individual surroundings of chromophores in an amorphous matrix have position uncertainties of the solvent molecules which are two orders of magnitude larger, hence allowing the pressure induced distance changes between solvent molecules after averaging over an ensemble of surroundings to be seen within the statistical fluctuations of the matrix molecules.

Every experiment proves something. If it doesn't prove what you wanted it to prove, it proves something else.

Anonymous

Chapter 3

Methods and Materials

3.1 Sample Preparation

3.1.1 Thionin and BODIPY

BODIPY (4,4-difluoro-5-(4-phenyl-1,3-butadienyl)- 4-bora-3*a*,4*a*-diaza-*s*-indacene-3-propionic acid) was bought as a powder from Molecular Probes, Thionin (3,7-diamino-5-phenothiazinium acetate) from Sigma. Both samples were used without further purification. A 0.01 M Tris/HCl buffer was used to create stock solutions with a pH of 7.5. Glycerol (Fluka, puriss.) was added to obtain a final water to glycerol ratio of 4:5. The concentrations of the dyes were adjusted to acquire an optical density of 0.6 to 1, the optimum range for hole burning spectroscopy, amounting to a final concentration in the range of 10^{-5} to 10^{-4} M for each dye which is sufficiently low to prevent clustering.

3.1.2 Cyclodextrin

Cyclodextrins (cyclohexaamylose, cycloheptaamylose) were bought from Sigma and used without further purification. Since cyclodextrins absorb in a wavelength range lower than 250 nm they do not interfere with the absorption bands of the hole burnt dye thionin. Therefore, the concentrations of cyclodextrins were chosen to provide a sufficient binding probability with thionin on one hand, but to minimize the influence of the cyclodextrins on the glass-forming abilities of the sample on the other hand. The final concentration of α-cyclodextrin (α-CD) amounted to $5 \cdot 10^{-4}$ M, the concentration of β-cyclodextrin (β-CD) to $5 \cdot 10^{-5}$ M with a base concentration of thionin of $5 \cdot 10^{-5}$ M. The concentration of β-CD was mainly limited by its low solubility.

3.1.3 DNA Oligonucleotides

Oligonucleotide duplexes were bought from Applied Biosystems and purified with HPLC at the laboratory of Prof. Chang (IAMS, Academica Sinica, Taiwan). The dried samples were dissolved in Tris/HCl buffer of pH 7.5 and stirred for at least four hours. After adding thionin with a concentration of $5 \cdot 10^{-5}$ M glycerol was added to obtain a glycerol/water ratio of 5:4. For the telomeric sequences of

$d(G_2T_2G_2TGTG_2T_2G_2)$ and $(d(G_4T_4G_4))_2$ additionally 0.15 M NACl was mixed to the sample to retain the quadruplex structure of the the oligonucleotides [97].

3.1.4 Phycocyanin

C-phycocyanin as well as its α-subunit of the cyanobacterium *Mastigocladus laminosus* were refined and purified by the group of Prof. H. Scheer (Botanisches Institut, Ludwig-Maximilians-Universität) and brought into a 10 mM $NaHPO_4/Na_2PO_4$ buffer with a pH of 7.5. The exact purification process can be found elsewhere [98]. The concentration of the chromophore was adjusted by evaporization of the solvent at ambient temperature to account for optimal hole burning efficiency. Evaporization times were in the range between 24 and 72 hours. Glycerol was added to the final protein solution to obtain a 4:5 mixture of protein buffer and glycerol.

3.2 Cryostats

All experiments were conducted in a homebuilt ^{4}He bath cryostat. The glass cells with the samples were placed into a sample holder and completely submerged in liquid helium for a fast freezing process ensuring a good glass quality. To lower the temperature and to prevent boiling of helium during the course of the experiments the vapor pressure was held at a constant value of about 30 mbar which corresponds to a liquid helium temperature of approximately 2 K.

3.3 Light Sources

3.3.1 Spectrophotometer

Absorption spectra at ambient temperature were recorded with a UV-2401 spectrophotometer from Shimadzu. A homebuilt nitrogen bath cryostat was used to take control spectra at 70 K with the sample cells immersed in liquid nitrogen.

3.3.2 Monochromator

The low temperature absorption spectra as well as the satellite hole burning spectra were recorded with a monochromator in 1m-Czerney-Turner setup (Jobin Yvon) with a Xe high pressure arc lamp (Osram, 75 W). Using a UV-blazed grating in 2nd order with a line density of 600 mm^{-1} and entrance and exit slit widths of about 100 μm a spectral resolution in the order of 1 cm^{-1} was achieved.

3.3.3 Dye Ring Laser

Hole burning and scanning was accomplished with a cw dye ring laser. One setup featured a Coherent 899-21 pumped by an argon ion laser (Coherent Sabre 10) at a pumping wavelength of 514 nm and a pumping power of 6 W in single line mode, another a Coherent 699-21 pumped by a frequency doubled neodymium vanadate laser (Coherent Verdi) with a pumping power of 5 W. The ring lasers were operated with rhodamine 6G and sulforhodamine 101 (Radiant Dyes) in

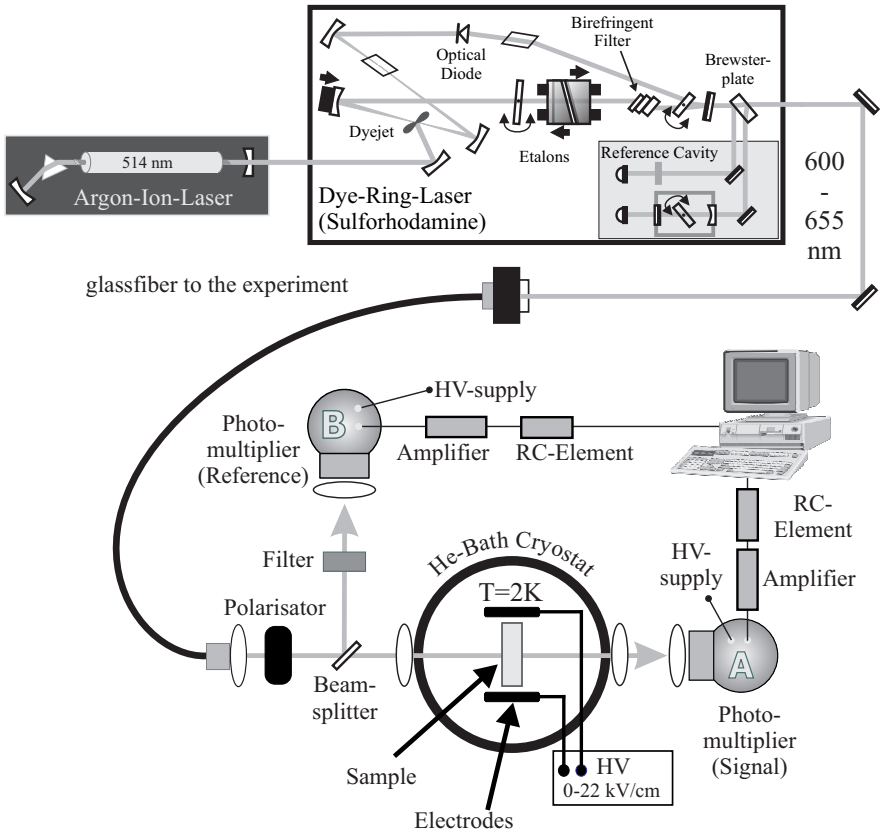

Figure 3.1: *Optical setup of the experiments.*

a spectral range between 16000 and 17850 cm^{-1} and 15200 and 16700 cm^{-1}, respectively. The output power of both laser systems was above 150 mW. Both lasers could be scanned over a range of 30 GHz with a spectral resolution of 500 kHz in mode lock. The wavelength check was done with a homebuilt scanning interferometer with a spectral resolution of 100 MHz.

3.4 Optical Setup

The laser light was coupled into a PMMA fibre and transmitted to the experiment. To avoid polarization artifacts the fibre was subjected to slight vibrations. Neutral density filters were used to tune the laser power down to the desired level. Hole burning itself was conducted with a power density of 10–1000 $\mu\mathrm{W/mm}^2$ depending on the sample and the hole burning efficiency. After hole burning times of up to 15 mins the hole depths were in the range of 5–25% of the inhomogeneous absorption band at the particular wavelength. For scanning the laser power was reduced by a factor of 10^2 to 10^3 to avoid additional hole burning during the scan. Before reaching the sample cell a part of the laser beam was coupled out to compensate for intensity fluctuations. Two photomultipliers (Hamamatsu R928) collected the transmitted light, two high frequency amplifiers (HMS 564) and two homebuilt RC smoothers processed the signals which were directed to an A/D converter. The obtained signal was the relative intensity of the transmitted light with respect to the reference light (*cf.* Fig. 3.1).

3.5 Experiments

3.5.1 Satellite Hole Burning

For the satellite hole burning spectra an absorption scan of the unburnt inhomogeneous band was made with the monochromator. After burning a hole at a certain wavelength the monochromator scan was repeated and the base spectrum subtracted to create a background free satellite hole spectrum.

3.5.2 Stark Effect

By applying high voltage supplied by two generators (fug HCN 14-6500 and 14-12500) to two steel plates at the sides of the sample cell, an homogeneous electrostatic external field of variable strength could be generated perpendicular to the direction of the laser beam. The maximum field strength in this work was $|\vec{E}_{\mathrm{ext}}| = 25\,\mathrm{kV/cm}$. A hole was burnt at some initial field strength and the voltage increased in 2 kV steps while subsequently taken hole scans at the various field strengths. Every hole scan was repeated four to five times to improve the signal-to-noise ratio. At the end of each series the voltage was reset to scan a control spectrum of the initial hole to account for spectral diffusion processes. For each wavelength two series with different polarization geometry were recorded by using a Glan-Taylor prism.

3.5.3 Pressure Tuning

Samples for the pressure tuning experiments were welded into small transparent plastic bags to ensure an isotropic spread of pressure inside the sample cell. Gaseous helium from a pressure cylinder was used to apply the pressure to the cell. A pressure sensor (Sensotec TJE/713-25) controlled the pressure with an accuracy of $10^{-3}\,\mathrm{MPa}$ up to 25 bar, the pressure at which liquid helium solidifies at 2 K. Similar to the Stark experiments an initial hole at ambient pressure was burnt and subsequently scanned multiple times while increasing the external pressure. Releasing the pressure at the end of the experiment allowed for a controlling scan of the hole.

3.6 Data Evaluation

3.6.1 Satellite Hole Burning

After subtracting the unburnt absorption spectrum from the burnt spectrum the dips in the background free spectrum were evaluated with respect to their spectral distance to the laser frequency. This was done for several burning frequencies all over the inhomogeneous absorption band. The assignment of vibrational modes for thionin in a glycerol/water glass was done by Weng *et al.* [99].

3.6.2 Stark Effect

The averaged spectra were fed to an evaluation routine written in Fortran 90 by J. Gafert based upon the formulae for Stark broadened and splitted hole

shapes from Schätz and Maier [77]. The core fitting routine was taken from the IMSL library [100]. Fitting parameters were the splitting and the broadening of the hole with increasing external electrostatic field as well as the angle between the transition dipole moment and the fixed dipole moment difference, while the initial parameters like hole width, hole depth and baseline slope were determined by a simple Lorentzian fit. The control spectra at the end of a Stark series were fitted to a Lorentzian as well and a linear evolution of hole width and depth due to spectral diffusion over the course of the experiment was assumed. Any parameters obtained with this method are still weighted with the Lorentz factor, which was evaluated by comparison with quantumchemical calculations.

3.6.3 Pressure Tuning

To estimate the compressibility the pressure shifts of the hole centers with increasing pressure were measured and plotted versus the hole burning frequency. The slope of the linear regression yielded the local compressibility κ, whereas the intersection of the regression function with the frequency axis yielded the vacuum frequency ν_{vac}. Pressure broadening effects were not taken into consideration in this work. Hole shapes were fitted to a Voigtian by Fourier transformation of the data.

When we try to pick out anything by itself, we find it is tied to everything else in the universe.

John Muir

Chapter 4

Thionin – A Model Chromophore

Together with its methylated relative methlene blue thionin[1] is the simplest derivative of the cationic phenothiazine family. Phenothiazinic compounds have widespread uses in agriculture, pharmacology, biology, phytochemistry and medicine [101]. While often used for staining of biological tissues derivatives with aliphatic sidechains have become especially interesting for biomedical applications because of their antibacterial, antiviral and antitumor properties [102–105]. To understand this behavior in detail and be able to synthesize special new derivatives for selective medical or pharmacological purposes the most essential point of interest is the mapping of intermolecular interactions between the compound and its target. Investigating the basic principles of the electrostatic contributions is the main focus of the next four chapters where thionin is regarded as a model system.

4.1 Thionin Tautomers

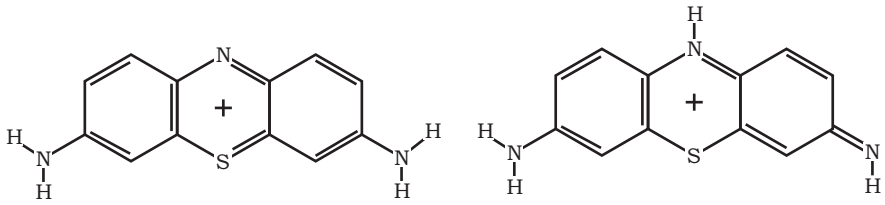

Figure 4.1: *The two tautomeric forms of thionin as proposed by Marek et al. [106]. The left form is referred to as amino form, the right as imino form.*

Thionin by itself is already an interesting molecule. Marek *et al.* [106] found by quantumchemical calculations that in an aqueous environment two tautomers should be viable (*cf.* Fig. 4.1). The amino form is a symmetric one where a proton is bound to the nitrogen atom of one of the outer aromatic rings. The imino form, however, is asymmetric with respect to the π-electron system because the proton is bound to the nitrogen of the central aromatic ring rather than to

[1] Although cationic dyes such as thionin are often spelled with the suffix "-ine" rather than "-in" naming conventions in this work will refer to the international colour index where thionin is listed under the CI serial number 52000 with the suffix "-in".

one of the outer rings. At sufficiently low temperatures the equilibrium of these tautomers can be trapped and spectrally resolved. Several high resolution hole burning techniques can help to elucidate and confirm the existence of the proposed tautomeric forms.

4.1.1 Absorption Spectra

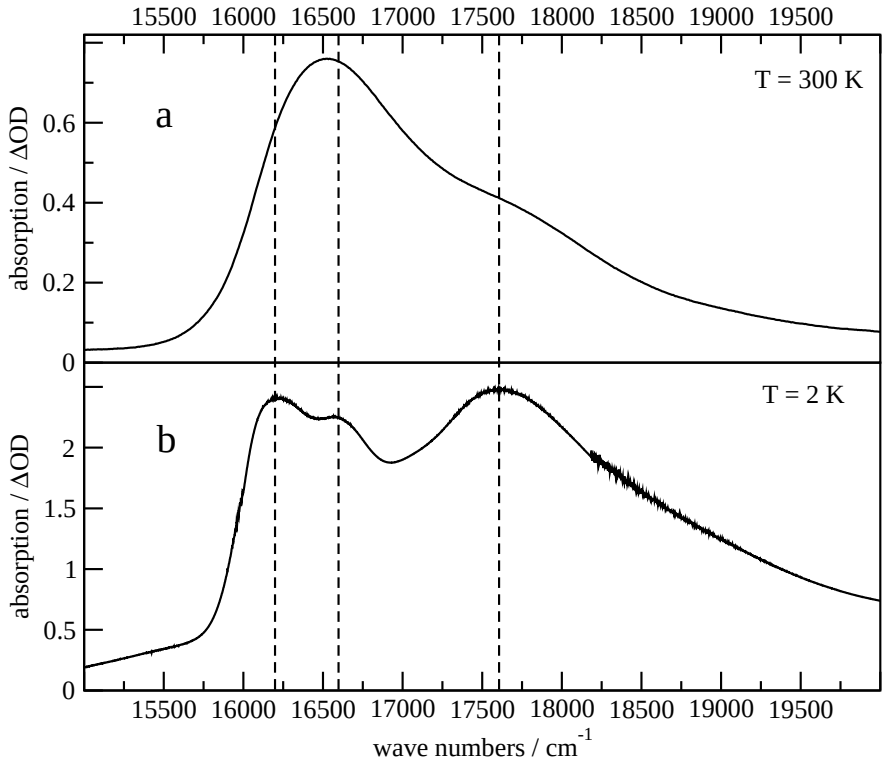

Figure 4.2: *Absorption spectra of thionin in glycerol/water at room temperature (a) and 2 K (b). The dotted lines indicate the absorption maxima of the main bands in the low temperature spectrum.*

Fig. 4.2 shows the absorption spectra of thionin dissolved in a glycerol/water mixture. The room temperature spectrum displays a broad inhomogeneous band at 16500 cm^{-1} (605 nm) with a broad shoulder to the blue side at around 17700 cm^{-1} (565 nm). There is no indication of distinct tautomers to be recognized. However, by lowering the temperature to 2 K the glycerol/water freezes to a glassy state and the features of the inhomogeneous absorption band sharpen. The main band splits into two clearly distinguishable bands at around 16200 cm^{-1} (617 nm) and 16600 cm^{-1} (602 nm). On the other hand, the shoulder to the blue gains significantly in intensity. Experiments with various concentrations of thionin show that the appearance of this band heavily depends on the amount of thionin in the sample and can therefore be attributed to oligomers of thionin. The overall chromophore concentration thus has to be kept low in order to rule out overlapping of the oligomer band with the monomer bands.

Fitting the absorption spectrum to Gaussians is only possible with a minimum of four bands as shown in Fig. 4.3. The two redmost bands at wave numbers of

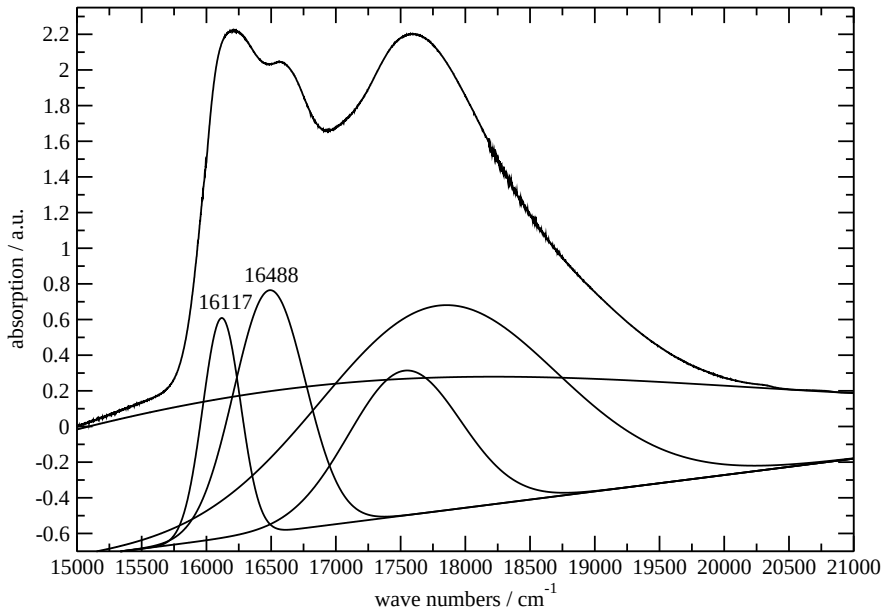

Figure 4.3: *Absorption spectrum of thionin at 2 K fitted with four Gaussians. The baseline has been fitted by a Gaussian and a constant slope. The numbers above the redmost bands indicate the wave numbers of the centers of the Gaussians.*

16117 cm^{-1} and 16388 cm^{-1} both have a relatively small width indicating the existence of two independent electronic origins connected to the two tautomers. The broad band at around 17600 cm^{-1} is most likely made up of a multitude of overlapping Gaussians belonging to the various oligomeric states of thionin. Those oligomers will not be regarded in the following discussion since high resolution hole burning is not possible in this spectral region. The majority of molecules contributing to the absorption spectrum in the region between 16000 and 16500 cm^{-1} can be ascribed to the tautomer bands. The hole burning experiments in this work solely focus on this region where sharp and sufficiently deep spectral holes can be produced.

4.1.2 Satellite Hole Burning

The group of Prof. Ta-Chau Chang of the Academica Sinica in the Republic of China has been able to perform a series of satellite hole burning experiments with various dyes over the last few years [67, 107–112]. Combined with normal mode calculations using Gaussian 92/DFT [113] at the HF/3-21G level to map the electronic ground state of the dye molecules their satellite hole burning studies showed two distinct sets of satellite holes for thionin in a glycerol/water glass [99].

Fig. 4.4 shows an example for a satellite hole burning experiment. After recording a reference spectrum of thionin a resonant hole was burnt at a burn frequency of 16592 cm^{-1}. The difference spectrum of the pre- and the post-burn spectra shows a sharp resonant hole at the burning frequency accompanied by a Franck-Condon shaped pseudo-phonon side band to the red made up by molecules that were excited accompanied by a creation of a phonon. The direct phonon side band is in this case not distinguishable from the large broad band of the photoproduct

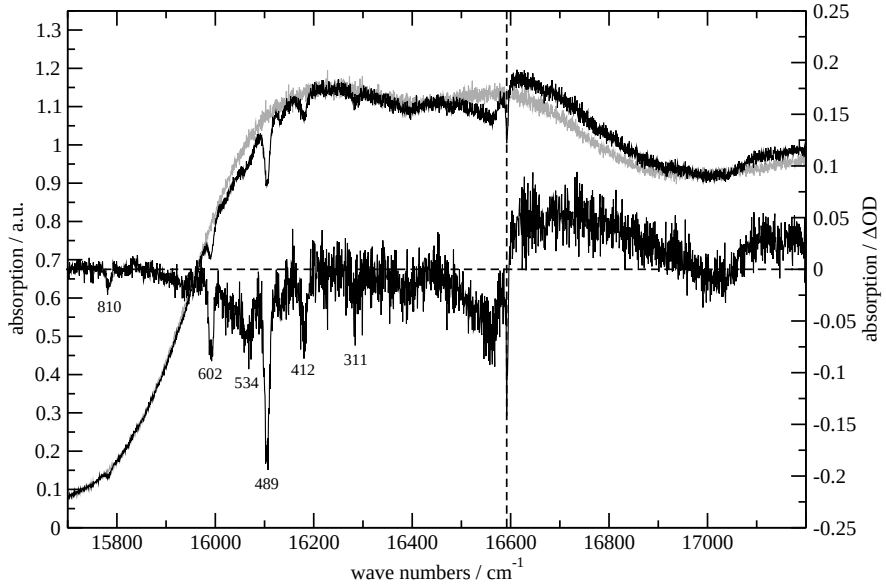

Figure 4.4: *Satellite hole burning spectra for thionin in a glycerol/water glass at 2 K. The hole was burnt at 16592 cm^{-1} (vertical dotted line). The graphs at the top are the pre-burn (light grey) and post-burn (black) spectra, the graph in the middle shows the difference spectrum. The horizontal dotted line indicates an absorption difference of zero. To the red side of the burn frequency several prominent non-resonant satellite holes are labeled with their wave number difference to the resonant hole.*

that appears as a positive absorption difference at the blue side of the resonant hole. However, the most interesting features are the red shifted non-resonant satellite holes. When burning a hole in the 16388 cm^{-1} band the satellite holes appear in the 16117 cm^{-1} band. Weng *et al.* [99] repeated those experiments for larger burn frequencies, thus shifting the appearance of those satellite holes to the 16388 cm^{-1} band. By doing that, they were able to observe small frequency changes in certain satellite holes, for example the 489 cm^{-1} hole shifted to 478 cm^{-1} and the 810 cm^{-1} hole to 798 cm^{-1}. By subsequently tracing the burning frequency over the whole absorption band of thionin they could assign two different sets of satellite holes to the main tautomer bands. The normal mode calculations showed that the two afore mentioned main vibrational modes at 489 cm^{-1} and 810 cm^{-1} are responsible for the inner ring motions of thionin. Other modes that differ in the two sets can be explained by overtones and summed up modes.

By comparison to experiments in PVB (polyvinylbutyral) films where only one set of vibrational modes appears, Weng *et al.* were able to assign the bands to the different tautomeric structures. The imino form has a much higher dipole moment than the amino form due to the larger π-electron system that is extended to the double bonded nitrogen atom in one of the outer rings. The stability of such a molecule critically depends on the ability to form hydrogen bonds to solvent molecules. In a glycerol/water matrix the formation of hydrogen bonds is fairly easy whereas in a PVB film there are no free protons accessible. The set of vibrational modes present in the PVB film displayed the same features as the set found for the 16388 cm^{-1} band of thionin in glycerol/water, so it is

straight forward to assume that the amino form – the only stable tautomer in PVB films – corresponds to the 16388 cm^{-1} band while the imino form as the less stable one can only exist in glycerol/water and appears as the 16117 cm^{-1} in the absorption spectrum. This is in line with the calculations of Marek *et al.* [106] who predicted the thermodynamical equilibrium of the tautomers to be shifted to that of higher symmetry. The bonding energy of a hydrogen to a nitrogen in the outer amino group is by about 10% higher than the one to the nitrogen inside the central moiety. The area beneath the Gaussian fits for the two tautomers is about 15% larger for the band at 16388 cm^{-1} supporting the assignment of the higher wave number band to the symmetric amino form.

By applying persistent spectral hole burning techniques this assumption can be substantiated. Furthermore they allow for the allocation of base parameters such as the isothermic compressibility, the quasi-homogeneous linewidth and the fixed dipole moment difference which will serve as benchmarks when evaluating the differences in those parameters upon interaction with various systems of biomolecular interest.

4.2 Homogeneous Linewidths

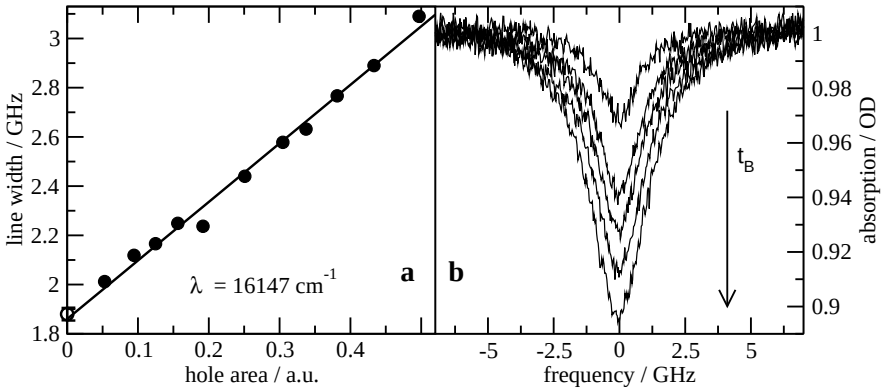

Figure 4.5: *Determination of the quasi-homogeneous linewidth of thionin in a glycerol/water matrix. (a) After an initial hole was burnt at 16147 cm^{-1} and scanned, additional exposure to laser light at the same spectral position led to further deepening and broadening of the hole. The hole area is plotted against the hole width. The linear extrapolation to zero area yields the quasi-homogeneous linewidth. (b) Some example holes at that burning frequency. The hole deepens and widens as the accumulative burning time increases.*

Fig. 4.5 shows an example of a hole burning experiment to determine the quasi-homogeneous linewidth of thionin. For every hole the burning power was kept as low as possible to avoid artificial hole broadening. Fig. 4.5(a) indicates that the laser intensity was low enough to allow for linear regression with a small error in the y-axis intercept.

By repeating this measuring procedure the burning frequency dependency of the quasi-homogeneous linewidth Γ_{hom} can be determined. The results are displayed

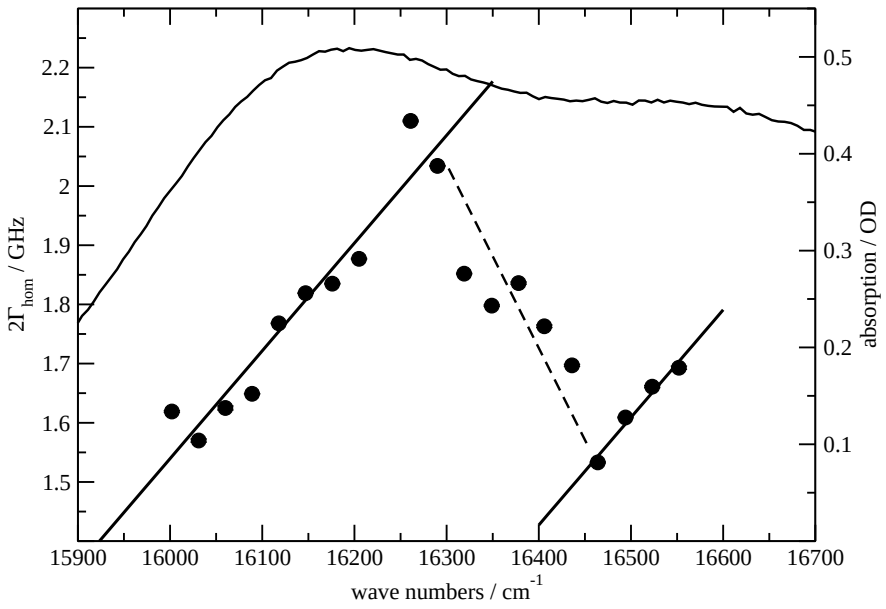

Figure 4.6: *Dependence of the quasi-homogeneous linewidth* Γ_{hom} *on the burning frequency. The errors of the data points are below the resolution limit. The lines drawn are a guide to the eye rather than actual linear fits. The background shows the respective part of the absorption spectrum of thionin in a glycerol/water matrix at 2 K.*

in Fig. 4.6 together with the absorption spectrum of thionin. The values shown are still the doubled linewidths $2\Gamma_{\mathrm{hom}}$ as they are directly taken from the experiment. Starting with a $2\Gamma_{\mathrm{hom}}$ of around 1.6 GHz the linewidth increases rapidly when scanning over the imino band to the blue. Upon reaching the intermediate spectral range where both the imino and the amino absorption overlap, the linewidth drops again until it reaches about 1.6 GHz whereupon it starts to rise again as the laser is tuned into the amino band. First of all it is worth noting that at each burning frequency in this area similarly narrow holes with a few GHz width could be burnt. This is a clear sign that both bands originate from separate electronic transitions. Holes burnt in vibrational bands are by orders of magnitude broader due to their drastically shortened lifetime. Secondly, the transition from the imino to the amino band is rather smooth. The spectral range between the two bands is a region of coexistence where each tautomer equally contributes to the formation of the subensemble making up the hole. And lastly, the rate at which Γ_{hom} is increasing with the burning frequency is roughly the same for both absorption bands. This supports the idea of tautomeric bands because Γ_{hom} should mainly depend on the coupling to the solvent and the relaxation rate of the excited electronic state. The geometry of the molecule should not play a significant role at all which leads to a similar behavior for both tautomers.

4.3 Stark Spectroscopy

The dipole moment differences $f \cdot \Delta\vec{\mu}_{\mathrm{mol}}$ and $f \cdot \Delta\vec{\mu}_{\mathrm{ind}}$ were determined by measuring the Stark effect. In Fig. 4.7 an example for a Stark experiment is given. At a fixed external electric field strength and a certain polarization geometry

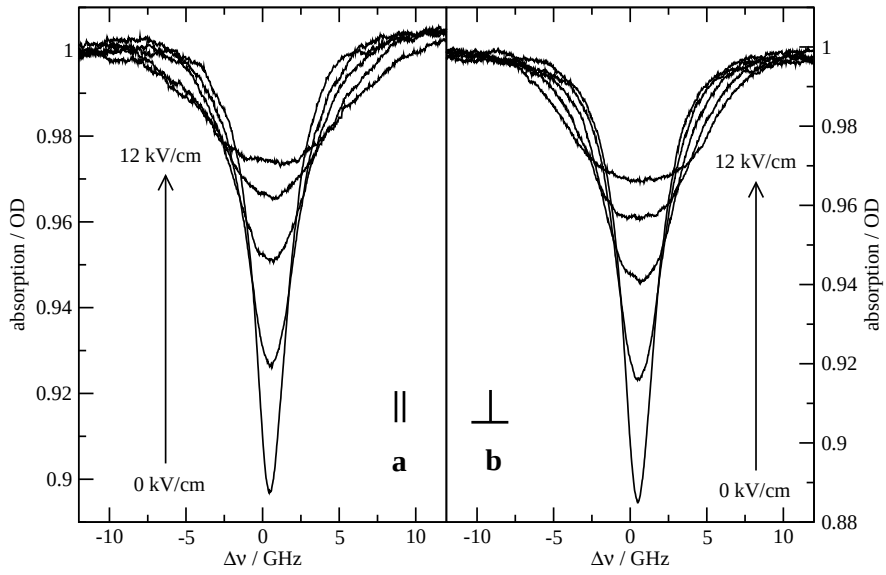

Figure 4.7: *Stark effect of thionin in a glycerol/water glass at 2 K. After burning an initial hole the external electric field was increased in steps and the changes recorded. The experiment was conducted at a burn frequency of 16181 cm^{-1} for two polarization geometries – in (a) the incident laser light was polarized parallel to the external electric field, in (b) perpendicular.*

a hole was burnt at 16181 cm^{-1}. While the electric field strength was increased in steps, the broadened hole was scanned repeatedly. The first thing to note is that both series of spectra look very similar – in neither of the holes scanned a large splitting is prominent, which has two reasons. The induced dipole moment difference is rather large for thionin, so the splitting is covered by the fast broadening. Furthermore, the angle θ between $\Delta\vec{\mu}_{\mathrm{mol}}$ and the transition dipole moment $\vec{\mu}_{\mathrm{fi}}$ is around 60°, so that the holes in the perpendicular polarization geometry split only slightly. Those circumstances increase the difficulty of obtaining good quality fits and accordingly reliable values for the dipole moment differences. While for lower field strength both polarization geometries are nearly indistinguishable, the splitting of holes becomes only discernible from the broadening if the holes are subject to a very high field strength, where the hole already covers the full spectral range accessible by finetuning the laser and the depth of the hole becomes to low to account for a good signal-to-noise ratio. Because of the enhanced interest in molecular properties rather than the interaction of the chromophore with the solvent, the focus in this work is on the fixed dipole moment differences.

The fitting results for the Stark effect spectra are shown in Fig. 4.8. The broadening σ and the splitting Δ are plotted *vs.* the strength of the external electric field E_0. Simultaneously to the best fitting hole parameters, the angle θ is allowed to run freely. Fig. 4.8(b) lets one main difficulty become obvious: θ is hard to determine for small values of E_0 because the splitting is small. Both polarization geometries tend to look similar, so the fitting routine often "decides" to favor an extreme value of 0° or 90° over the real values. In the example, after presetting the angle to an estimated 60° θ immediately is fitted to 90°. Concomitantly, the

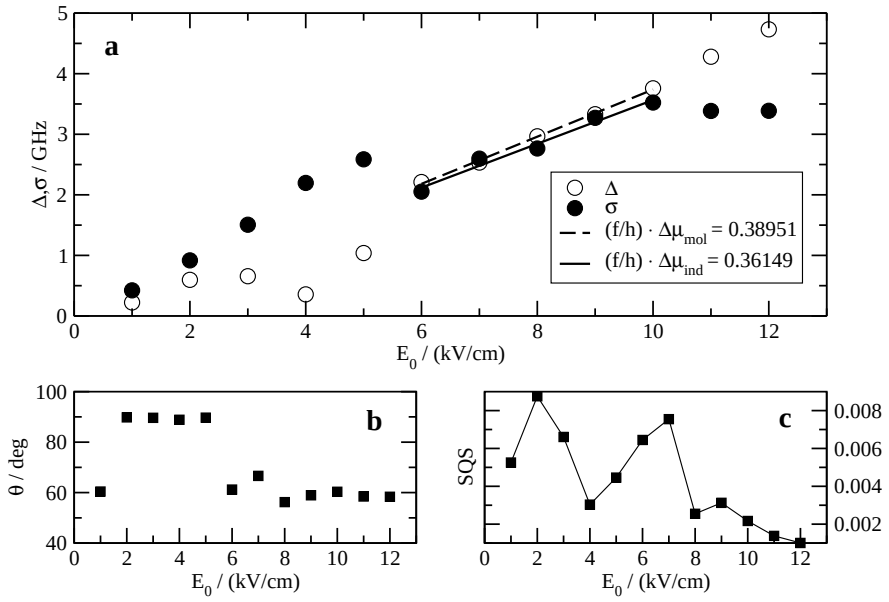

Figure 4.8: *Fit results of the Stark effect experiments in Fig. 4.7. (a) shows the broadening σ and splitting Δ in GHz. The slopes of the linear regressions yield the modified dipole moment differences $f \cdot \Delta\vec{\mu}_{\mathrm{mol}}$ and $f \cdot \Delta\vec{\mu}_{\mathrm{ind}}$. The best fitting angle θ for each external field strength is depicted in (b), the mean square error, a measure for the quality of the fit in arbitrary units, in (c).*

actual splitting is underestimated with rising external field strength allowing the broadening to be fitted to a larger value. Only at a field strength of about 6 kV/cm the disparities in the spectra become to large for the routine to be fitted with a θ of 90°, thus the angle jumps back to a more reasonable value of 60° degrees. At that point Δ and σ are returning to their actual values, which is why in the linear regression to obtain $f \cdot \Delta\vec{\mu}_{\mathrm{mol}}$ and $f \cdot \Delta\vec{\mu}_{\mathrm{ind}}$ only the values above 5 kV/cm are taken into consideration. A good parameter to check the validity of the linear regression is the y-axis intercept – at zero field strength neither broadening nor splitting should occur, so the intercepts for both regressions should be zero. The fits in the example meet this requirement rather well, rendering them trustworthy enough to reflect the actual dipole moment differences.

4.4 Pressure Tuning

Fig. 4.9(a) shows the behavior of a hole burnt in thionin under increasing isotropic pressure. Two notable changes can be observed: First of all the width of the hole increases in the same degree as the depth decreases so that the area of the hole remains the same. This indicates that the repeated scanning after each pressure change does not cause more molecules to be photochemically burnt, thus leaving the number of molecules contributing to the hole unvaried. In Fig. 4.9(b) the contrarious trend of the width and the depth is depicted. Secondly, the center of the hole shifts to the red with increasing pressure in a linear fashion (*cf.* Fig. 4.9(c)). The focus of this work rests on the evaluation of the parameters associated with this linear shift, namely the isothermic compressibility κ and the vacuum frequency ν_{vac}, which can be determined by plotting the constant hole

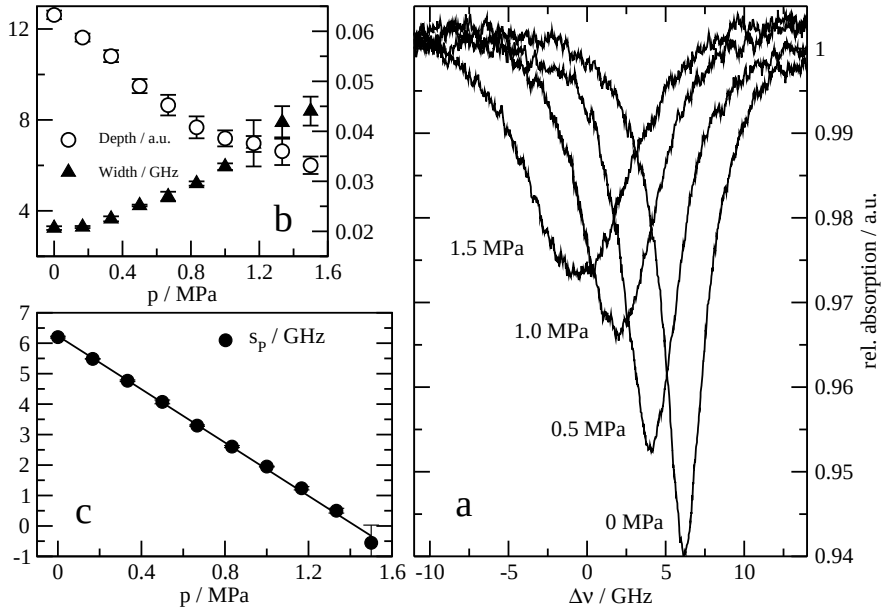

Figure 4.9: *A hole in thionin under pressure: (a) shows the changes in hole shape upon exerting increasing pressure on a spectral hole in thionin in a glycerol/water glass at $T = 2\,K$. (b) depicts the decreasing hole depth and the concomitant increase in hole width with increasing pressure. (c) shows the spectral position of the hole center relative to the initial position right after burning. A linear fit yields the pressure shift $s_\mathrm{P}/\Delta p$.*

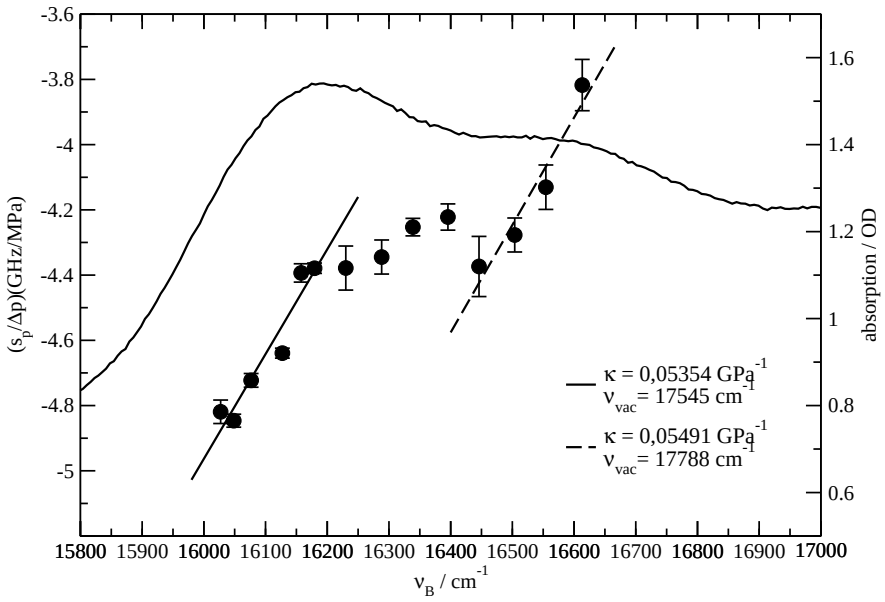

Figure 4.10: *Shift of the hole center s_P per unit of pressure Δp for Thionin in a glycerol/water glass at $T = 2\,K$. In the background the low temperature absorption spectrum is underlain. The "s"-shaped distribution of data points along the burning wavenumber ν_B allows the distinction of two subregions corresponding to the absorption bands. The gradient of the linear fit for both subregions indicates the isothermic compressibility κ, the intersection with the spectral axis the vacuum wavenumber ν_vac.*

shift per unit of pressure $s_P/\Delta p$ against the excitation energy.

The experiments were repeated for various wavelengths along the two redmost absorption bands of thionin. Fig. 4.10 shows the dependency of $s_P/\Delta p$ on the burning wave number ν_B. When comparing the course of the values of $s_P/\Delta p$ with the absorption bands, one can find a linear increase across the redmost band followed by a region of constant $s_P/\Delta p$ that passes into another linear ascend that coincides with the appearance of the next absorption band further to the blue. The gradient of linear regressions fitted to both of the regions of ascending $s_P/\Delta p$ is approximately the same for both absorption bands and leads to values of the isothermic compressibility κ of about $0{,}54\,\mathrm{GPa}^{-1}$. Considering the two proposed geometries of the thionin tautomers by Marek *et al.* [106], it seems rather straightforward to associate the two bands with the origins of the first electronic transitions for the tautomers. Similar to the homogeneous linewidth experiments this result can be seen as an affirmation of the existence of tautomers in low temperature regimes. The equality of κ for both tautomers is reasonable seeing that κ only depends on the surrounding solvent. Both tautomers have the same charge and take up the same space – so the solvent is expected to arrange in roughly the same fashion around both tautomers. The quantitative value of κ is consistent with that of other molecules in a glycerol/water glass [38]. By extrapolating the linear regression to a hole shift of zero the vacuum frequencies ν_{vac} were determined to $17550\,\mathrm{cm}^{-1}$ and $17790\,\mathrm{cm}^{-1}$, respectively. For glassy systems those values reveal rather large solvent shifts of about $1400\,\mathrm{cm}^{-1}$. The experiments could unfortunately not be expanded to higher wave numbers. As seen at the increasing error bars of $s_P/\Delta p$ the hole quality decreases dramatically beyond $16600\,\mathrm{cm}^{-1}$.

The important thing in science is not so much to obtain new facts as to discover new ways of thinking about them.

Sir William Bragg

Chapter 5

Color Effects in Homogeneous Linewidths

In biophysical applications of optical spectroscopy the chromophore plays the most important role. Consequently, over the last decades a lot of work has been put into the development of synthetical fluorescent probes to suit the needs of the investigated systems [114, 115]. Different design criteria have to be met to ensure maximum information gain with as little interference in naturally occurring processes as possible. The most prominent among those criteria are:

- *Intrusion:* To be effective in living systems chromophores will have to be introduced into cells without disrupting the cells' functionality. A proper carrier system to insert optical probes into cells must be in place.

- *Detectability:* Different methods of optical detection require dyes to have certain features like high fluorescence yield, longevity upon cycled excitation, high absorption coefficients or phosphorescence. In the case of persistent hole burning spectroscopy suitable chromophores must be photoreactive and provide a large Debye-Waller factor.

- *Specificity:* Probes should be able to specifically bind or attach to a known target within the assayed system. Often living systems provide a large variety of different components – the ability to pick out a single component on its own depends largely on the ability to specifically design a molecule to selectively bind to this component.

The main focus in this chapter lies on the specificity of dyes. The binding behavior relies mainly on the way the molecule interacts with its environment so the complete assessment of its electrostatic nature is a precondition to estimate the specificity.

Taking a look at two dyes with hole burning spectroscopy – BODIPY and thionin – reveals remarkable differences in their color effects of the homogeneous linewidth and the Stark spectra.

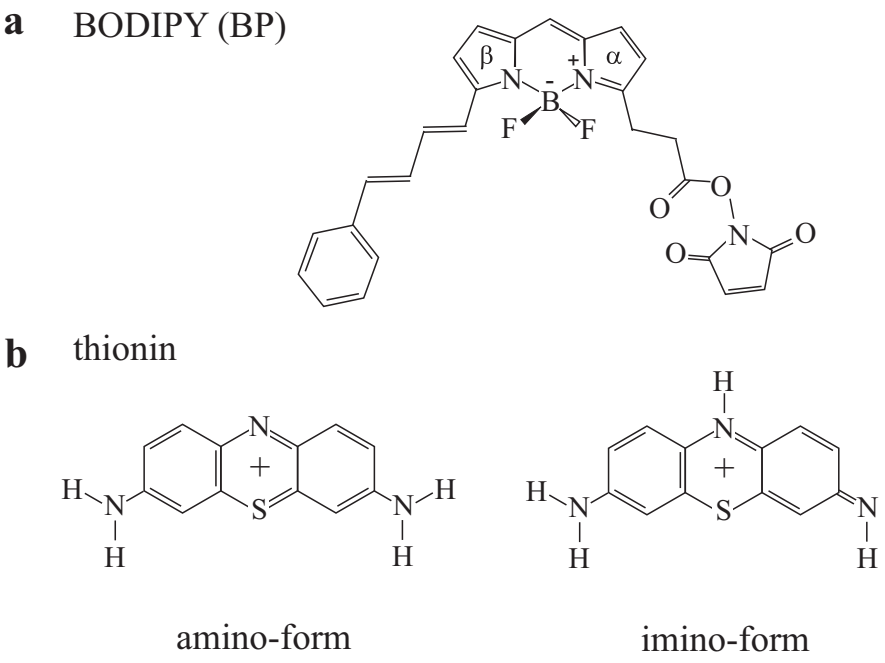

Figure 5.1: *(a) Chemical structure of the used BODIPY dye in contrast to (b) the tautomeric structures of thionin.*

5.1 The Dye BODIPY

BODIPY is a short form for 4,4-difluoro-4-bora-3*a*,4*a*-diaza-*s*-indacene dyes, developed and patented mainly by Molecular Probes, Eugene (Oregon). The defining core element of these dyes are three aromatic rings with a N_2BF_2 group in the middle ring. Various side groups can be attached to the outer rings, thus defining the spectroscopic properties of the dye [116]. Usually BODIPY dyes are used as reactive fluorescent labels because of their extraordinarily high extinction coefficient and their good photostability. BODIPY dyes can be covalently bound to any organic compound using carbon chains as linkers.

The specific BODIPY dye – 4,4-difluoro-5-(4-phenyl-1,3-butadienyl)-4- bora-3*a*,4*a*-diaza-*s*-indacene-3-propionic acid, succinimidyl ester – used in the work of M. Stübner [27] is shown in Fig. 5.1(a)[1]. This dye has been investigated in a series of experiments by the group of T.-C. Chang and, in joint projects, also by groups of the author's group [24, 111, 117], where the propionic end group has been attached via an amino linker to the phosphate groups of various oligonucleotides.

The absorption spectrum of BODIPY in a glycerol/water glass consists of four bands of which the redmost with its center at 16808 cm^{-1} is the most prominent. Its shape is nearly Gaussian with a width of about 350 cm^{-1}. A much less intense shoulder to the blue can be distinguished at 17100 cm^{-1}. Pressure tuning experiments revealed a bathochromic solvent shift in glycerol/water with a mag-

[1]The term BODIPY refers to this variant of the dye family from now on.

nitude of about 865 cm^{-1}. Two inhomogeneous absorption bands at 18015 cm^{-1} and 18352 cm^{-1} will not be taken into account in the following discussion.

5.2 Stark Spectroscopy Of BODIPY And Thionin

5.2.1 BODIPY

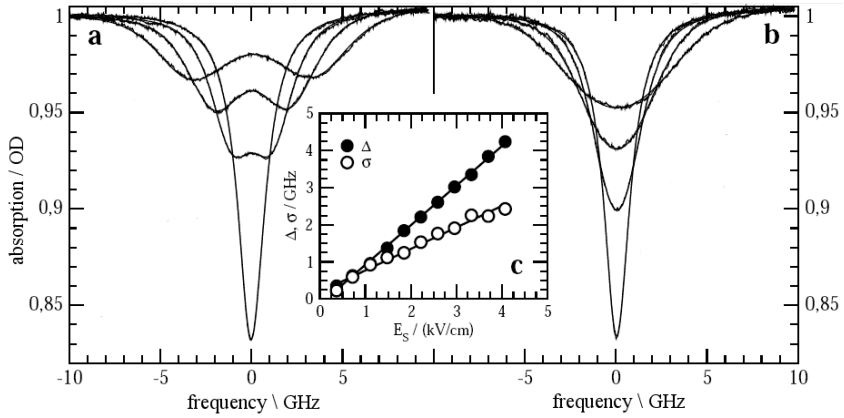

Figure 5.2: *A typical Stark experiment for BODIPY attached to a thymin decamer at a burn wave number of 16660 cm^{-1}: Subsequent hole scans upon increasing the external electric field strength from 0 kV/cm to 4 kV/cm for parallel alignment of the external electric field and the laser polarization (a) and perpendicular alignment (b). The inset shows the fits of the hole splitting Δ and the broadening σ with increasing field strength. The data is taken from the thesis of M. Stübner [27].*

Fig. 5.2 shows the results of a typical Stark experiment done for BODIPY covalently attached to a thymin decamer. The original hole was burnt at 16660 cm^{-1} in the far red edge of the inhomogeneous absorption band of BODIPY. Even for relatively low external electric fields there is a clear splitting visible when the exciting laser light is polarized parallel to the external field (*cf.* Fig. 5.2(a)). On the other hand for the perpendicular excitation geometry (*cf.* Fig. 5.2(b)) only a broadening of the hole can be measured. The magnitude of the splitting as well as of the broadening scale linearly with the field strength as can be seen from the inset in Fig. 5.2. From fitting the data according to the theory of Schätz and Maier [77] the angle between the transition dipole moment and the fixed dipole moment difference can be estimated to 30°.

A large hole splitting always indicates a large difference in the molecular dipole moments for the ground and the excited state. For BODIPY this is quite reasonable: The central aromatic ring that contains the N_2BF_2 moiety is very highly polarized due to the large electronegativity of the BF_2 group causing a strong dipole moment along the symmetry axis of the aromatic ring system. Generally

spoken a large dipole moment is usually subject to large changes upon electronic excitation of the π-electron system of the chromophore, so a large hole splitting can be expected.

5.2.2 Thionin

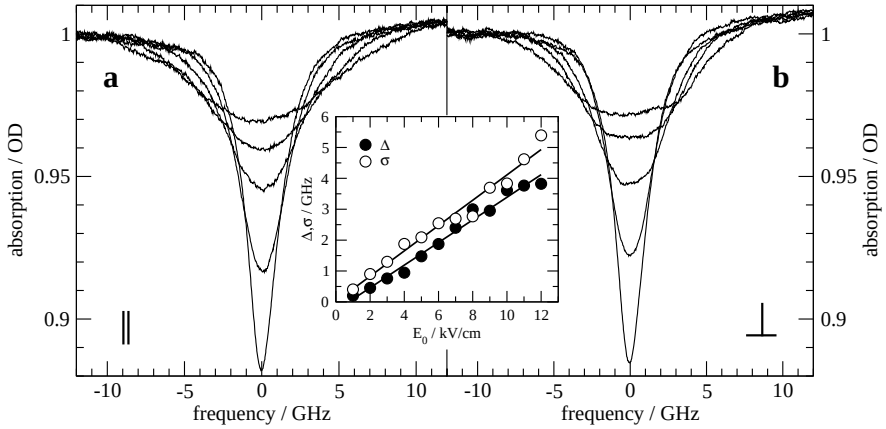

Figure 5.3: *A typical Stark experiment for thionin in a glycerol/water glass at a burn wave number of 16080 cm^{-1}: Subsequent hole scans upon increasing the external electric field strength from 0 kV/cm to 12 kV/cm for parallel alignment of the external electric field and the laser polarization (a) and perpendicular alignment (b). The inset shows the fits of the hole splitting Δ and the broadening σ with increasing field strength.*

As already mentioned in the previous chapter, the dipole moment differences in thionin are small compared to those in BODIPY. Moreover the exiguous hole splitting is mainly superimposed by the hole broadening so that it is very hard to actually determine the angle as well as the quantitude of the relevant parameters. Fig. 5.3 shows another typical Stark experiment in a similar fashion as Fig. 5.2. For thionin, however, in both excitation geometries the holes basically just broaden leaving nearly identical hole shapes in parallel (Fig. 5.3(a)) and perpendicular (Fig. 5.3(b)) geometry. On closer inspection the hole shape for the perpendicular geometry spectra tends to flatten out in the center which is a sign of an onsetting hole splitting. Only a careful fitting procedure can refine this splitting that is even smaller than the hole broadening, which can be seen from the inset in Fig. 5.3. The angle between the transition dipole moment and the fixed dipole moment difference can be estimated to around 55°.

Even more notable is the fact that for the Stark experiments with thionin the maximum external electric field strength was tripled in comparison to the BODIPY experiments. Although the initially burnt holes were similar in depth and width the dipole moment differences for BODIPY are much larger than the respective ones for thionin. This may indicate that thionin by itself has a significantly smaller molecular dipole moment than BODIPY.

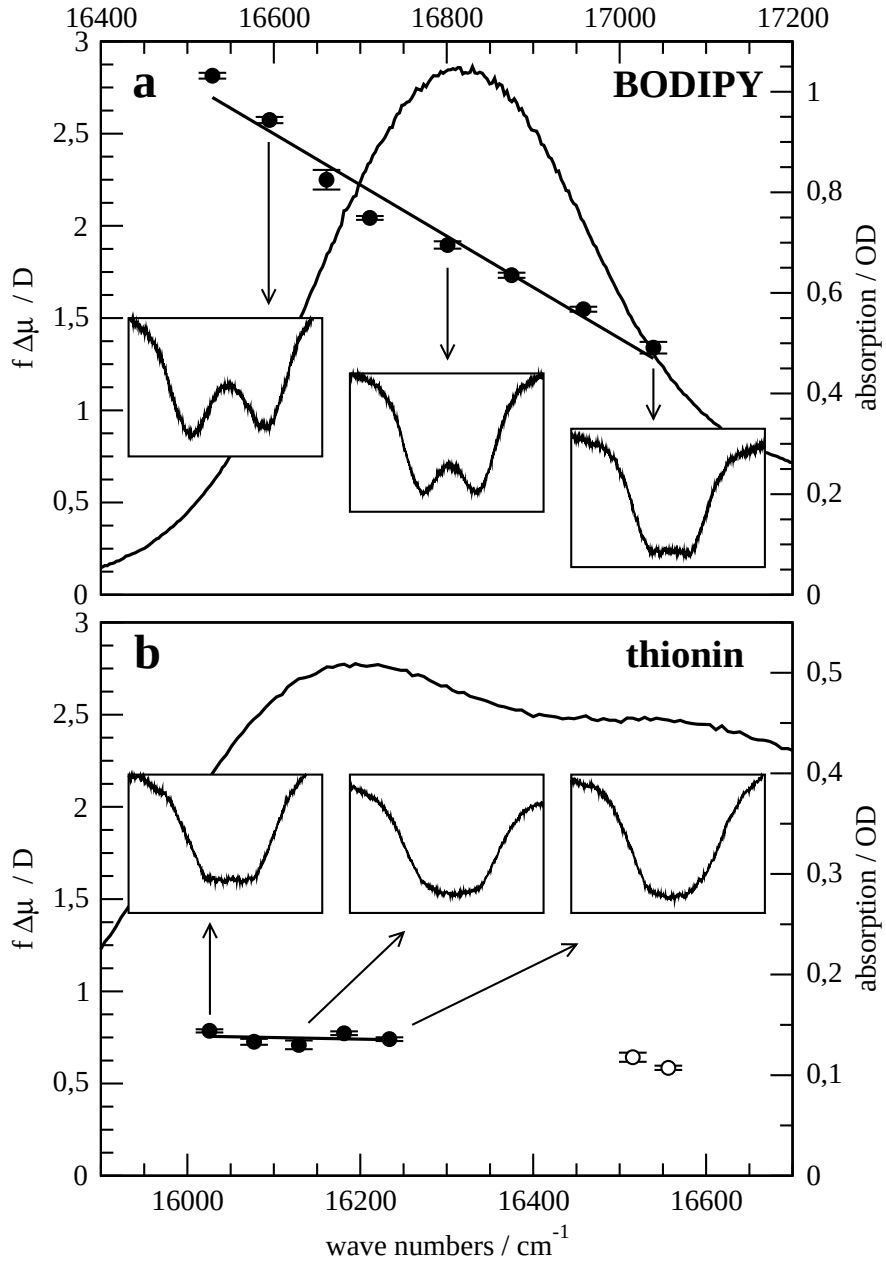

Figure 5.4: *The color effects of the hole splitting for BODIPY and thionin. (a) shows the decrease in hole splitting from the red edge of the BODIPY inhomogeneous absorption band to the blue edge. The overall values for the splitting are rather large. (b) shows the hole splitting for different wave numbers in thionin. Here the rather small values stay the same over the whole red edge of the inhomogeneous absorption band. Additionally, experimental values for the blue absorption band are indicated with open circles. The insets for both (a) and (b) show the hole spectra for the largest applied external electric field in each case, depending on the burning wave number. The absorption spectra are shown in the background.*

5.2.3 Color Effects in Stark Spectroscopy

Upon repeating the experiments over the spectral regions accessible to stable hole burning for both thionin and BODIPY there is also a clear difference regarding the color effects of the dipole moment differences. We focused on the

intrinsic dipole moment differences as for those the fitting procedure gives more reliable results.

In Fig. 5.4 the respective data for both dyes can be seen. Fig. 5.4(a) shows the fixed dipole moment difference Δ as a function of burning wave number for the BODIPY chromophore. The redmost inhomogeneous absorption band is plotted in the background. There is a strong decrease of Δ when going from the red edge of the absorption band to the blue. The initial large value of $\Delta = 3\,\mathrm{D}$ at $16500\,\mathrm{cm}^{-1}$ is approximately halved when burning holes at $17050\,\mathrm{cm}^{-1}$. The decrease is perfectly linear with the wave number. At crucial points the respective maximum field strength spectra for parallel polarization geometry are shown in the inset to illustrate the decrease in hole splitting.

Fig. 5.4(b) represents the findings for the thionin experiments. The spectral range for the experiments does not cover the whole absorption band since in the intermediate region between the two tautomeric forms the hole quality was not sufficiently good to extract the already poor splitting with satisfactory accuracy. However, the trend is quite clear: The overall low dipole moment differences do not change at all when going from the red edge to the blue edge of the imino absorption band. The two open circles represent measurements done for the amino absorption band where the magnitude of hole splitting is analog to the one in the imino band. Again, the insets serve as guide for the eye to indicate the just slightly flattened hole centers for the spectra taken at maximum external electric field strength.

5.3 Color Effects in Homogeneous Linewidths

5.3.1 Homogeneous Linewidth Experiments

Fig. 5.5 shows two series of sequential hole burning at the same spectral position for both BODIPY and thionin. Depending on the efficiency of the phototransformation at various burning wave numbers the initial time for hole burning varied between 10 and 30 seconds at very low burning powers in the order of a few tens of $\mu\mathrm{W/mm}^2$. After scanning the hole was deepened and widened by adding some further burning time in increasing steps. For both BODIPY as well as thionin the holes retained to a very good approximation a Lorentzian shape indicating that neither power nor energy correlated artificial broadening played a major role. In Fig. 5.5(b) and (d) the scans for different burning times can be seen.

The hole spectra were then fitted to Lorentzians. According to Breinl *et al.* [62] the hole width should increase linearly with the number of burnt molecules, thus with the hole area. Fig. 5.5(a) and (c) show the regression done for the hole widths of BODIPY and thionin respectively – the agreement of the data with the linear fits is very good. For each burning wave number the intercept of the linear fit with the y-axis was determined. This value is twice the quasi-homogeneous linewidth.

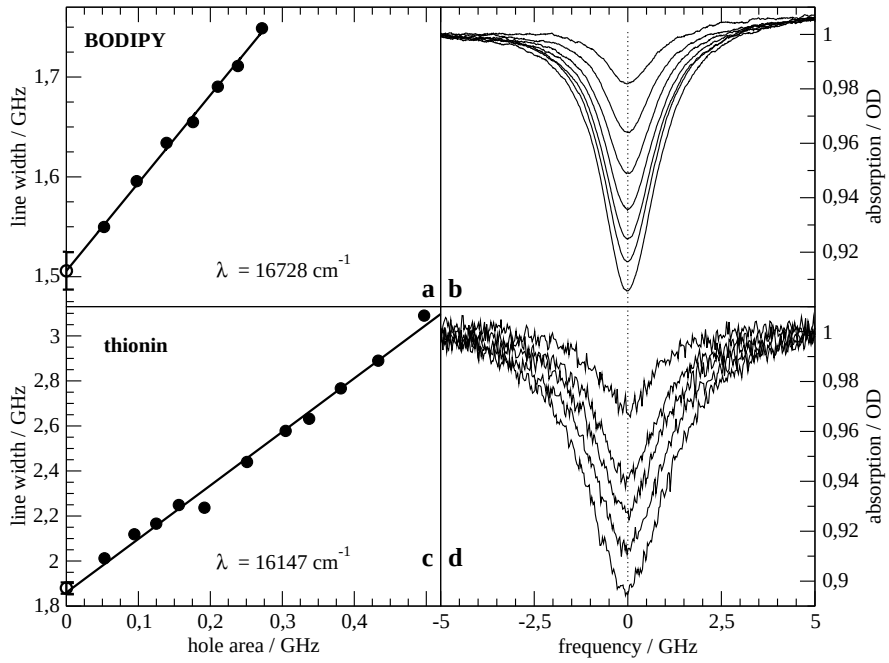

Figure 5.5: *Examples of hole burning series for BODIPY (a,b) and thionin (c,d) at the given burn wave numbers: (b) and (d) show the increase of hole width and depth at the same spot of the sample with increasing exposure time to the burning laser light. The power was kept sufficiently low to prevent artificial power broadening. Burning times ranged from 10 seconds up to 15 minutes. (a) and (c) show the dependency of the hole width on the hole area. The hole spectra were fitted to Lorentzian lines. Extrapolation to a hole area of zero yields twice the quasi-homogeneous linewidth* $2\Gamma_{\mathrm{hom}}$.

In Fig. 5.6 those values have been gathered and plotted for the particular burning wave number. There are remarkable patterns to be observed: For BODIPY the trend is very unambiguous – the linewidth decreases proportional to the wave numbers from about 1.8 GHz in the far red edge of the inhomogeneous absorption band to 1.1 GHz in the far blue. While the values themselves are rather small the relative narrowing of the homogeneous linewidth amounts to 40%. The pattern of the data points for thionin is more complicated, but can be understood when considering the existence of two independent absorption bands due to the two independent tautomers. First of all, the data is more scattered for thionin than it is for BODIPY. This can be ascribed to the fact that hole burning in BODIPY in general is easier than in thionin. Comparison of Fig. 5.5(b) and (d) reveals a much worse signal-to-noise ratio in thionin, mostly because of the poorer glass forming qualities. However, the z-shaped pattern can be broken into three parts. Starting from the most bathochromically shifted region up to around 16250 cm^{-1} the linewidth increases constantly. Between 16250 and 16400 cm^{-1} the linewidth drops again until from 16400 cm^{-1} it starts to rise again. The linear fits depicted in Fig. 5.6(b) have roughly the same slope as could be expected from tautomeric molecules.

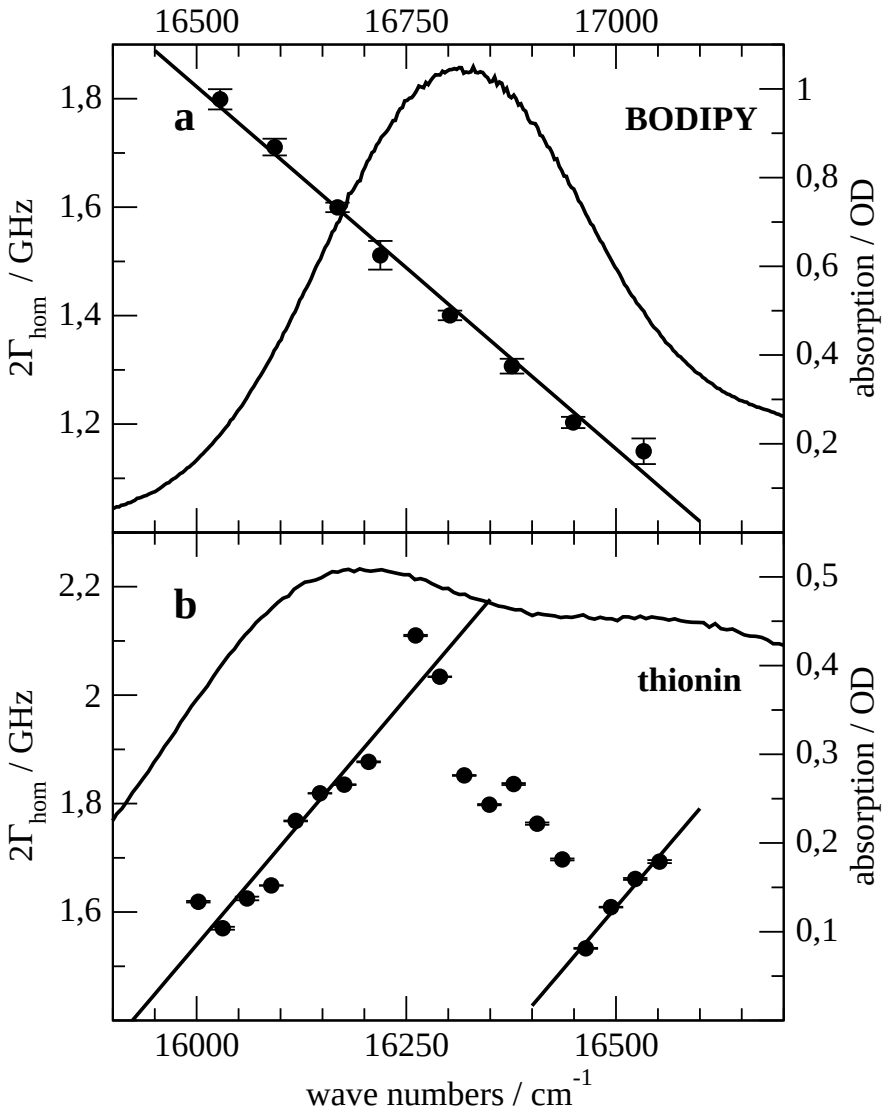

Figure 5.6: *The color effects for the homogeneous linewidth measurements found with BODIPY (a) and thionin (b). For BODIPY (a) the linewidth decreases in a linear fashion from the red to the blue edge. For the two thionin tautomers (b) each band displays a linear increase in the linewidth as the burn frequency is tuned from the red to the blue edge with a decrease between the bands. Each plot shows the relevant absorption spectrum in the background.*

5.3.2 A Spectral Diffusion Model

A first, albeit quite obvious remark concerns the fact that there are color effects in the quasi-homogeneous linewidth at all. An inhomogeneous absorption band is made up of a single electronic transition to the first electronically excited state. Color effects necessarily have to stem from the interaction of the chromophores with their environments since the electronic transition does not change its relaxation properties along the course of the absorption band when observed on its own.

There are very few reports on color effects in quasi-homogeneous linewidths in literature. Avouris *et al.* [118] found a linear color effect in the linewidth of rare earth ions embedded in an amorphous silicate matrix. Avouris and Morgan [119] investigated manganese ions in the same matrices coming to the same conclusion of phonon-assisted energy transfers. Those experiments found a uniform broadening in linewidth when going from the red to the blue. Accordingly, the effects were explained in terms of a change in electron-phonon coupling along the inhomogeneously broadened absorption band [120].

For the experimental findings at hand a completely new approach must be considered [121]. A site-correlated electron-phonon coupling strength, as proposed by Avouris [118, 119], relies on the phonon properties in the amorphous matrix to change. BODIPY and thionin are both subject to a fairly large bathochromic solvent shift, so the stronger coupling between chromophore and solvent will be found at the red edge of the absorption band for both dyes. However, since the solvent of glycerol/water is the same for the BODIPY as well as the thionin sample, a phonon related color effect should yield the same trend regardless of the probe used. The antithetic behavior of two dyes in the same matrix demands dye related changes along the absorption bands to be the main cause for the color effect in the probe-solvent coupling.

The second large cause for line broadening in amorphous systems is the phenomenon of spectral diffusion [122–125]. Glasses display a non-ergodic behavior on every time scale because of the lack of long range order[126]. As temperature decreases equilibration processes were shown to cover time scales of up to weeks [125]. Naturally those diffusive processes only cause small changes in the structural short range order, hence only small changes in the probe-solvent coupling strength, but with a sufficiently high resolution technique such as persistent spectral hole burning those changes can be mapped in the hole broadening. In experiments where a hole burning series can take up to tens of minutes to be completed, broadening by spectral diffusion processes has to be expected. A first and hitherto generally accepted simplified approach to represent spectral diffusion dynamics is the introduction of so called *two-level systems* (TLS) [127, 128]. The structural dynamics of an amorphous system is broken up in an ensemble of pairwise independent subsystems which are modeled in a way that each of the subsystems can only exist in one of two possible states. Analytically the best approximation for such a TLS is a double well potential and at sufficiently low temperatures the transition between one and the other state is made by tunneling. The amorphous system will be perceived as being caught in a random state consisting of a set of microscopical substates and every flip of a TLS is regarded as a relaxation process towards equilibrium. The time dependence of this relaxation behavior can be modeled as logarithmic allowing for the asymptotical relaxation towards thermal equilibrium.

Again, there are several possibilities to account for a site dependent color effect in hole broadening with the application of TLS theory. Reasons that only depend on changes in the solvent such as the density of TLS [129, 130] in the vicinity of the chromophore can be disregarded because for the same solvent the same

gradient for the homogeneous linewidth should be found regardless of the probe used. Any cause for opposite color effects to occur must be sought in the way the specific probe interacts with the TLS.

5.3.3 Differential and Total Color Effect

To be able to bring the different color effects in a quantitative context, one can define new parameters [121]. For any given quantity q that provides a color effect along the inhomogeneous absorption band with the wave number ν, a suitable definition for the total color effect C_t is

$$C_\mathrm{t} = \frac{\Delta q}{q_0} \tag{5.1}$$

and for the differential color effect C_d

$$C_\mathrm{d} = -\frac{1}{q_0}\frac{\partial q}{\partial \nu}. \tag{5.2}$$

Here, the parameter q_0 is the mean value of q found at the maximum of the absorption band, so that C_t is the average of C_d taken over the whole inhomogeneous absorption band from q_min to q_max:

$$C_\mathrm{t} = -\int_{q_\mathrm{min}}^{q_\mathrm{max}} C_\mathrm{d}\, d\nu \tag{5.3}$$

For the linewidth experiments, q will be assigned to the quasi-homogeneous linewidth and q_0 to its respective mean value at the center of the absorption band.

Table 5.1: *Color effect values for BODIPY and thionin. σ_0 is the full Gaussian width of the inhomogeneously broadened long wavelength absorption band, s_0 the average solvent shift, Γ_0 the quasi-homogeneous hole width at the band maximum, C_d the differential and C_t the total color effect in the hole width as defined in the text.*

dye	$\sigma_0/\mathrm{cm}^{-1}$	s_0/cm^{-1}	σ_0/s_0	Γ_0/GHz	$C_\mathrm{d}/\mathrm{cm}^{-1}$	C_t
BODIPY	302	865	0.35	1.40	$0.95 \cdot 10^{-3}$	0.29
thionin (imino)	300	1425	0.21	1.76	$-1.0 \cdot 10^{-3}$	-0.31
thionin (amino)	n.e.	1308	n.e.	1.57	$-1.2 \cdot 10^{-3}$	n.e.

In Table 5.1 the particular values for the BODIPY and thionin measurements are listed along with the average solvent shift s_0 and the Gaussian width σ_0 for each absorption band involved. For the amino band of thionin σ_0 could not reliably be estimated because of the interference with the multitude of Gaussians making up the thionin dimers and oligomers in the absorption spectrum.

5.3.4 BODIPY: Dipole-Dipole Coupling

When looking at BODIPY there is the prominent color effect in the Stark experiments to be explained at first. Stübner quite convincingly traced the increase of the fixed dipole moment difference in BODIPY when tuning the burning wave number from the blue to the red edge back to the fluor atoms at the central N_2BF_2 moiety [27]. Their large electronegativity provides a preferred target for solvent molecules to form hydrogen bonds. Hydrogen bonds always cause hypsochromic solvent shifts because upon excitation of the probe molecule their strength becomes less. Consequentially, for a chromophore like BODIPY with an overall bathochromic solvent shift the molecules with weaker hydrogen bonds should be found on the red edge of the inhomogeneous absorption band. This is perfectly in line with the increased dipole moment differences found at lesser wave numbers – strong hydrogen bonds weaken the dipole moment of the bonded molecule because the partial charges of the fluor atoms become smaller. Thus, the dipole moment of a BODIPY molecule with weak hydrogen bonds retains its initially large value and therefore its large dipole moment differences upon electronic excitation.

The color effect in the dipole moment difference is the key to understanding the color effect in the homogeneous linewidth for BODIPY: Table 5.1 shows a value of 0.35 for σ_0/s_0 which is somewhat bigger but in the same order as the respective value of 0.29 for C_t. This indicates that the dominant forces causing the solvent shift may be responsible for the color effect in the linewidth as well. The main interaction between TLS and the chromophore will occur via dipole-dipole coupling. The larger the coupling strength between the TLS dipole and the probe dipole, the higher the contribution to the hole broadening from a single TLS flip will be. The experiments support that thesis – the further to the red side of the absorption band molecules are excited, the broader the linewidth will become owing to the increase in the dipole moments of the involved molecules.

5.3.5 Thionin: Ion-Dipole Coupling

For thionin the situation seems much more complicated. The following discussion will only put the imino band into focus, but the arguments qualitatively still hold for the amino band as well. Despite the fact that the magnitude of C_d for thionin is similar to that of BODIPY, C_t has not only a different sign, but is significantly larger in its absolute value than the respective value for σ_0/s_0 hinting that the interactions that are responsible for the solvent shift are not the main reason for the color effect in the homogeneous linewidth.

As already seen from Fig. 5.4(b) the dipole moment differences are neither large nor changing a lot with the burn wave number. That means that dipole-dipole interactions will only play a minor role for thionin. The fairly sizable bathochromic solvent shift of about $1300\,\mathrm{cm}^{-1}$ suggests that the major contribution stems from dispersive interactions. Dispersive interactions occur when the probe molecule polarizes the solvent molecules which in turn polarize the probe molecule again. That way the induced dipoles are always aligned to each other in such a way that

the excitation energy for the probe molecule will be lowered, hence shifted to the red. Dispersive interactions are in terms of distance dependence the weakest of the first and second order multipole interaction forces, however, for molecules with large polarizations they will dominate the solvent shift.

Quite in contrast to the BODIPY dye, thionin is an inherently charged molecule leading to ion-dipole interactions between the charge and the dipoles of the environment. Although those interactions are much stronger than dipole-dipole interactions or dispersive interactions, they can not contribute to the solvent shift because upon excitation the net charge remains the same, both in magnitude as well as distribution over the molecular frame. That will change the energy of the ground and the excited state in the same way yielding a net solvent shift of zero. Upon freezing the thionin sample the environment that was polarized by the ionic charge will be fixed in space. Flipping a TLS in this setup will in fact cause an increase in coupling strength because its associated dipole moment will be aligned with the Coulomb field of the charged thionin. Yet again this alone will not be able to add to a site-dependent hole broadening because the increase will affect both the excited as well as the ground state in the same fashion.

The only difference comes from the dispersively polarized dipoles in the environment. A Coulomb field of a charge can effectively be shielded by surrounding dipoles. The higher the polariziation of the solvent molecules, the larger the dielectric permittivity and consequentially the shielding capacity of the solvent will be. At the redmost edge of the inhomogeneous absorption band the dispersive interaction will be strongest [88], hence the dielectric permittivity will be larger. Flipping a TLS at the red edge will accordingly have a lesser effect on the coupling to the charge of the molecule because its dipole moment will be shielded more effectively against the Coulomb field. By moving from the red to the blue edge the solvent polarization due to dispersive forces will get weaker and fluctuations of the TLS dipoles will have a larger impact on the coupling strength to the thionin molecules. Congruously, the homogeneous linewidth will increase when moving to higher excitation wave numbers. Of course there will still be dipole-dipole interactions but they will be preponderated by the ion-dipole interaction which is a lower order effect.

5.4 Summary

The experiments at hand have shown in a unique way that depending on the nature of the solute molecules, a rich diversity of complementary effects and interactions has to be considered when judging color effects. For the first time, similarly constructed experiments have been juxtaposed with completely oppositional outcomes in the trend of color effects. It has also been proved with thionin as example that the method of spectral hole burning can be a handy tool to investigate interaction types that do not directly influence the solvent shift such as ion-dipole interactions. Hand in hand with Stark spectroscopy measurements as backup, the experiments provided insight in site-correlated differences in local dielectric permittivity for thionin and hydrogen bonding strength for BODIPY.

Determination of homogeneous linewidths can be a valid tool to disentangle different interaction contributions of a single molecule within a given amorphous environment according to its solvent shift.

In all science, error precedes the truth, and it is better it should go first than last.

Hugh Walpole

Chapter 6

Pressure Tuning Spectroscopy of Oligonucleotides

While the last two chapters dealt with the already complicated behavior of thionin in a solvent by itself, the next step is to actually employ the chromophore for its biophysical purpose – as optical probe monitoring the interactions, dynamics and structure of other, biologically relevant molecules such as desoxyribonucleic acid (DNA). By understanding the detailed features of dyes interacting with specific DNA molecules in a selective way a multitude of new possible applications based on nanomanipulation of DNA will open up in the future [131–136].

DNA has long been known to interact with phenothiazinium and other planar dyes [137, 138]. Especially the cytotoxicity of those dyes due to their capability of photoinduced DNA cleavage or mutation evoked interest among scientists to investigate the binding properties of phenothiazines to DNA [30, 139–141]. However, through controlled employment of engineered derivatives otherwise toxic effects may be turned to a therapeutic use by selectively affecting the accessibility of enzymes to the DNA molecule or inhibiting DNA replication. The main binding mode of smaller molecules with aromatic cycles to DNA is the so-called *intercalation* [142, 143]. Unlike bulkier agents planar chromophores can slip between base pairs being held in place by π-π electron stacking which relies on dispersive interactions due to the often large polarizabilities of the involved molecules [144]. Depending on the base pair composition of the DNA and the structure of the intercalating molecule the intercalation strength, periodicity and effectiveness can vary greatly.

Apart from intercalation there are two other common binding modes present in the interaction of dye molecules with DNA: *minor groove binding* and *major groove binding*. Whenever a molecule is too large or too less polarizable to be effectively stacked between adjacent base pairs it may attach itself to the sides of the polynucleotide chain. Because of the natural helicoidal appearance of DNA there are indentations between the actual base pairs. Sugar units sticking out in angles of 120° rather than 180° cause those folds – also referred to as *grooves* – to be uneven in width. The larger of the two grooves is called the *major grooves* where most enzymes and proteins dock to the DNA. The *minor groove* has only recently become the focus of research, its main role in protein-DNA recognition

is mostly still unclear [145, 146].

For three sets of different oligonucleotides – a short linear duplex of guanine–cytosine base pairs, a strand of telomeric DNA and a synthetically created thrombin aptamer – the intercalating and groove binding abilities of thionin have been investigated by means of pressure tuning spectroscopy of spectral holes. By comparing the local isothermal compressibility for each sample to that of free thionin possible binding sites could be characterized via their mechanical stability.

6.1 DNA And Its Components

DNA as the carrier of the genetic code for living organisms is apart from proteins one of the most important and ubiquitous molecules in biology. Although Watson and Crick resolved the structure of DNA more than half a century ago [147] a lot of its principles of functionality remain a mystery still. DNA in its original form is a set of two polymers with a remarkably simple assembly of only a few components. However, the enormous length of native DNA, its flexibility and its ability to interact with its surrounding as well as itself in a large variety of ways make it essential to regard the dynamics and the statistical mechanics of the molecule.

6.1.1 DNA Bases

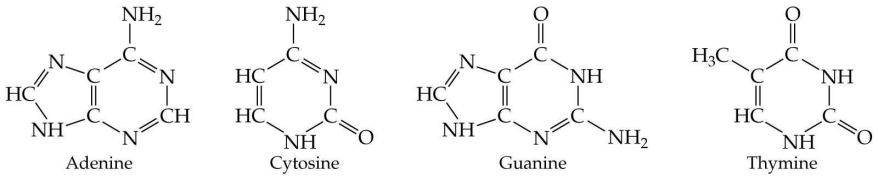

Figure 6.1: *Chemical structures of the four bases found in DNA.*

The defining elements of DNA are the four nucleic bases that are responsible for storing the genetic information. Fig. 6.1 features the chemical structures of the four naturally occurring DNA bases. Adenine (A) and guanine (G) as the larger ones are purine derivatives with two organic carbon cycles while thymine (T) and cytosine (C) are built on a pyrimidine base. Thymine is replaced by uracil (U) in ribonucleic acid (RNA) which is a conversion intermediate to translate the genetic code from the DNA into the construction of proteins and enzymes. The bases are attached via a covalent bond to one of their nitrogens to the backbone that lines up several nucleic bases to a single DNA strand.

The DNA holds the information about how proteins are to be built. Proteins, however, are made up from 20 amino acids. Obviously the small pool of only four different nucleic acids is not large enough to attribute one nucleic to one

amino acid each. Therefore, groups of three nucleic acids define the code for each amino acid. The abundance of threefold base combinations can account not only for the amino acids but for special controlling sequences such as the "stop" code TAA which defines the end of a protein or blank information which does not code anything at all. Blank or "degenerate" information helps making the information stored in DNA more resistant to replication faults or single point mutations.

6.1.2 Nucleotides

Each of the functional bases forms over a β-N-glycoside bond together with a 2-desoxy *D*-ribose unit the so-called *nucleoside*. The pentose sugar is the main part of the DNA backbone. By attaching a phosphate group to the sugar the *nucleotide* is completed. On the free side of the sugar a phosphate group from another nucleotide can bind to form an effectively endless chain of nucleotides, a polynucleotide. The phosphate groups serve as spacers ensuring an always constant gap of about 4 Å between two neighboring functional groups in a linear string of nucleotides. However, due to strong $\pi - \pi$ electron interactions between the aromatic rings of the bases it is more favorable to twist the bases against each other by approximately 30°. This way the distance between the aromatic moieties can be reduced to 3.4 Å without having to compress the length of the strand. With each base twisted in that fashion the pile of aromatic rings eventually winds up in a helicoidal structure.

Due to the asymmetry of a single nucleotide the endpieces of each polynucleotide are different. The common denotation to tell the ends apart is to name them by the number of the only free carbon atom of the ribose unit at the fringes. The end of the backbone starting with a phosphate group is called the 5'-terminus, the opposite end the 3'-terminus. The usual direction of writing down the sequence of nucleic bases is from the 5'- to the 3'-terminus.

6.1.3 Base Pairings And Quartet Structures

A very convenient coincidence is the complementary nature of the nucleic bases in terms of hydrogen bonding. Two possible base pairings are easy to form because thymine and adenine as well as guanine and cytosine fit seamlessly together. The geometrical structure of the base pairs is given in Fig. 6.2. A single stranded DNA molecule will therefore always be bound to a complentary chain that attaches itself in a opposite direction to the first matching the nucleic sequence with the correct base partners. Although there is no information gain by adapting an inverted sequence, the advantages are obvious:

- *Stability:* The hydrogen bonds strengthen the molecule and protect the functional groups from binding to unwanted molecules.
- *Hydrophilicity:* The more hydrophobic nucleic bases will be wrapped up in the inside of the helix leaving the hydrophilic ribose units on the outside improving the solubility in aqueous environments.

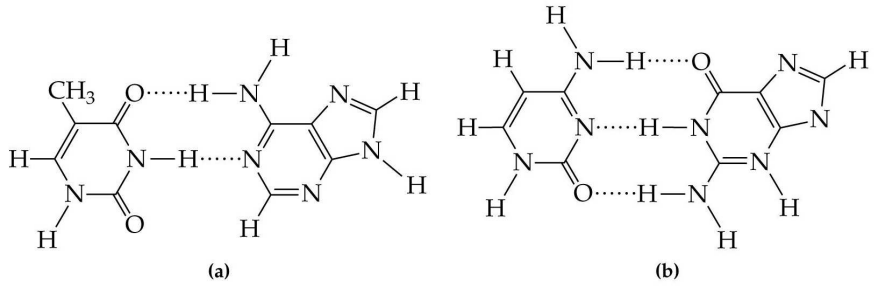

Figure 6.2: *Chemical structures of the naturally occurring base pairings in DNA. Dotted lines represent hydrogen bonds. In (a) the base to the left is thymine, the one to the right adenine. In (b) the left base is cytosine, the right guanine. The ribose unit connects to the bottom left nitrogen atom of each pyrimidine and to the bottom right nitrogen of the pentacyclic ring of the purine bases. That means that the helix' minor groove for each base pair lies below the structures drawn in the scheme, the major groove above.*

- *Safety:* Genetic information is very sensitive to accidental damage or loss. When a single base in one strand is damaged or lost, the information is still stored in the "backup" strand increasing the chance of information retrieval.
- *Copying:* Building up a new DNA helix is actually quite simple with two independent information copies. Certain replication proteins just separate the two strands from each other and fit a new strand of matching base pairs to each of them.

Another possibility to form bonds between nucleic bases often occurs in guanine rich regions of DNA strands. Fig. 6.3 shows the guanine quartet structure where four guanines form a square planar network of hydrogen bonded bases. While the usual base pairs detailed above are connected in a Watson-Crick bonding geometry, guanine quartets – or guanine tetrads – are linked in a fashion called Hoogsteen geometry. Although Hoogsteen geometries are perceived to be slightly more stable than the Watson-Crick structures [148], the stacking interactions that entail Watson-Crick geometries are more favorable, thus limiting naturally occurring Hoogsteen bonds to a few exceptions like guanine quartets.

G-quartets are very notable in terms of their polymorphism [149]. Since four different DNA strands contribute to the formation of the planar guanine array the quartets can be classified by various parameters:

- *Strand Stoichiometry:* The number of different strands contributing to the formation of the G-quartet. A single strand may constitute one edge of the tetrad, loop back and make up for one or two more or even all of the strands at the edges. There are monomolecular, bimolecular, trimolecular and quadromolecular G-quartets possible.
- *Strand Connectivity:* When one strand loops back to form another of the tetrad backbone, there are various possibilities in which order the strands connect to each other – crossed over the middle of the guanines or along one edge.

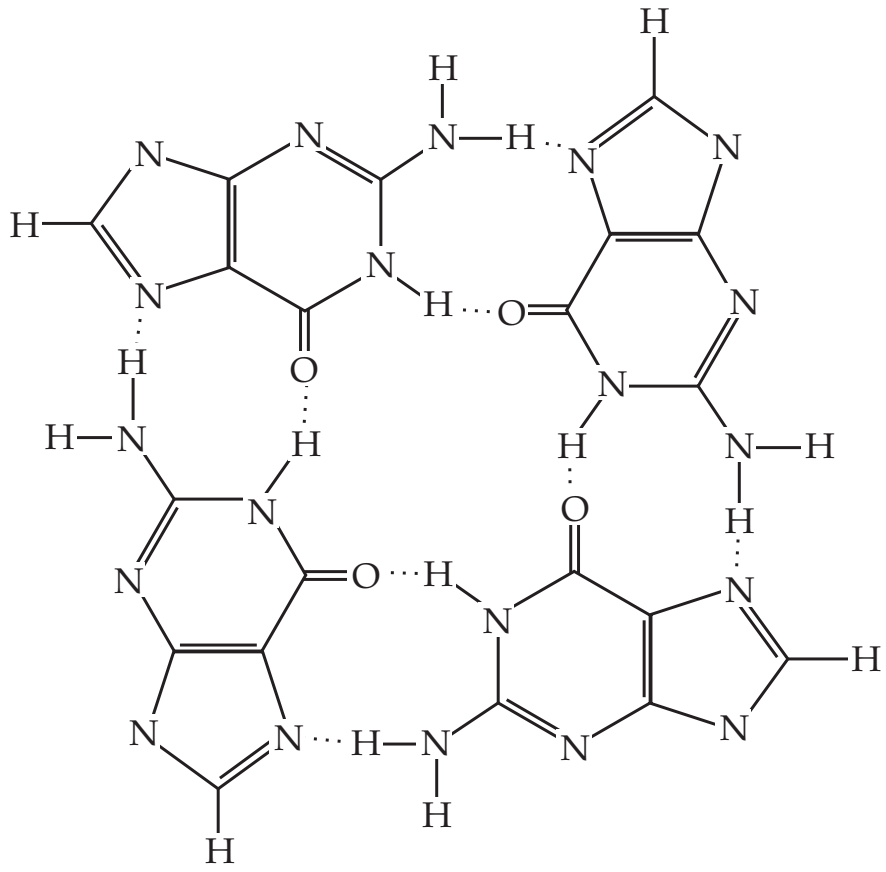

Figure 6.3: *Chemical structure of the guanine quartet structure. Dotted lines represent hydrogen bonds.*

- *Strand Polarity:* With four strands there are 16 combinations for the directions in which the strand may run along the G-quartet edges.

Piling up several G-quartets yields a structure referred to as G-quadruplex. Because of the fairly large gap in the center of each quartet this tube-like geometry is often stabilized by positively charged metal ions incorporated in the center between two adjacent stacks of tetrads. The best fitting cations are potassium and strontium, closely followed by sodium.

6.2 Selected Oligonucleotide Structures

Because of the sheer multitude of possible DNA structures it is vital to pick out several model systems of educational value or known biological function to pin down the crucial points in the interaction scheme of thionin with DNA. First a short dodecameric nucleotide of repeating base sequence is presented to find peculiarities in the intercalation properties. Then a naturally occurring section of eukaryontic telomeric DNA is investigated and finally a synthetic oligonucleotide known to be fundamental in the manipulation of the protein thrombin.

6.2.1 Linear Duplex

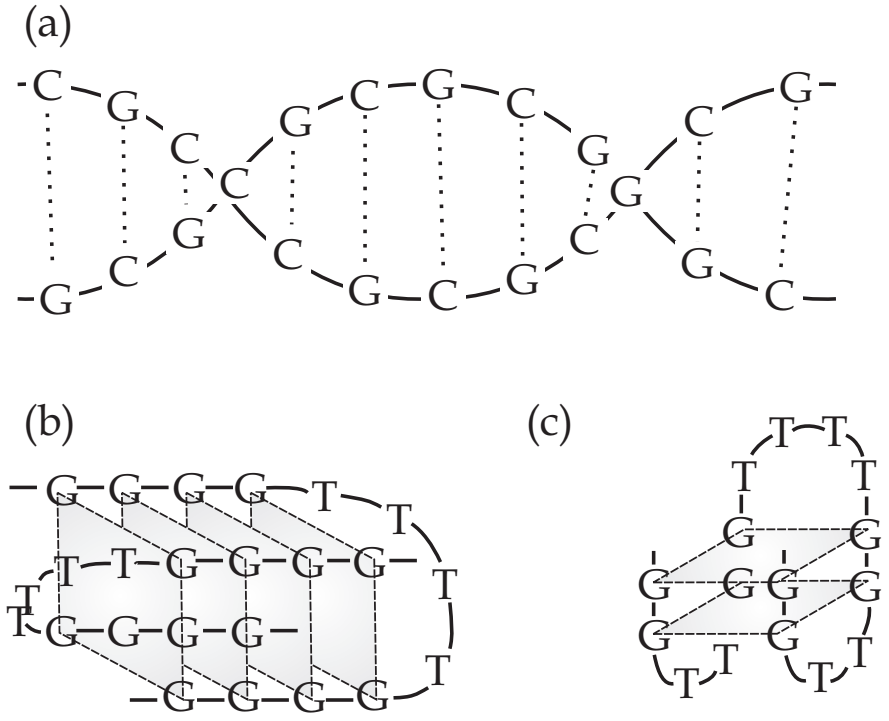

Figure 6.4: *Chemical structure of the oligonucleotides used in this work: (a) a linear duplex of GC (LD), (b) telomeric DNA found in* Oxytricha *(Oxy) and (c) the thrombin aptamer (Apt). LD consists of two single strands with six repeating guanine–cytosine sequences that are bound to each other in reverse direction. Oxy is made up of two hairpin structures held together by four G-quartets. Between the quartet layers there are sodium ions incorporated. Apt is a monomolecular structure which forms two G-quartets. Again a sodium ion helps stabilizing the quartets.*

Fig. 6.4 (a) gives a scheme of the dodecameric oligonucleotide. Each of the strands is made up from alternating guanine and cytosine bases giving rise to stacking G–C base pairings with alternating orientation. It is known from quantum chemistry calculations that those kind of base pairings offer the best stacking interactions. Alternating G–C stacks provide a stacking energy of about 0.63 eV per pair, considerably more than for example alternating A–T stacks which only provide an interation energy of 0.14 eV per pair. As already mentioned in 6.1.2 double stranded DNA will coil up in a helicoidal fashion with a coiling angle of about 30° per base pair. LD as a dodecameric structure will therefore be wound up once around its axis leaving only a small minor and major groove for molecules to bind. With a helix diameter of about 18 Å the whole structure is not long enough to bend. LD will assume the form of a rather stiff helix with about 40 Å length from end to end.

Short strands of duplex DNA with known and repeating base sequence often serve as model systems to investigate the intercalation behavior of planary dyes within certain sequences of native DNA [150–152]. For phenothiazinium dyes there are several indicators that not only the intercalation structure may vary with base pairs and geometry of the dye but that depending on the

ionic strength of the solute other binding modes are possible too. Tuite and Kelly found considerable red shifts in spectral titration studies of methylene blue and thionin but an isosbestic point was lacking [141]. At present the exact binding properties of those dyes to polynucleotides is not fully understood yet.

Phenothiazinium dyes have extraordinarily strong photosensitizing and photodamaging capacities when bound to DNA. Unravelling the damaging mechanisms is inevitably linked with gaining detailed knowledge of the dye photochemistry and its impact on the DNA.

6.2.2 Telomeres

Cell division in living organisms relies on the correct transfer of all genetic information. Within every cell the information is split up among several DNA polynucleotides, the chromosomes. Replication of the information stored in the chromosomes is accomplished by separating the inversely identical strands of the double helix and building up new counterstrands for each original strand. Separating the strands in the first place requires molecular machines within the cells to take care of that, the so-called DNA polymerase III. This protein complex copies base per base starting form the 3' end of a single DNA strand. When starting to unzip a chromosome for one of the strands – the one having its 3' end at this side of the chromosome – the polymerase can work flawlessly. The complementary strand, however, runs in the opposite direction. Thus the replication is done backwards in a piecewise fashion. The starting points for those pieces are defined by RNA primers which are set at certain initializing points along the copied strand. After both strands have been successfully copied the DNA ligase connects both newly emerged strands again behind the polymerase.

This works very nicely until the other end of the chromosome is reached. Since RNA primers can not be put at any given position the last piece of the strand that is being copied backwards from the last primer to the end can not be duplicated. The new chromosome is therefore always several nucleic bases shorter than its template [153]. To prevent loss of vital information the end pieces of chromosomic DNA only contain base sequences without any genetic code, sometimes up to hundreds of thousands of base pairs. Those terminal sequences are called *telomeres* and are specific in their base composition depending on the organism [29].

A common feature of nearly all eukaryotic telomeres is the relative abundance on guanine bases. Examples for base motifs are TTAGGG (human DNA), TTGGGG (bacterium *Tetrahymena thermophila*), TTTGGG (algae *Oxytricha*) or TTAGG (silkworms). Apart from providing informationless material the telomeres also contribute to the protection of the chromosomes. Open ended polynucleotides tend to aggregate with other nearby nucleotides so the chromosomic termini anneal themselves by forming guanine quartet structures.

The quartet structure used in this work is a common structure from the telomeric DNA of *Oxytricha* (Oxy) (Fig. 6.4 (b)). It consists of two single strands of $G_4T_4G_4$ which form hairpinlike structures: The guanines bind to each other with a loop of thymines. Two of those hairpins can form a quadruplex structure. Several experiments confirmed the cross connectivity of the native telomeric structure of Oxy where the guanines of the same strand are placed in diagonally opposite edges of the tetrad [154–156]. Oxy is a mechanically very stable nucleotide well suited to protect the chromosomic termini from agglomeration. The stability is further enhanced by the incorporation of cations, mostly sodium or potassium ions which are found in abundance within cells.

The importance of telomeres was only discovered in the late seventies of the last century [157, 158]. Every reproduction cycle of a cell shortens the telomeric sequences leading to its slowing and eventually its cessation. Senescence of cells thus is terminated by the number of cell divisions rather than chronological time. However, to elongate the normal lifespan of a generation of a cell and its duplicates an eukaryiotic ribonucleoprotein called *telomerase* can replicate the telomeric sequences of the chromosomes. This mechanism seems naturally well balanced – cells that divide too fast can not be targetted by the telomerase and will quickly be no longer replicable due to their too short telomeres. Cells that divide more slowly will get their lost telomeric sequences replaced and can be replicated much longer. Controlling of the telomerase activity can be consequently used to control the reproduction and proliferation of cells.

Any disturbance in the normal telomerase activity can lead to unnatural replication behavior. Cancer cells for example are known to be immortal because there seem to be mechanisms that allow for a greatly enhanced telomerase activity. Tumors can therefore proliferate endlessly promoting cancer. The main target for the fight against cancer nowadays focuses on regaining control of the telomerase in tumor cells or inhibiting telomerase activity by introducing counteracting drugs. To be able to specifically target cancer cells without destroying healthy cells it is of vital importance to know exactly how telomeres are interacting with telomerase and telomerase inhibiting drugs.

6.2.3 Aptamers

Aptamers are synthetically created oligonucleotides designed for antagonizing special proteins [159, 160]. Their evolution is usually monitored by systematic *in vitro* refinement of competitive protein binding of a multitude of potential nucleotides until one optimum structure is found.

One of the first aptameres to be developed was the α-thrombin aptamer (Apt) [161]. Its structure can be seen in Fig. 6.4 (c). A monomolecular chain of thymines and guanines can be stabilized by a single cation to form a structure similar to a rocking chair. The eight guanines form two quartet structures while the thymines form the loops connecting the strands at the edges of the G-tetrad. Apt displays

an extraordinarily high affinity to thrombin and inhibits its activity.

Thrombin is an enzyme that emerges from the ubiquitous proenzyme prothrombin and is responsible for the conversion of fibrinogen to fibrin. Fibrin molecules are fibrinogen proteins that are lacking certain amino acid sequences protecting the proteins from aggregation. While fibrinogens are unable to clump up, fibrin monomers can form a tight polymer network that can serve to seal lesions in blood vessels. Thus, thrombin activity has a large impact on blood clotting and blood clotting related diseases like thrombosis and apoplexy. Sytematical inhibition of thrombin with Apt helps combatting those malfunctions of the blood circuit. The further development of pharmaceutical agents relies on the knowledge of the interactions of aptamers with their specific targets.

6.3 Absorption Spectra

Low temperature absorption spectra at $T = 2\,\mathrm{K}$ of all samples are shown in Fig. 6.5. The quality of the oligonucleotide spectra is lesser because of the low concentration of oligonucleotides and consequently thionin and the ensuing lower optical density. Each spectrum displays a main peak to the very red edge entailed by a somewhat smaller band on the blue shoulder. Although the blue shoulder seems to be lower in intensity for the oligonucleotide samples this is only caused by the lower intensity of the hypsochromically shifted oligomer band of thionin. For Oxy and Apt the spectral positions of about 16200 and $16550\,\mathrm{cm}^{-1}$ remain unchanged compared to the free thionin spectrum, but for LD there is a bathochromic shift of $\delta = 200\,\mathrm{cm}^{-1}$ for each band.

In each band holes of similar width could be burned for every sample confirming the existence of two independent electronic excitations. The bands can be assigned to the tautomeric forms of thionin, namely the imino form (red band) and the amino form (blue band) [99, 162].

6.4 Binding Properties Of Thionin

The isothermic compressibility κ is an excellent parameter to estimate the binding capabilities of a dye to a target molecule [162]. Exertion of isotropic pressure will lead to a decrease of the average distance between solvent molecules and the dye shifting the potential and therefore the absorption energy. Oligonucleotides are more stable than the solvent cages formed around a free dye. If a dye is closely bound to an oligonucleotide it can be expected that the DNA shields the dye from the surrounding solvent molecules. κ as a local parameter in the vicinity of the dye will accordingly decrease because the solvent molecules can not penetrate the stable shell of the DNA formed around the dye and the deformation of the DNA itself will be considerably smaller. Dependent on the magnitude of this decrease in κ certain binding modes and geometries can be

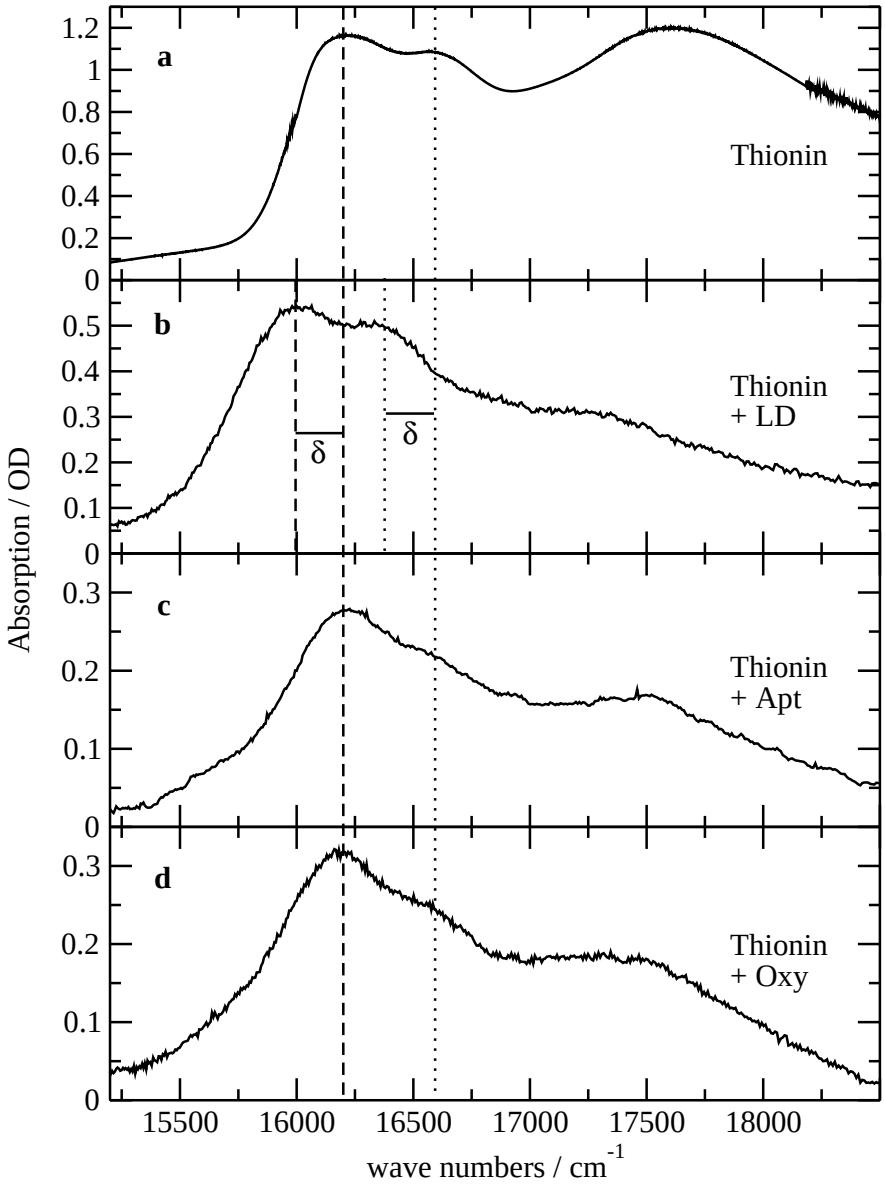

Figure 6.5: *Absorption spectra of (a) thionin, (b) thionin with LD, (c) thionin with Apt and (d) thionin with Oxy, each taken in a glycerol/water glass at $T = 2\,K$. Only for the sample of thionin with LD the redmost absorption bands display a bathochromic shift of about $\delta = 200\,cm^{-1}$.*

verified or ruled out.

6.4.1 Thionin As Reference

As already detailed in Chapter 4 Fig. 6.6(b) shows an example of holes under pressure burnt in thionin in a glycerol/water glass. The initially sufficiently deep and somewhat narrow hole broadens and flattens if isotropic pressure is exerted upon the sample. Low pressures of around $\Delta p = 1.5\,\mathrm{MPa}$ suffice to shift the center of the hole by about 6 GHz (*cf.* Fig. 6.6(a)). The hole center shifts

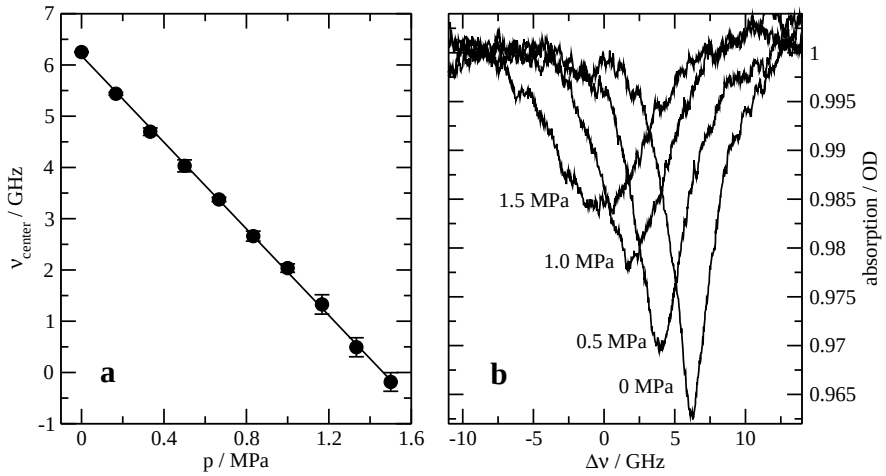

Figure 6.6: *Pressure tuning experiment for thionin in a glycerol/water glass at $T = 2\,K$. The hole was burnt at 16390 cm^{-1}. (a) shows the shift of the hole center upon increasing pressure. (b) shows some of the hole spectra at various pressures.*

perfectly proportional to the applied pressure.

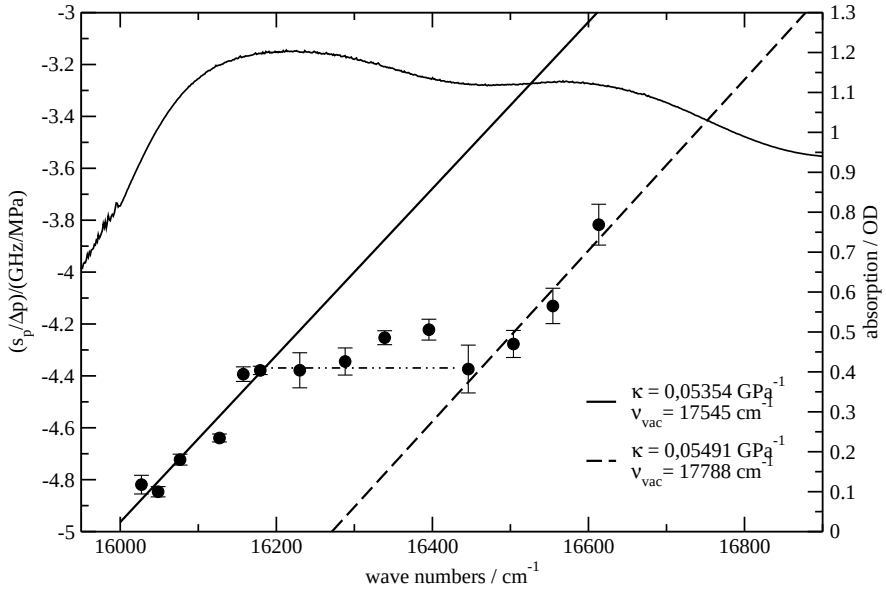

Figure 6.7: *The dependency of the hole shift per unit of pressure $s_p/\Delta p$ on the burn wave number for thionin in a glycerol/water glass. The low temperature absorption spectrum is shown in the background. The pattern for $s_p/\Delta p$ with the burning frequency is z-shaped: After an increase at the red edge of the inhomogeneous absorption band there is a region of constant $s_p/\Delta p$. At the blue edge $s_p/\Delta p$ increases again with the same slope as at the red edge.*

Repeating the experiments for holes burnt all over the inhomogeneous absorption band the hole shift per unit of pressure $s_p/\Delta p$ depends on the burning wave number. Fig. 6.7 shows this dependency with the absorption spectrum of thionin in the background. Two regions of similarly increasing $s_p/\Delta p$ are discernible, separated by a spectral region of approximately constant $s_p/\Delta p$. While the

slopes correspond to the two tautomers of thionin, namely the imino form for the red band and the amino form for the blue band, the holes in between are made up by molecules in both tautomeric geometries thus cancelling their hole shifts to an average and therefore constant value – this is quite a reasonable pattern for overlapping species of molecules [163]. The gradient of the rise of $s_\mathrm{p}/\Delta p$ with the wave number can be used to calculate the isothermic local compressibility κ for each tautomer. Both have about the same value of $\kappa = 0.054 \pm 0.010\,\mathrm{GPa}^{-1}$. It is reasonable for the parameters to have the same magnitude because the solvent environment is not likely to change upon a tautomeric transition. The compressibility will therefore remain unchanged regardless of the tautomerisation. The numbers obtained for κ by themselves just reflect local properties of the solvent around the dye and may, in some cases, differ from the compressibility of the pure solvent. However, they serve as calibration parameters for the experiments with DNA.

Apart from κ the second parameter that can be extracted from the data is the vacuum wave number ν_vac that determines the size and direction of the solvent shift. For thionin the solvent shift is with $\nu_\mathrm{vac} = 1350\,\mathrm{cm}^{-1}$ fairly large and bathochromic.

6.4.2 Linear Duplex

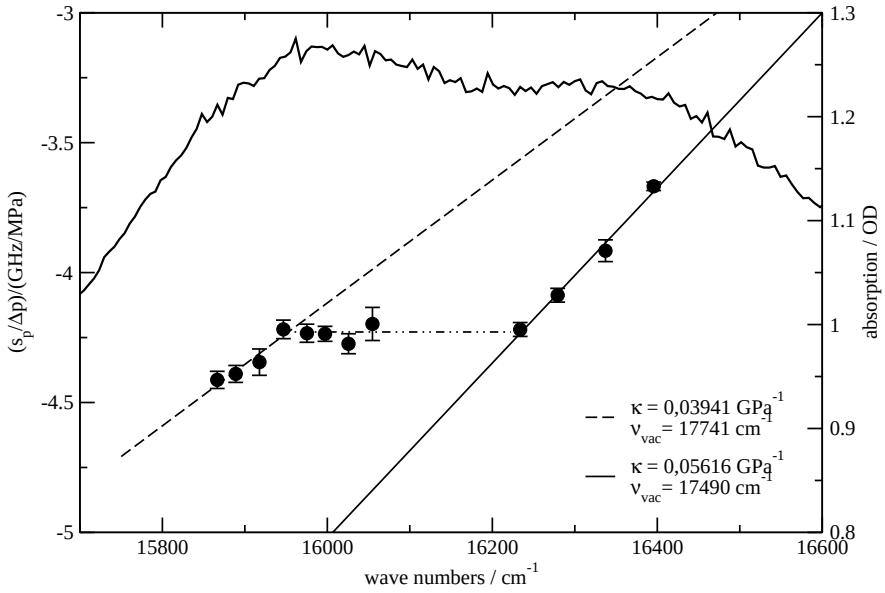

Figure 6.8: *The dependency of the hole shift per unit of pressure $s_\mathrm{p}/\Delta p$ on the burn wave number for thionin with LD. The low temperature absorption spectrum is shown in the background. Along the red side of the inhomogeneous absorption band the slope for $s_\mathrm{p}/\Delta p$ with the burn frequency is more gently inclined than on the blue side. Between the two tautomeric absorption band $s_\mathrm{p}/\Delta p$ remains constant.*

Fig. 6.8 shows the results for the pressure tuning experiments in thionin mixed with LD in glycerol water. The data points are not as evenly spaced as for

pure thionin because in the intermediate region between the two tautomer bands hole burning is not possible with sufficient quality. This is most likely caused by electron transfer induced quenching effects when thionin is brought into the vicinity of guanine bases [164, 165]. However, again there are three regions discernible: At the blue edge and the red edge there are linear increases of $s_\mathrm{p}/\Delta p$, while in the spectral region in between the pressure shift remains constant.

The most interesting observation concerns the difference between the gradients of both onsets. For the blue absorption band the compressibility is with $\kappa = 0.056 \pm 0.004\,\mathrm{GPa}^{-1}$ of the same magnitude as for free thionin. But for the red band the slope is significantly less inclined and yields $\kappa = 0.039 \pm 0.009\,\mathrm{GPa}^{-1}$, a value approximately 40% less than for the corresponding absorption band in free thionin. Satellite hole burning studies suggested that the redmost absorption band corresponds to the imino form regardless of the bathochromic shift that both tautomer bands undergo. A 30% decrease in compressibility is evidence for a very effective shielding of the dye against solvent molecules which can only be provided by intercalation. Furthermore, the mechanical stability of the duplex DNA seems very good. For the amino form the case is different. The display of an unchanged value for the compressibility rules out any intercalative binding to DNA. The red shift of the absorption bands implies some interaction of the amino form with LD, but the data can not provide evidence for a detailed description of the binding mode. One possibility is that the amino simply attaches itself to the outside of the chain remaining as much exposed to the solvent as free thionin. There also might be a groove binding mechanism if the groove is large enough to hold both solvent molecules as well as the thionin. In that case isotropic pressure would still cause to compress the immediate surrounding of the thionin found in the grooves in the same way as the pure solvent around a free thionin.

6.4.3 Telomer

Fig. 6.9 shows the pressure tuning results for thionin bound to oxy. The hole quality in the blue edge of the absorption band was not satisfyingly good to justify an estimation of hole shifts. For both oxy and apt the low concentration paired with an impact on the glass forming abilities hampered the burning of narrow holes with a low signal-to-noise ratio. Therefore the data shown only applies to the redmost absorption band where a smooth linear incline with $\kappa = 0.045 \pm 0.003\,\mathrm{GPa}^{-1}$ can be found. This value is about 20% smaller than the respective one for free thionin.

First of all, there is no additional solvent shift to offset the absorption spectrum of thionin with oxy from that with free thionin. Since the change in compressibility suggests a binding of thionin to oxy the interaction has to rely on types that do not contribute to the solvent shift. A very likely interaction would be purely Coulombic interaction that does not change in magnitude when exciting molecules from the ground to an excited state and thus does not contribute to the overall solvent shift. Also the decrease in κ is only not as large as the change for the intercalating thionin in LD. Together with the Coulombic interaction

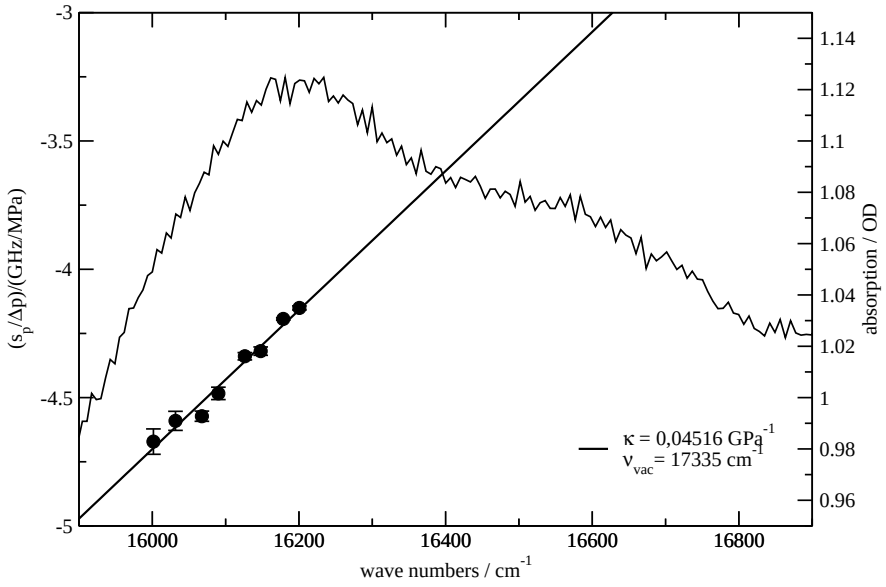

Figure 6.9: *The dependency of the hole shift per unit of pressure $s_\mathrm{p}/\Delta p$ on the burning wave number for thionin with oxy. The low temperature absorption spectrum is shown in the background. At the red side of the inhomogeneous absorption band the slope for $s_\mathrm{p}/\Delta p$ with the burn frequency is constant. The hole quality at the blue edge did not allow an evaluation for the second tautomer band.*

type and the fact that sodium ions are incorporated into the G-quartet structure the most likely binding mode will be external stacking. The thionin attaches itself to the top or the bottom of the G-tetrad only shielded by the loop of thymines against the solvent. This shielding is not as effective as for intercalating chromophores so the compressibility remains closer to the compressibility of free thionin.

6.4.4 Aptamer

Lastly, Fig. 6.10 depicts the results of the pressure tuning experiments done for thionin with apt. The picture is similar to that of oxy: The hole shift $s_\mathrm{p}/\Delta p$ increases linearly with increasing burning wave number ensuing a compressibility of $\kappa = 0.049 \pm 0.007\,\mathrm{GPa}^{-1}$. Although the value is somewhat smaller than the one for free thionin it is larger than for thionin with oxy.

The core part of apt is basically the same as for oxy, a stack of G-quartets stabilized by incorporated sodium ions. With the same solvent shift it is reasonable to assume that thionin will be stacking externally to the G-tetrad here as well. The slightly higher compressibility may be caused by the different geometrical arrangement of the loop parts connecting the strands making up the quartets. For apt the loops are connected edge to edge on both sides of the stacks whereas for oxy the loops span diagonally over the tetrads. A chromophore nested in a stacking fashion upon the tetrad will be less shielded against influence of the solvent for apt because the loops will not stretch directly over the dye molecule.

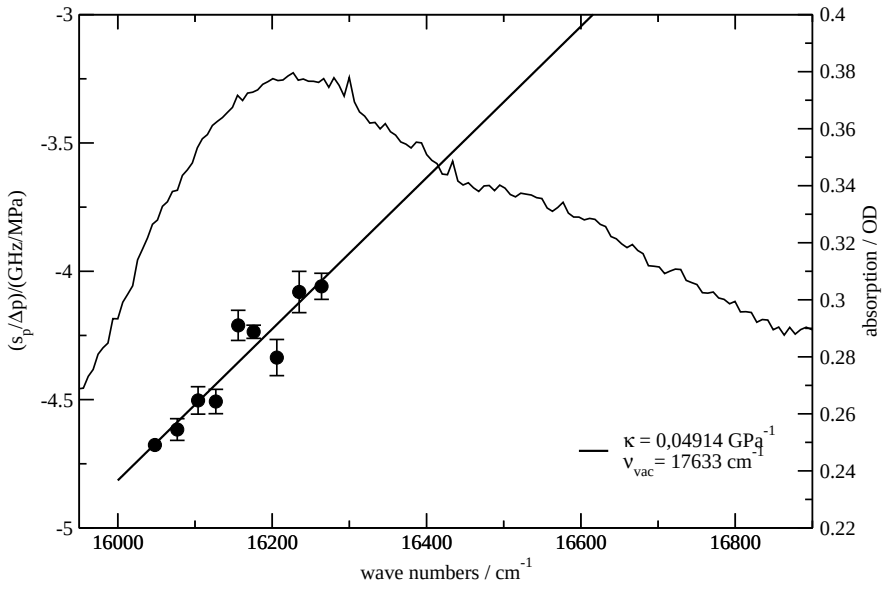

Figure 6.10: *The dependency of the hole shift per unit of pressure $s_p/\Delta p$ on the burn wave number for thionin with apt. The low temperature absorption spectrum is shown in the background. Along the red side of the inhomogeneous absorption band the slope for $s_p/\Delta p$ with the burn frequency is constant. The hole quality at the blue edge did not allow an evaluation for the second tautomer band.*

6.5 Summary

For three different DNA binding partners the interaction modes of thionin could be investigated [162]. The proposed binding mechanisms can be convincingly supported by deliberation of mechanical stability, geometrical structure and solvent shifts. In the case of G-quartets thionin seems to bind in an external stacking mode solely by Coulombic interactions. For a linear DNA duplex of G–C base pairs a difference in binding behavior for the two tautomers is found. Although the inhomogeneous absorption spectra give no hint on these binding modes pressure tuning experiments can help to identify them by unequal values of the isothermic local compressibility. The imino form has a significantly lower compressibility than the amino form in the presence of the linear duplex thus hinting at the selective intercalation of only one species of thionin into the G–C base pairs.

The most exciting phrase to hear in science is not "Eureka!" but rather "Hmm... that's funny...".

Isaac Asimov

Chapter 7

Pressure Tuning Spectroscopy of Cage Complexes

Having established thionin as a chromophore that can probe its immediate surrounding and the mechanical stability thereof, it is rather straightforward to try to incorporate thionin in the inside of large molecules as an optical sensor. A very suitable family of molecules for that purpose are cyclodextrins (CD), cyclic compounds of saccharose units in various sizes capable of forming conic structures with a cavity in which guest molecules can be inferred. After their discovery in 1891 by Villiers [166] the two naturally occurring CDs in bacteria – α- and β-CD – were characterized and identified by Schradinger in the period from 1903 to 1911 [167]. Until the late 1960s it was not possible to produce CDs synthetically in large amounts for industrial purposes. From then on CDs have given rise to a large field of research by themselves with over a thousand publications a year dedicated to the uses in various areas of application [34, 168, 169].

CDs have a lot of properties that make their deployment in medicine and pharmacy very useful:

- *Inclusion Complexes*: Smaller molecules can fit inside the cavity provided by the CD. Most inclusion complexes are such that one CD incorporates a single guest molecule but larger structures with two or more CDs capping larger guest molecules are possible as well. Those complexes are not formed with covalent bonds making the formation completely reversible.

- *Amphotericity*: The outside of the CD cones is hydrophilic whereas the inside is more hydrophobic. This means that hydrophobic molecules that would not be soluble in hydrophilic environments can be wrapped in a CD complex which has an increased solubility. Especially for drugs and pharmaceutical agents that are hydrophobic the transportation over body fluids which are usually hydrophilic can be eased by use of CDs.

- *Nontoxicity*: CDs are completely biodegradable by mammals and do not exhibit any biohazard when taken in small doses. Due to its high resistance to biodegradation by β-amylase, CDs are usually metabolized within the colon by the microflora. The metabolism products are maltose and glucose which are both harmless to the organism. Furthermore, CDs are taste- and odorless so they are perfectly suited as drug carriers.

- *Adaptability*: The modification of side chains allows CDs to fulfil specialized purposes while at the same time maintaining their encapsulation capabilities. Depending on the modification several key parameters like fluorescence, solubility, surface activity or affinity to proteins and enzymes can be purposefully altered. Thousands of CD derivatives have been investigated in the last decades and found their ends in various areas of medical, pharmaceutical or biochemical application.

- *Bioavailability*: Most drugs have to be delivered to cells to be most effective. While unprotected drugs are often destroyed during the application process, encapsulated CD complexes can deliver the drug unharmed to cell membranes where the bulky CD can not pass through but the drug is released and absorbed by the membrane. This bioavailability enhances the efficiency of drugs and at the same time reduces the necessary doses.

In our case thionin serves as a sensor with known features to probe the complex formation abilities of CDs. Especially the thermodynamic stability of CD complexes can be investigated by means of pressure tuning spectroscopy. Two types of CDs – α- and β-CD – have been mixed with thionin to evaluate the inclusion properties.

7.1 Structure of Cyclodextrins

CDs are rings of α-1,4-linked D-glucopyranose units who form a doughnut shaped truncated cone. The size of the cone varies with the number of glucopyranoses: The smallest CD is for steric reasons the α-CD with six sugar units, the largest naturally occurring CD consists of eight such units. Larger rings with up to hundreds of glucopyranose units can be synthesized but they are very unstable due to the inability to form a sufficient number of hydrogen bonds between the hydroxy groups of neighboring sugar units [170]. The hydroxy groups at the narrow end of the truncated cone are denoted as primary, the ones at the wide end as secondary hydroxy groups. All natural CDs are very rigid structures where only some conformational freedom is allowed in the rotation of the primary hydroxy groups and the dihedral twisting of the 1,4-carboxy linker group [171].

7.1.1 α-Cyclodextrin

Fig. 7.1 shows the chemical structure of α-CD. The secondary hydroxy groups are connected via hydrogen bonds, however, the small radius of the α-CD cone only allows the formation of four out of six pssible hydrogen bonds between the hydroxy groups. Therefore the solubility of α-CD in water is comparably good because the remaining hydroxy groups can form hydrogen bonds with water molecules.

7.1.2 β-Cyclodextrin

Fig. 7.2 shows the chemical structure of β-CD. Other than for α-CD the hydroxy groups can build up a full hydrogen bonding network among themselves. The solubility in water is for β-CD an order of magnitude smaller than for α-CD.

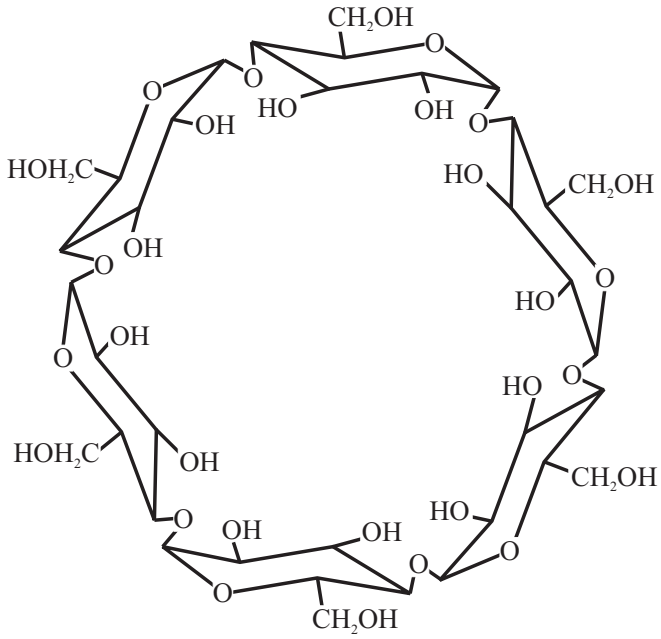

Figure 7.1: *Structure of α-cyclodextrin: Six α-glucopyranose units are linked in a ringlike fashion to form a hexamaltose torus.*

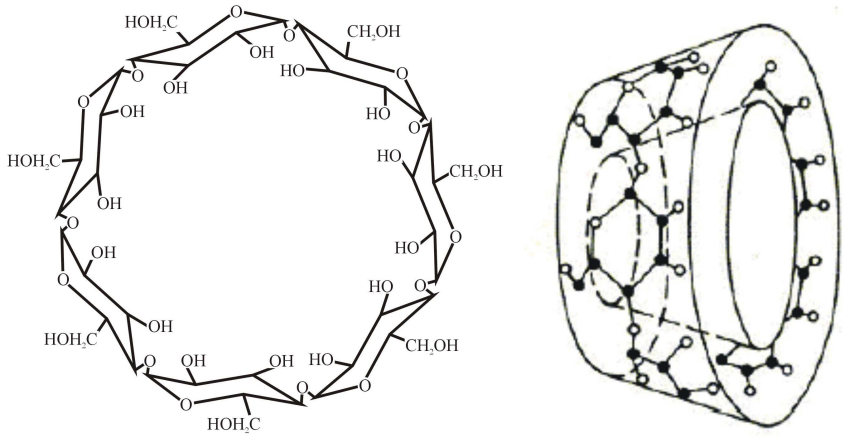

Figure 7.2: *Structure of β-cyclodextrin: Seven β-glucopyranose units are linked in a ringlike fashion to form a heptamaltose torus. The right side shows a sketch of the truncated conical shape of β-cyclodextrin where the narrow end of the cone is practically closed due to the small distance between the CH_2OH groups pointing inwards.*

For the basic types of CDs, Table 7.1 lists some relevant features necessary for the discussion of the experiments. While the depth of the cavity is approximately the same for all CDs the cavity diameter varies greatly with the number of glucopy-

Table 7.1: *Characteristic dimensions and parameters for α-, β- and γ-CD [172].*

	α-CD	β-CD	γ-CD
Number of glucopyranose units	6	7	8
Cavity depth in Å	7.9-8.0	7.9-8.0	7.9-8.0
Cavity volume in Å^3	174	262	427
Cavity diameter (wide end) in Å	5.2	6.4	8.3
Cavity diameter (narrow end) in Å	4.7	6.0	7.5
Solubility in mol/l H_2O ($T = 298\,K$)	14.5	1.85	23.2

ranoses. For α-CD the diameter is so small that an inclusion complex should not be possible with aromatic molecules like thionin, while β-CD provides a larger cavity capable of holding aromatic rings.

7.2 Absorption Spectra

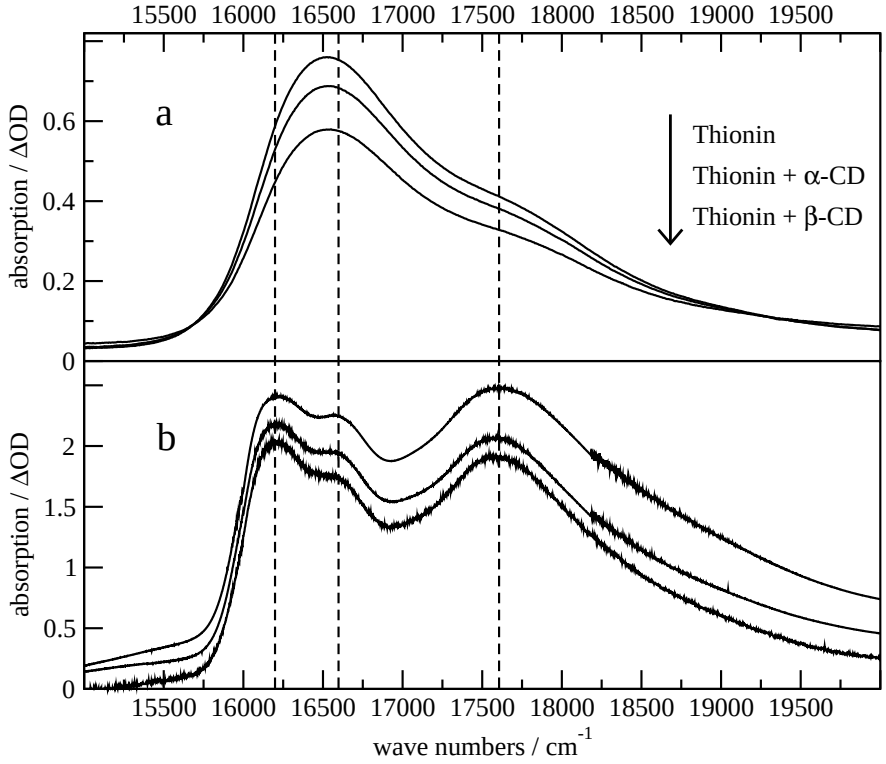

Figure 7.3: *Absorption spectra of free thionin, thionin with α-CD and thionin with β-CD at $T = 300\,K$ (a) and $T = 2\,K$ (b). All spectra were recorded with glycerol/water as a solvent.*

Fig. 7.3 shows the absorption spectra for the samples of thionin with α-CD and β-CD in a glycerol/water glass in comparison to the spectrum of free thionin. Both the room temperature spectra (Fig. 7.3(a)) as well as the low temperature spectra at $T = 2\,K$ (Fig. 7.3(b)) do not display any significant difference between

the three samples. Again, upon freezing the sample the oligomer band at around 17600 cm^{-1} gains intensity while the two redmost bands can be associated with the imino and the amino form of thionin. In this spectral region there is no contribution from the CDs that only absorb light in the UV region. Holes of sufficient depth could be burnt in either of the tautomeric thionin regardless of the presence of CD. The quality of the spectra even increased because both CDs enhanced the glass forming abilities of the samples.

7.3 Satellite Hole Burning Spectra

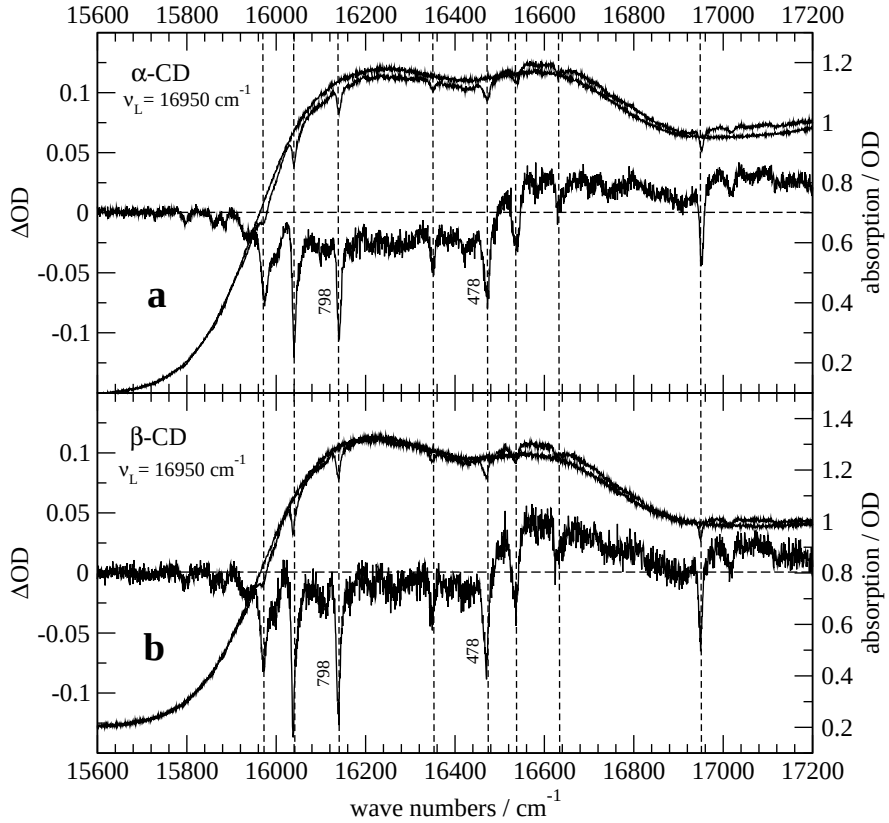

Figure 7.4: *Satellite hole burning spectra of thionin with α-CD (a) and thionin with β-CD (b). All spectra were recorded with glycerol/water as a solvent. The diagrams show the pre- and post-burn absorption spectra along with the difference spectrum. The figure shows the difference for some prominent holes to the burning position in wave numbers. Vertical dotted lines indicate the position of the most prominent satellite holes.*

Fig. 7.4 shows satellite hole burning spectra taken for thionin with α-CD (a) and thionin with β-CD (b). For several minutes a zero phonon hole was burnt at 16950 cm^{-1} and a second broadband absorption spectrum taken after the unburnt spectrum. The difference spectrum shows the typical distribution of red-shifted satellite holes for thionin. The holes at 478 and 798 cm^{-1} are crucial in determining the tautomeric state of the thionin at the inhomogeneous absorption bands: Both are known to relate to the inner ring motion and many other satellite holes are overtones or combination modes [99, 173]. Their frequencies shift to 489 and 809 cm^{-1}, respectively, when the tautomeric state changes from

the amino to the imino form. In the results at hand, those holes do not shift in comparison to free thionin for both samples, α-CD and β-CD. Apparently there is no interaction between thionin and the particular CD strong enough to cause changes in the vibrational modes. This documents the fact that the interactions, if any, are most likely hydrogen bonds and van der Waals forces.

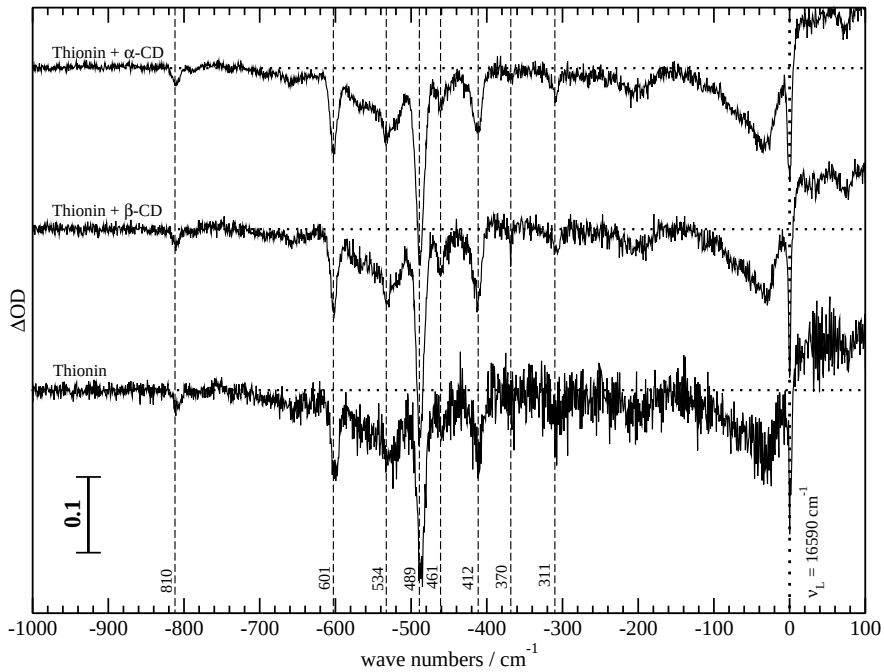

Figure 7.5: *Difference spectra of satellite hole burning measurements of thionin with α-CD, thionin with β-CD and free thionin. The infrared spectrum of thionin is highly resolved in its first excited electronic state. All spectra were recorded in a glycerol/water solvent and the zero phonon holes were burnt at 16590 $^{-1}$ each. The spectra are offset for reasons of clarity, the dotted horizontal lines indicate zero difference for each spectrum.*

Fig. 7.5 shows only the difference spectra for another burning wave number. When burning holes at 16590 cm^{-1} the spectra for the α-CD, the β-CD and the free thionin sample exhibit satellite holes at exactly the same spectral positions. The signal-to-noise ratio for the CD samples are slightly better due to the improved glass forming qualities. From the satellite hole burning experiments alone there is no hint that thionin interacts with CD at all.

7.4 Homogeneous Linewidth Measurements

An exemplary experiment to determine the quasi-homogeneous linewidth is shown in Fig. 7.6: The sample was thionin with α-CD, the hole was burnt at 16010 cm^{-1}. Fig. 7.6 (a) shows the linear increase of the hole width with the hole area, Fig. 7.6 (b) the respective hole spectra with increasing burning time. The experiments in β-CD were conducted in the same way and the spectra look quite similar.

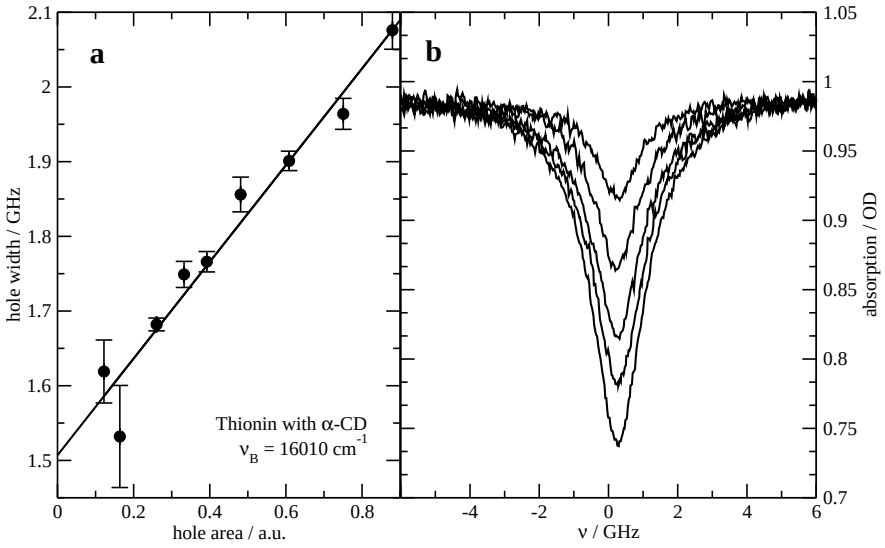

Figure 7.6: *Successive hole burning of thionin with α-CD at a burn wave number of 16010 cm^{-1}. (a) shows the linear dependency of the hole width with the hole area as the hole is burnt for longer times. The intercept of the linear fit with the y-axis denotes the double quasi-homogeneous linewidth. (b) shows some example spectra for increasing burning times.*

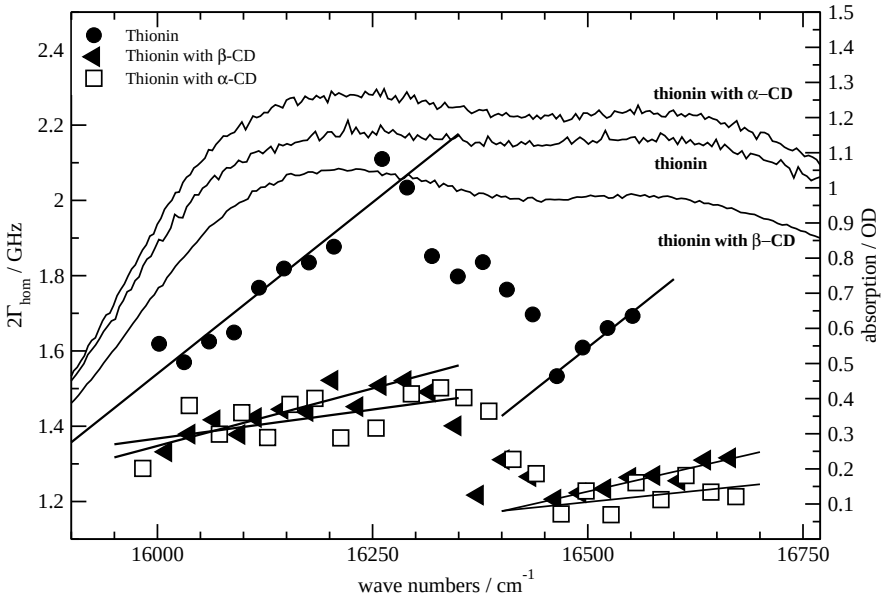

Figure 7.7: *Color effects of the quasi-homogeneous linewidth for the CD samples. Both thionin with α-CD (white squares) as well as thionin with β-CD (black triangles) show qualitatively the same color effect as free thionin (black circles): Two regions of increasing linewidth with wave number are intersected by an intermediate region of dropping linewidth. The broadband absorption spectra for all samples are shown in the background.*

The experiments for the determination of the quasi-homogeneous linewidth were repeated for burning wave numbers all over the inhomogeneous absorption band. In Fig. 7.7, the results for the CD samples are shown in comparison to the

previously presented results for free thionin. First of all, the two steps in the trend of the linewidth can be found for thionin mixed with either of the CDs as well. The intermediate region between 16300 and 16450 $^{-1}$ shows a decrease of the linewidth with wave number at about the same rate for each of the samples. Furthermore, the tautomers can be found in the CD samples as well because the linewidth increases along the course of the particular inhomogeneous absorption bands in a similar fashion.

However, for both α- and β-CD, the values of the quasi-homogeneous linewidth are reduced and the increase in linewidth as the burning laser is tuned to the blue is not as pronounced as for free thionin. Hecht *et al.* [121] explained the rather unexpected color effect with ion-dipole couplings of thionin with surrounding two-level systems (TLS). For thionin with either CD this behavior still prevails, but the efficiency of the coupling is diminished. When thionin engages with CD in some way to form a supramolecular complex the solvent molecules have to rearrange around the chromophore. On one hand the solvent accessibility to thionin is restricted to the part of thionin that is not engaged with a CD, while on the other hand the binding geometry is optimized towards maximum coupling strength between CD and thionin. This leads to two different effects. First, the overall coupling strength between thionin and the remaining TLS is weakened lowering the homogeneous linewidth in general. And secondly, due to the lowered density of TLS around the thionin shielded by CD the possibilities for flipping a TLS are more limited leading to only a moderate color effect in comparison to free thionin.

Between α- and β-CD the differences are however small. Note that the linewidth experiments are only able to tell something about the existence of the formation of a supramolecular complex, but not the exact shape. There may very well be different configurations for α- and β-CD that lead to the same solvent accessibility.

7.5 Pressure Tuning Spectroscopy

To be able to estimate whether thionin can be incorporated within the CD cavity, pressure tuning spectroscopy was used to estimate the local compressibilites around the chromophore. Fig. 7.8 depicts an example for a pressure tuning experiment, in this case for thionin with β-CD. In Fig. 7.8 (b) several holes for various values of the isotropic pressure can be seen – they shift to the blue as the pressure is increased. Fig. 7.8 (a) shows the perfectly linear dependency of this shift according to the pressure. The experiments for α-CD were conducted in a similar fashion and yielded comparable results.

7.5.1 α-Cyclodextrin

For α-CD the color effect is presented in Fig. 7.9. It is quite obvious that there is no significant difference between free thionin and thionin with α-CD. The course of the increase in pressure induced hole shift is nearly identical for both samples and the values for the slopes, the local compressibilities, are the within the expected error margin the same for both tautomers. The fact, that the overall

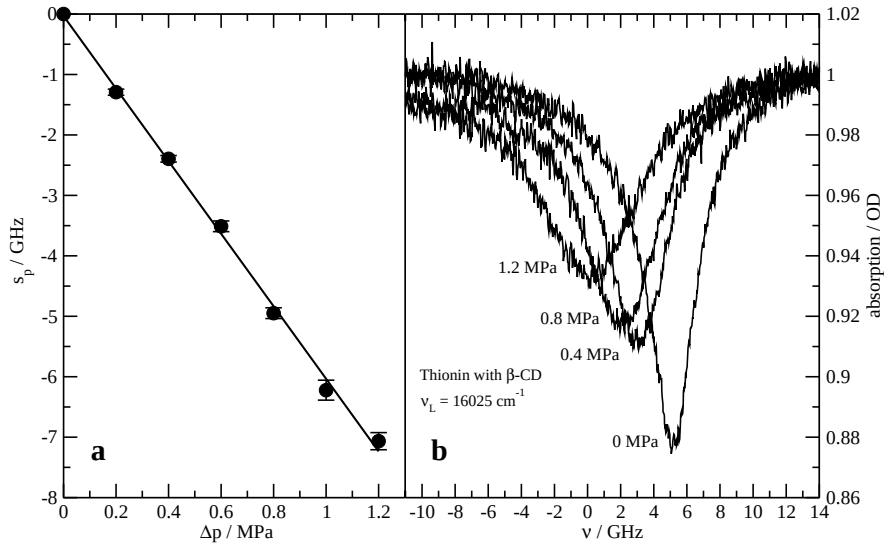

Figure 7.8: *Pressure tuning of thionin with β-CD at a burn wave number of 16025 cm^{-1}. (a) shows the linear dependency of the pressure shift of the hole center s_p with increasing pressure Δp. (b) shows some example spectra for increasing pressure.*

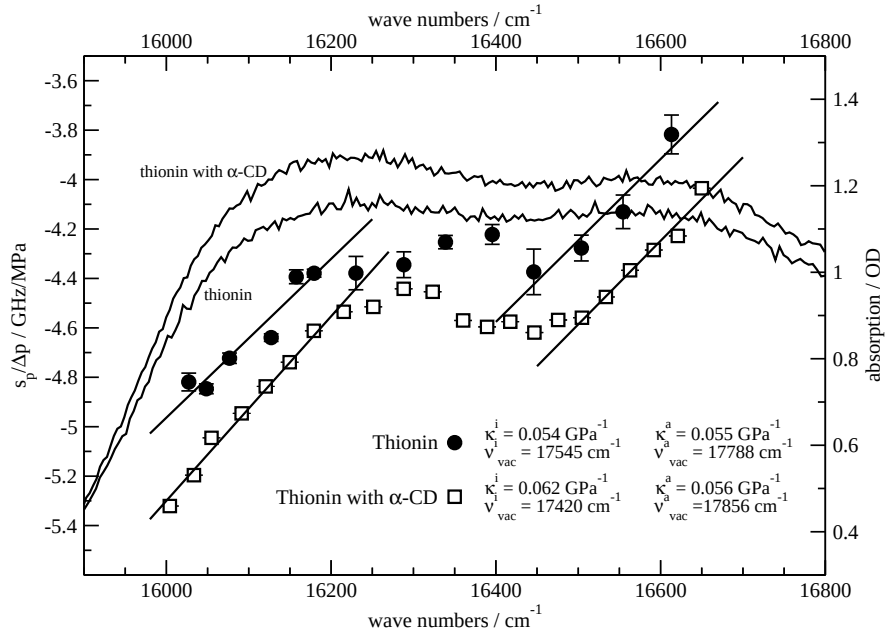

Figure 7.9: *Color effects in pressure tuning of thionin with α-CD. Similarly to thionin the increase of the hole shift per unit of pressure $s_p/\Delta p$ is constant for each of the inhomogeneous tautomer absorption bands with a region of constant $s_p/\Delta p$ in between. The values for the compressibility κ are nearly the same for free thionin and thionin with α-CD.*

pressure shifts are larger for thionin with α-CD can be attributed to a slightly blue shifted vacuum frequency, possibly due to a change in hydrogen bonding compared to free thionin. This shift can not be affected by pressure because of the rigidity of the hydrogen bonding network made up by α-CD, so the overall

absorption spectrum remains unchanged.

It is noteworthy, that the quasi-homogeneous linewidth for thionin with α-CD differs a lot from the one of free thionin, whereas the compressibility appears to be the same. In fact, thionin does form some kind of complex with α-CD – due to sterical reasons it is just not able to slip inside the cone and replace the water molecules inside. Therefore, the compressibility does not change, but the homogeneous linewidth which depends on the individual structure of the surrounding solvent molecules does.

Although thionin is a charged molecule it is fairly hydrophobic. This is documented by the experimental evidence that thionin is hardly soluble in cold water but easily soluble in hot water. Generally, hydrophobic molecules are favorable guests in the hydrophobic interior of the CD cone: The previously very loosely bound water molecules inside the CD get pushed out by more hydrophobic guests so that the solvation energy is lowered. However, the cavity diameter of α-CD is with around 5 Å (*cf.* Table 7.1) too small to host a thionin molecule of roughly the same width. The thionin molecules will just cling to the outside of the α-CD molecules unable to supersede the water molecules in the CD cavity.

On the other hand the hydrophobicity is antagonized by the strong ion-dipole interactions between the charged thionin and the solvent molecules. Just like in the case of the free thionin any hydrophobically ordered structure around the chromophore can not be stabilized, thus displaying the same local compressibility for both samples.

7.5.2 β-Cyclodextrin

Guo *et. al.* already showed experimentally and theoretically that phenothiazine derivatives can be incorporated within β-CD [174]. The geometrical dimensions of β-CD and thionin fit very well together: The inner diameter of the cone is about 1 Å larger than the width of the thionin molecule. The chromophore can therefore be expected to displace water molecules from the cavity of β-CD and orient itself with the long axis along the rotational symmetry axis of the host. Various quantumchemical calculations showed that the homocyclic central aromatic moiety will be able to penetrate to about half its length into the inside of the CD cone.

Fig. 7.10 shows the pressure tuning data for thionin with β-CD in comparison with free thionin. Unlike for thionin with α-CD the parameters for the β-CD sample are quite different. Although the typical z-shaped distribution of data points that indicates the presence of two independent tautomeric states of thionin remains unchanged, the slope of the increase of the pressure induced hole shift $s_\mathrm{p}/\Delta p$ is larger than for the free chromophore. The data points are more scattered for the amino band, but the values for the compressibilities κ are similar for both tautomer bands. With a magnitude of approximately $0.094\,\mathrm{GPa}^{-1}$ they are by over 70% larger than the compressibilities for free thionin which are about $0.055\,\mathrm{GPa}^{-1}$. As a consequence the vacuum frequencies ν_vac for thionin with β-CD are about $450\,\mathrm{cm}^{-1}$ smaller than the respective

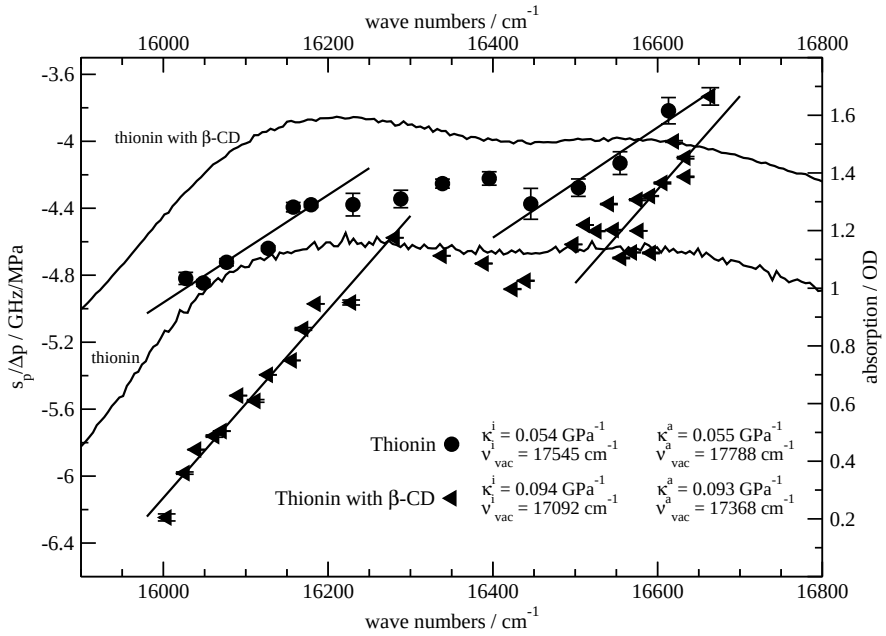

Figure 7.10: *Color effects in pressure tuning of thionin with β-CD. Similarly to thionin the increase of the hole shift per unit of pressure $s_\mathrm{p}/\Delta p$ is constant for each of the inhomogeneous tautomer absorption bands with a region of constant $s_\mathrm{p}/\Delta p$ in between. The values for the compressibility κ are enhanced by a factor of about 1.7 for thionin with α-CD in comparison to those of free thionin.*

frequencies for free thionin.

The most surprising observation is the increase in compressibility. β-CD is a very rigid and stable molecule – a guest molecule within the cavity should be shielded very well against pressure from the outside and the local compressibility of a chromophore should be smaller than in its free state. This can be seen from the changes in the vacuum frequencies: The solvent shift $s_0 = \nu_0 - \nu_\mathrm{vac}$ is for the β-CD sample by about $450\,\mathrm{cm}^{-1}$ smaller than for the free chromophore. When the chromophore forms a supramolecular complex with β-CD it gains interaction energy and the excitation shifts to the red. However, due to the rigidity of the caging complex this solvent shift can not be influenced by pressure, so the vacuum frequency is shifted to the red by the same value. On the contrary, the interaction with the solvent molecules is greatly reduced because the solvent molecules are being kept out of the hydrophobic interior of the β-CD cone. This causes a blue shift which can be influenced by pressure. Concerning the absorption energies those two different contributions cancel each other out, so that the overall spectral position for thionin embedded in the β-CD cavity remains unchanged with regard to the free chromophore.

When considering the β-CD only, the compressibility should decrease because it is much more difficult to compress the rigid CD structure. But the compressibility measured by pressure tuning in hole burning spectroscopy is a local parameter dependent on the local environment. This immediate surrounding of the chromophore gets changed drastically upon embedding the guest molecule in the CD

cavity. While the water molecules get displaced from the cavity itself, the outside of the CD cone as a hydrophilic surface attracts more solvent molecules. For the thionin being only partially inside the CD cone this means there is a large gradient in solvent density along its long axis. Furthermore, the planar thionin molecule in the annular CD opening allows for small spaces next to the aromatic rings that will initially not be occupied by water molecules due to the hydrophobic repulsion. Upon exertion of pressure, however, the displacement of the molecules at the outside of the CD cavity will be larger than for solvent molecules around a free thionin molecule, because they can slip into the void spaces inside the cone. The hydrophobic effects can only partially counteract the density gradient in this case. Although the β-CD is rigid by itself the solvent molecules that experience very large displacements are responsible for the dispersive interactions with the thionin, the main cause for pressure induced hole shifts. For this reason the local compressibility does not map the stability of CD but rather the ability of solvent molecules to penetrate the hydrophobic inside of CD when it is coordinated with a guest molecule.

7.6 Summary

Pressure tuning spectroscopy is a formidable tool to uncover structural details in the complexation of smaller guest molecules within CD [175]. Most importantly, those details can often not be detected when using conventional absorption spectroscopy. In the experiments at hand neither the absorption spectra nor the vibrational spectra showed any indication of the formation of a supramolecular complex. First of all, the local compressibility is a good parameter to estimate whether a probe molecule can be incorporated into the CD cavity. Secondly, it can also be used to evaluate the behavior of the solvent in the immediate vicinity of the complex. Depending on the space the guest molecule occupies within the CD cone the local compressibility can even increase when solvent molecules find small voids to fill up inside CD. A high compressibility can be used as indicator how well the complex partners match. A very interesting application might be a controlled separation of the guest molecule from the cavity by external pressure.

For the presented experiments, α-CD is not found to form inclusion complexes with thionin due to steric hindrances. β-CD on the other hand is large enough to contain the thionin moiety at least partly, regardless of the conformation. Although there are no differences in the broadband absorption and the formation of satellite holes, the local compressibility and the vacuum frequencies displayed differences. The vacuum frequencies for thionin in β-CD shifted to the red – a sign for the mechanical rigidity of the β-CD structure. The compressibilities, however, increased for both thionin tautomers. This can be explained by a large gradient in solvent density along the guest molecule and the subsequent increase in displacement of solvent molecules in the immediate vicinity of the chromophore.

A good theory is like a good joke: It is short and the last line is quite unexpected.

Harold Friedman

Chapter 8

Stark Spectroscopy of Phycocyanines

Photosynthesis is nature's main way of providing plants and bacteria with the energy they need to survive. Every photosynthesis system relies on capturing the sunlight in molecular excitations, guiding the energy as fast as possible through a transfer chain to the reaction center and inducing photochemical reactions that can be used to synthesize energy storing molecules. To that end very efficient chromophores adapted to the spectrum of the sunlight need to be employed. The most prominent example is chlorophyll – a chromophore bound to light-harvesting complexes of green plants and photosynthetic bacteria.

The protein provides the optimal environment for the chromophore with regards to photostability, longevity, energy transfer and spatial localization at the thylakoid membrane. However, chlorophyll has two main absorption bands in its spectrum: The Soret band with an absorption between 400 and 500 nm and the Q_y band with an absorption between 600 and 700 nm. In the spectral range between 500 and 600 nm chlorophyll can not absorb light efficiently and therefore appears green in color.

Especially under water the main contribution to the overall spectrum of sunlight lies in this region – plants living under water like algae or submarine bacteria need to employ a different system to viably run photosynthetic processes. Already in the first half of the 19^{th} century submarine cyanobacteria, red and blue algae were investigated for their abundance of blue and red chromophores. Those dyes were found to be covalently bound to the so-called biliproteins, named after their first discovery in mammal bile. As research progressed several different types of biliproteins containing various chemically related dyes, the bilins, were discovered and classified. The compilation of biliproteins varies from organism to organism, depending on their natural habitat and the adaption to the most efficient photosynthesis.

One of the more popular and better investigated cyanobacteria is *Mastigocladus laminosus*. Its specific compilation of biliproteins, the phycobilisome, is shown in Fig. 8.1. The central unit is made up of a stack of three hemidiscoidally aligned allophycocyanines. Antenna of phycocyanine and phycoerythrocyanines stacks are attached to the core via linker polypeptides. The prefix *c* denotes the origin of

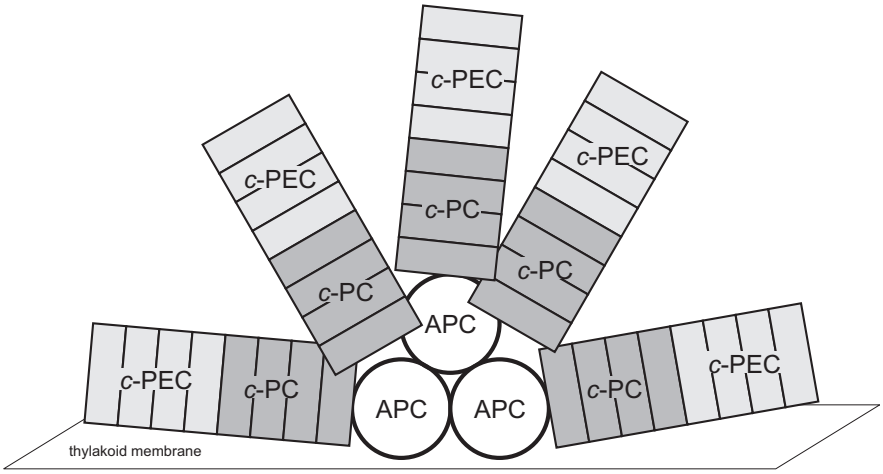

Figure 8.1: *The schematic structure of the phycobilisome in Mastigocladus laminosus [176]. The central core is made up of allophycocyanines (APC). Attached to the core are antennas consisting of stacks of phycocyanine (c-PC) and phycoerythrocyanine (c-PEC).*

the biliproteins, in this case cyanobacteria. *c*-Phycocyanine is one of the antenna pigments responsible for gathering light energy and directing it to the central allophycocyanine core.

8.1 *c*-Phycocyanine

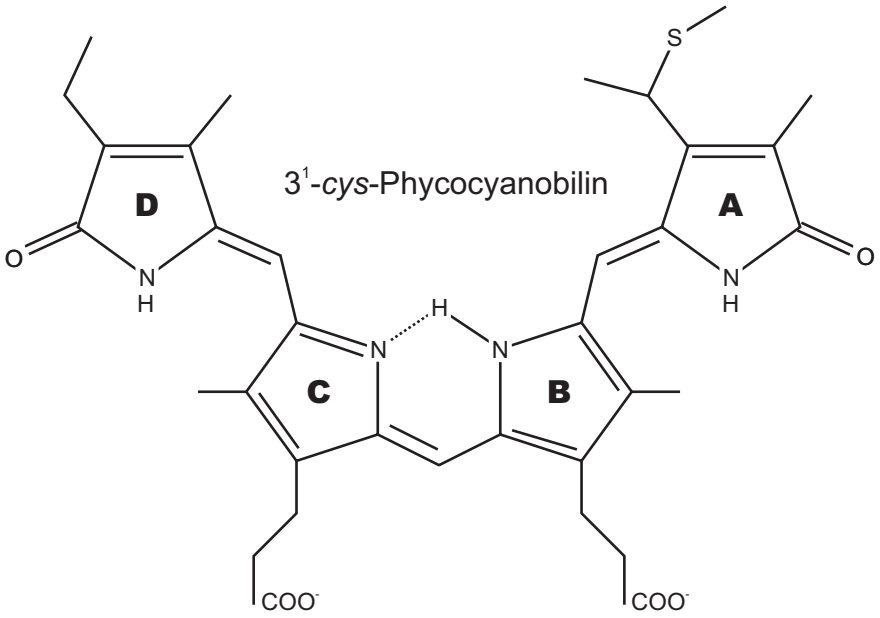

Figure 8.2: *The chemical structure of the chromophore 3^1-cys-phycocyanobilin. It consists of four pyrrole rings labeled A to D, beginning from the protein near aromatic ring. The chromophore is bound over a thio-ether bridge to cysteines within the c-phycocyanine.*

While the existence and function of *c*-phycocyanine (c-PC) was known long before, its exact structure could only be resolved in 1985 by X-ray crystallography [177]. It was found that the protein consists of two subunits, α and β. The α-subunit carries only one chromophore, while the β-subunit contains two chromophores [178]. All of the chromophores are of the same type called 3^1-*cys*-phycocyanobilin (PCB) – the chemical structure is shown in Fig. 8.2. Like most bilins it is a tetrapyrrole chain with modifying prostethic side groups altering the spectral absorption bands and adjusting it to the desired maximum absorption wavelength.

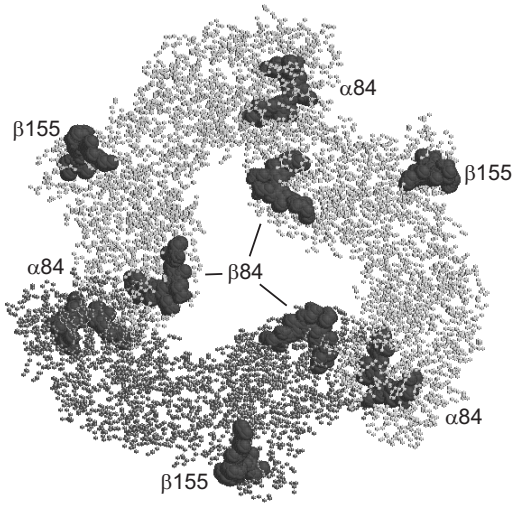

Figure 8.3: *The ball and stick model of a c-phycocyanine trimer. The monomers are colored in different shades of grey with the phycocyanobilins given in spacefill presentation. Each monomer consists of two subunits: The α-subunit contains only one chromophore at amino acid position 84, while the β-subunit contains besides the chromophore 84 a second chromophore in an outer loop at amino acid position 155.*

Under certain circumstances c-PC can form trimers. Three monomers aggregate to build a toroidal structure which can stack to hexamers. Fig. 8.3 shows such a trimer in a coarse model. The nine chromophores are marked dark grey and are denoted with the name of the subunit they belong to and the number of the amino acid residue they are bound to. The bilin dyes will bind via a thio-ether bridge to cysteine residues 84 and 155. In a monomer energy transfer between the different bilins is possible, due to their spatial proximity and the associated Förster radii. For a trimer the energy transfer processes get even enhanced because chromophores of neighboring monomers get to lie within close range to each other. It has been proven with femtosecond laser spectroscopy and quantumchemical Förster transfer calculations that especially the transfer between α84 PCB and β84 PCB of an adjacent monomer subunit is very efficient [179–181], because their intermolecular distance is only about 21 Å. The distance between the β84 PCB and β155 PCB in a monomer is with 34 Å much larger in comparison [182].

PC in general is an interesting protein for hole burning studies because it contains an intrinsic chromophore that absorbs in the visible region and can undergo photochemical transitions upon excitation [47, 56, 183]. The possibility to prepare the subunits, the monomers and the trimers in separate samples gives rise to comparative experiments with regards to spectral color effects in the homogeneous linewidth and the dipole moments.

8.2 Absorption Spectra

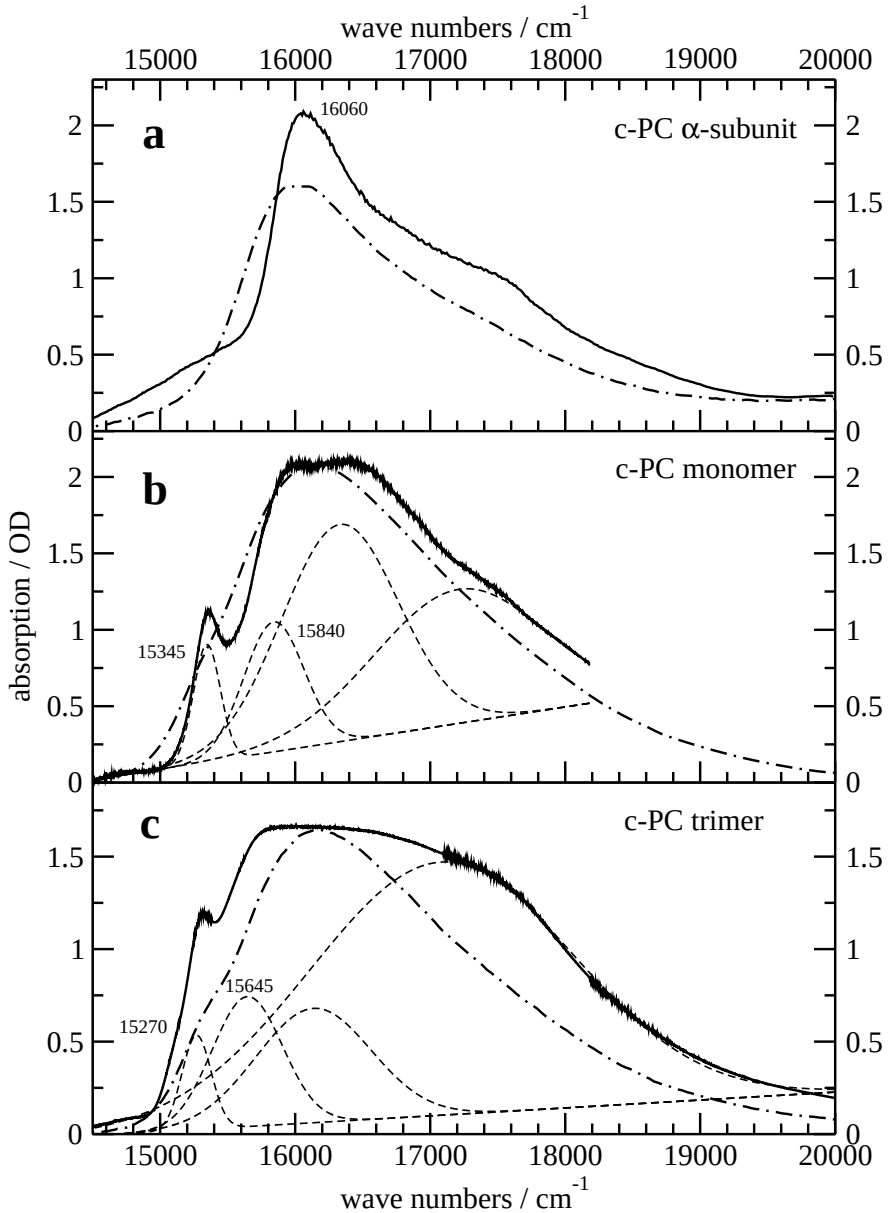

Figure 8.4: *The room temperature (dot-dashed line) and low temperature (continuous line) absorption spectra of the α-subunit (a), the monomer (b) and the trimer (c) of c-phycocyanine in a glycerol/water glass. For the monomer and the trimer four Gaussian lines on a linear background have been fitted to the spectra. In each spectrum the main peaks are denoted with the respective wave numbers of their centers.*

Fig. 8.4 shows the low temperature broadband absorption spectra of the α-subunit (a), the monomer (b) and the trimer (c) of *c*-phycocyanine in a glycerol/water glass at $T = 2\,\mathrm{K}$. The spectrum of the α-subunit does not deviate very much from the room temperature spectrum shown with a dot-dashed line. The two main absorption bands at 16060 and around $17500\,\mathrm{cm}^{-1}$ experience a slight blue shift but the overall structure remains the same. For both the monomer and the trimer, however, the main peak at around $16100\,\mathrm{cm}^{-1}$ splits in two seperate peaks, one slightly red, the other slightly blue shifted. Moreover, a prominent side band at the red shoulder of the main peak appears at around $15300\,\mathrm{cm}^{-1}$ for both the monomeric and the trimeric c-PC.

The room temperature spectrum of the α-subunit in a glycerol/water glass appears to be the same as in a pure aqueous environment. As expected upon freezing there is no band split to be observed, because only one chromophore ($\alpha 84$) is contributing to the absorption band. But for the sample in glycerol/water the main peak is hypsochromically shifted by about $60\,\mathrm{cm}^{-1}$ whereas low temperature spectra of the α-subunit dissolved in water shift approximately $100\,\mathrm{cm}^{-1}$ to the red [184]. This may be explained by the changed solvent accessibility of the chromophore depending on the solvent polarity. Homoelle and Beck showed that upon decreasing solvent polarity the tertiary protein structure of the α-subunit can be changed allowing the chromophore a better access to solvent molecules [185]. Adding a less polar solvent like glycerol to an aqueous solution of c-PC causes configurational changes in the $\alpha 84$ chromophore – the strong decrease in fluorescence yield and the concomitant drop in absorption intensity of the visible band suggest the formation of a cyclic state of PCB. Much like a chromophore in a denatured protein, this porphyrinlike configuration absorbs stronger in the UV than in the visible spectral region [186]. Moreover, PCB is loosened in its protein pocket, thus allowing new paths for radiationless decay and lowering the fluorescence. The chromophore gets exposed to the bulk solvent reducing its strong coupling with the electron transfer states in the protein environment itself, thus shifting the absorption band to the blue.

For the monomer and the trimer there is a band splitting visible, as could be expected from a multi-chromophore protein. In contrast to c-PC in a pure water solvent there is an additional shoulder at around $15345\,\mathrm{cm}^{-1}$ for the monomer and around $15270\,\mathrm{cm}^{-1}$ for the trimer. Comparison with spectra of mutated c-PC where the $\beta 155$ PCB is missing suggest that the blue peak at $16400\,\mathrm{cm}^{-1}$ in the monomer spectrum can be assigned to $\beta 155$ PCB [184]. Along with the existence of a broad band at wave numbers above $16500\,\mathrm{cm}^{-1}$, the red shoulders indicate that depending on the solvent accessibility the $\alpha 84$ and $\beta 84$ chromophore display various configurational states.

8.3 Homogeneous Linewidth

Homogeneous linewidth experiments have been conducted in all of the samples. Evidently the red shoulder found in the monomer and the trimer sample may be ascribed to electronic origins since narrow holes could be burnt in either of

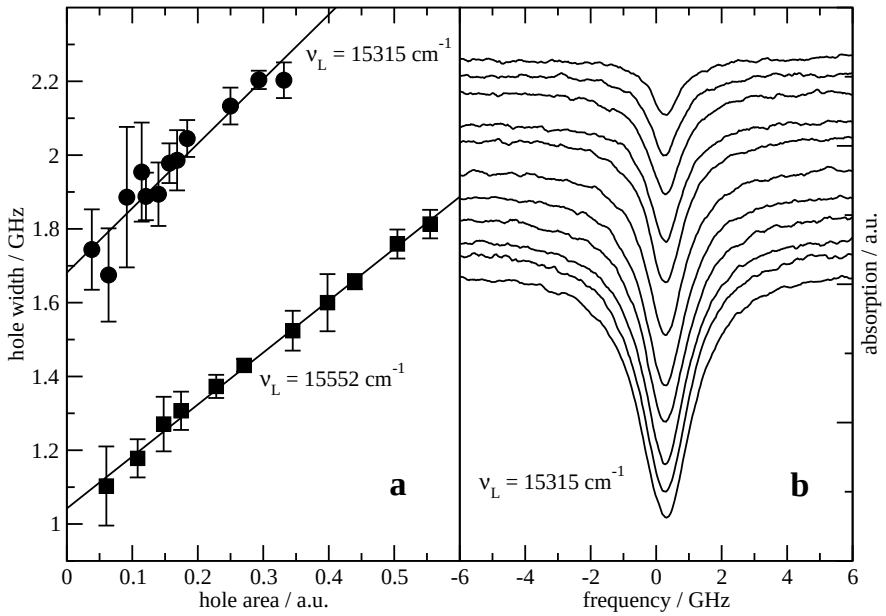

Figure 8.5: *An example for the measurement of the homogeneous linewidth in the c-PC trimer. (a) shows the linear extrapolation of the linewidth to zero hole area for two different burning wave numbers ν_{L} yielding two different cutoffs at the y-axis. (b) shows the respective hole spectra for $\nu_{\mathrm{L}} = 15315\,cm^{-1}$. Burning times increase from top to bottom. The spectra are offset for reasons of clarity.*

the two redmost bands. Fig. 8.5 shows an example of such an experiment: In (b) the successively scanned spectra with increasing burning time are shown, in (a) the line width is plotted against the hole area for two distinct burning wave numbers. The measurements for the monomer and the α-subunit were conducted in a similar manner.

Fig. 8.6 shows the color effects for the three samples. The hole burning range was limited by the optical setup on the far red edge and the disappearance of sufficiently deep zero-phonon holes on the far blue edge.

The α-subunit shows a uniform trend in its color effect. Along the red edge of the main absorption peak the quasi-homogeneous linewidth increases with the burning wave number in a linear way. Similarly to chapter 5 the total color effect C_{t} and the differential color effect C_{d} can be evaluated. With a value of 1.4 GHz at the base of the absorption band and a value of 2.2 GHz at the band maximum C_{t} amounts to -0.36 and C_{d} to $1.37 \cdot 10^{-3}/\mathrm{cm}^{-1}$. Those values are on the same order as the respective values for thionin (*cf.* chapter 5). The color effect is on the same order of magnitude as for BODIPY, but displays the an unexpected trend of increasing linewidth with excitation wave number. This seems rather sensible, because just like thionin PCB exists in its protonated form when bound to c-PC [56]. As mentioned before, in a glycerol/water glass with over half of the solvent molecules being less polar molecules than water α84 is very exposed to the solvent. Thus, the same criteria as for thionin apply in this case: The charged chromophore induces a large ion-dipole coupling with the solvent molecules in its surrounding. Yet those interactions will not contribute to the solvent shift

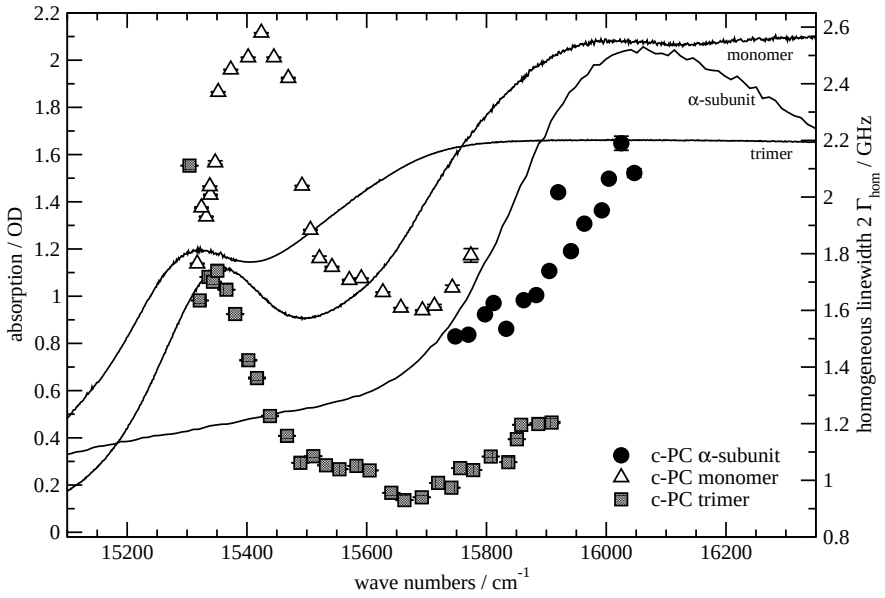

Figure 8.6: *Color effect of the homogeneous linewidth in the c-PC α-subunit, the c-PC monomer and the c-PC trimer. The linewidth for the α-subunit (black circles) shows a linear increase with wave number along the red edge of the inhomogeneous absorption spectrum. The patterns for the monomer (open triangles) and the trimer (shaded squares) display a large increase in the spectral region between the redmost peak and the main absorption bands. The inhomogeneous low temperature absorption spectra for each sample are shown in the background.*

because the charge does not change upon excitation to a higher electronic state. The solvent shift seems to be mainly caused by dispersive interactions, so the molecules with a strong dispersive interaction with the surrounding will be found at the red edge of the inhomogeneous absorption band. Those dyes will experience a larger shielding of their Coulomb field due to the better alignment of solvent dipoles. Spectral diffusion processes like a flipping of a TLS will hence have a lesser impact on the ion-dipole coupling for chromophores with strong dispersive interactions. Accordingly, the homogeneous linewidth will be lower for chromophores on the red edge of the inhomogeneous absorption band. Dipole-dipole interactions are considered to only play a minor role in the solvent shift, because the dipole moment differences of PCB do not change significantly over the inhomogeneous absorption band and are thus not able to evoke spectral color effects.

For the monomer the pattern seems more complicated: At the red edge of the absorption band at $16000\,\mathrm{cm}^{-1}$ the linewidth is similar to the α-subunit. In the region between this band and the redmost shoulder there is a rapid increase, coming to a maximum which has an about 60% larger homogeneous linewidth. After that the values drop again when the burning wave number is tuned over the peak of the shoulder and into its red edge. Obviously the maximum in the homogeneous linewidth coincides with the best overlap between the two redmost inhomogeneous absorption bands. That means that the linewidth is a direct evidence of the energy transfer occurring between the chromophores making up

the absorption bands.

The situation in the trimer sample is analog: A steep increase with decreasing wave number coincides with the overlap of the red absorption shoulder and the red edge of the main absorption band. However, for the trimer sample the decrease at the red edge of the absorption shoulder can not be seen due to technical limitations of the experimental setup. A common feature for both monomer and trimer is the positive gradient in the linewidth when tuning the burning wave number towards the maximum of the absorption peak at around $16000\,\mathrm{cm}^{-1}$. In this region the samples show the same behavior as the α-subunit. Interestingly, the overall values of the data points for the trimer and the monomer differ by a factor of about 1.6. This applies to all spectral regions – up to now it is still unclear what the cause for the discrepancy is.

8.4 Stark Spectroscopy

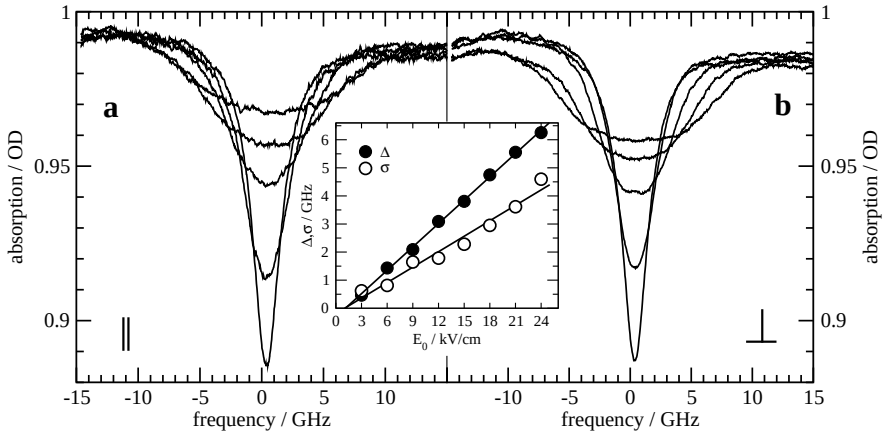

Figure 8.7: *An example for a Stark effect experiment in the c-PC α-subunit. (a) and (b) show the hole spectra for a hole burnt at $\nu_\mathrm{L} = 15930\,cm^{-1}$ in parallel and perpendicular polarization geometry, respectively. In (b) the holes slightly flatten with increasing external field strength indicating a hole splitting, which is relatively small compared to the broadening. The inset shows the fitting values for the hole splitting Δ and the hole broadening σ and the linear dependency on the field strength.*

Stark effect experiments were conducted for all three samples. Fig. 8.7 shows the respective results of a single burning position for the α-subunit, Fig. 8.7 the results for the c-PC trimer. For each series of measurements the hole splitting was very weak and occurred in the perpendicular polarization geometry. The angle θ between the fixed dipole moment difference $\Delta\mu_\mathrm{fix}$ and the transition dipole moment μ_fi was in every case around 55°, the angle at which both parallel and perpendicular polarization yield the same spectra because the splitting distributes evenly over the different experimental geometries. Under these conditions it is very hard to get reliable results for the fitting procedure because the broadening of the holes covers up the splitting. The insets of the diagrams in Fig. 8.7 and Fig. 8.8 show the fitted values for the hole splitting and the hole broadening dependent

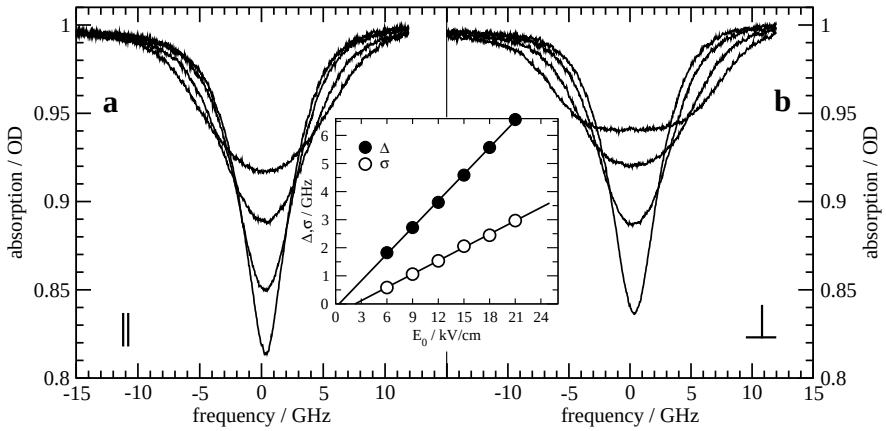

Figure 8.8: *An example for a Stark effect experiment in the c-PC trimer. (a) and (b) show the hole spectra for a hole burnt at $\nu_L = 15310\,cm^{-1}$ in parallel and perpendicular polarization geometry, respectively. In (b) the holes slightly flatten with increasing external field strength indicating a hole splitting, which is relatively small compared to the broadening. The inset shows the fitting values for the hole splitting Δ and the hole broadening σ and the linear dependency on the field strength.*

on the field strength. A linear regression for the data points results in the fixed and induced dipole moment differences scaled by the Lorentz factor f.

8.4.1 α-Subunit

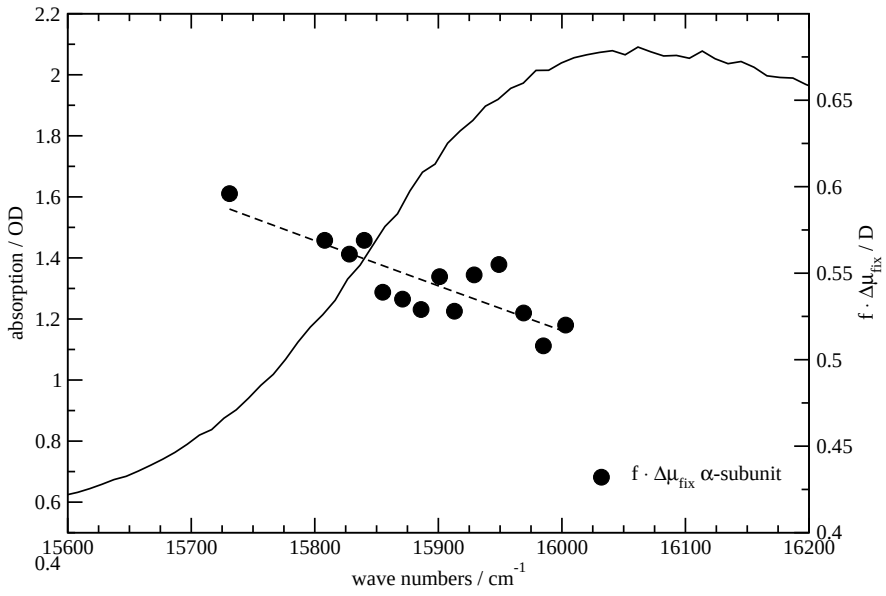

Figure 8.9: *Color effect in the Stark splitting for the c-PC α-subunit. The data points (black circles) show the hole splitting modified by the Lorentz factor; the dotted line is a guide for the eye. The inhomogeneous low temperature absorption spectrum is shown in the background.*

In Fig. 8.9 the color effect in the Stark experiments for the α-subunit is given. The data points represent the measured hole splittings calculated back to the

mitigated fixed dipole moment difference $f \cdot \Delta\mu_{\text{fix}}$. Two things are very obvious in this diagram: First of all, there is a slight uniform decrease in $f \cdot \Delta\mu_{\text{fix}}$ with rising burning wave number. And second, the overall values are only around 0.5 D which is much less than quantumchemical calculations would suggest. Simulations for the $\alpha 84$ chromophore in phycoerythrocyanin, a dye very similar to PCB, yield a ground state intrinsic dipole moment of about 25 D [187]. The expected dipole moment differences are much larger than the actually obtained experimental results.

This means that the polarity of the probe inside the protein is reduced in large parts. A main reason for this effect is the abundance and impact of charge transfer states that mix locally with the excited states of the PCB. Neighboring amino acid residues are known to donate electrons to the chromophore especially the protonated nitrogen atoms in the pyrrole rings [187, 188]. The mixing of the charge transfer dipole moments obviously leads to a strong adaptation of the dipole moments in the ground and excited state, resulting in a rather strong reduction of the Stark effect. Effectively, the probe molecule appears to be a kind of supermolecular complex: The charge transfer states superimpose dipole moments on the fixed dipole moment of the chromophore itself, thus reducing the overall dipole moment to a very small value.

A second crucial factor is the high local order of the protein environment in the immediate vicinity of the chromophores. The arrangement of the chromophores at the protein binding sites seem to be structurally determined within narrow margins. This hampers the distinction between induced and fixed dipole moment differences because the field of an ordered crystal can induce a well defined dipole moments. It is very likely that those directed induced dipole moment differences are on the same order of magnitude as the fixed molecular dipole moment difference, but in an antiparallel orientation. This would mean that in spite of a large fixed dipole moment difference the hole splitting would stay small.

For the experiments at hand those circumstances seem to be true, so that a determination of the Lorentz factor, which would reveal interesting insights in the dielectric constants within proteins, is not feasible.

8.4.2 Monomer and Trimer

The results for the monomer and the trimer are given in Figs. 8.10 and 8.11 respectively. Additionally to the scaled fixed dipole moment differences $f \cdot \Delta\mu_{\text{fix}}$, which are represented with shaded symbols, the random induced dipole moment differences $f \cdot \Delta\mu_{\text{ind}}$ are shown with open symbols. The lines in the diagrams are merely guides for the eye and do not resemble an actual fit.

For both the monomer and the trimer experiments the results show the same pattern: In the red absorption shoulder $f \cdot \Delta\mu_{\text{fix}}$ is fairly large in comparison to the values when tuning the laser to higher wave numbers and into the main inhomogeneous absorption band. $f \cdot \Delta\mu_{\text{ind}}$ is small when burning holes into a single band but rise to larger values when the burning wave number is cho-

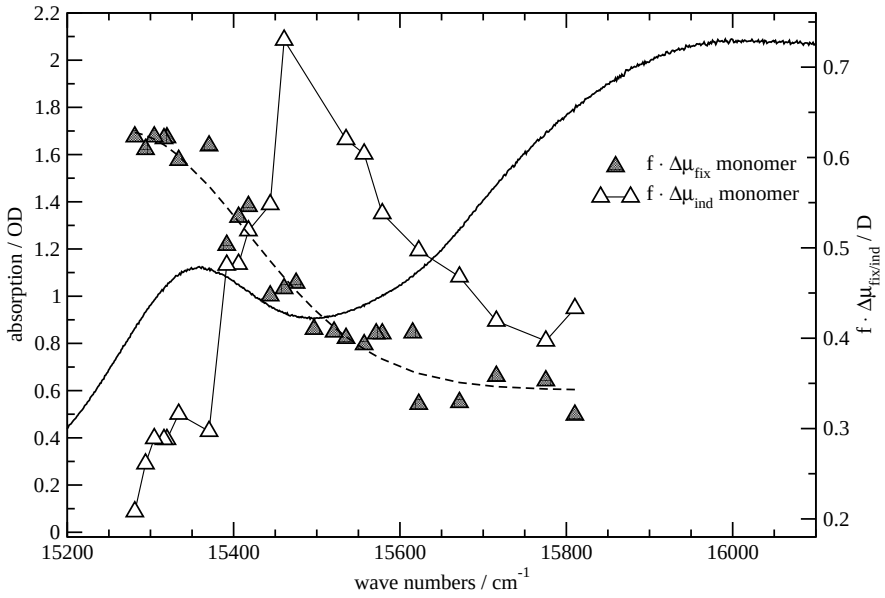

Figure 8.10: *Color effect in the Stark splitting and broadening for the c-PC monomer. The data points show the hole splitting (shaded triangles) and broadening (open triangles) modified by the Lorentz factor; the dotted line and the line connecting the broadening data points are guides for the eye. The inhomogeneous low temperature absorption spectrum is shown in the background.*

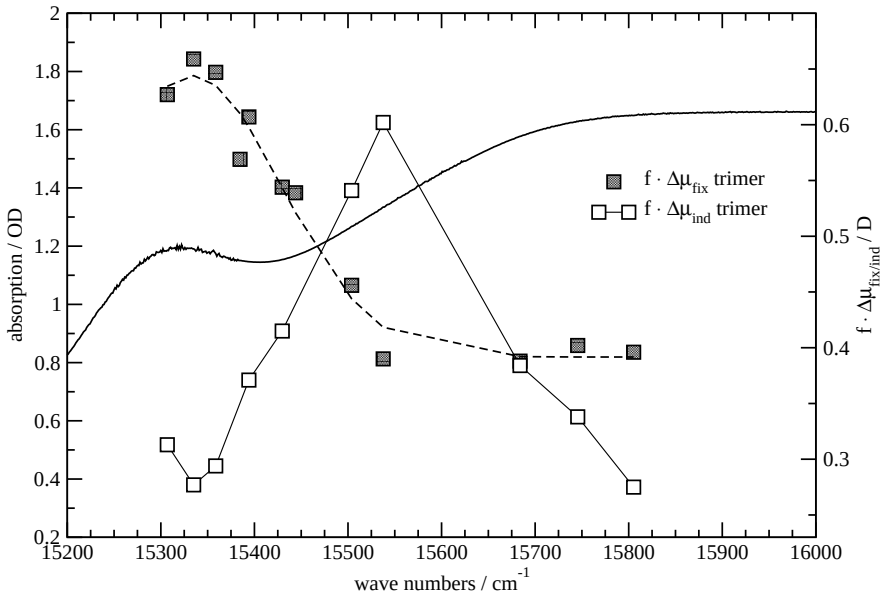

Figure 8.11: *Color effect in the Stark splitting and broadening for the c-PC trimer. The data points show the hole splitting (shaded squares) and broadening (open squares) modified by the Lorentz factor; the dotted line and the line connecting the broadening data points are guides for the eye. The inhomogeneous low temperature absorption spectrum is shown in the background.*

sen in an intermediate region where the inhomogeneous absorption bands overlap.

First of all, it is important to not that for the monomer as well as the trimer there are multiple chromophores involved in the formation of holes. Sauer and Scheer suggested that especially for the trimer excitonic coupling between the distinct chromophores in the different subunit should occur [179]. However, in the trimer with its three-fold symmetry the nonaxial dipole moments should cancel out leaving only a dipole moment – and therefore dipole moment differences – oriented along the symmetry axis of the protein. Regardless of the polarization geometry the splitting of holes should be of similar magnitude in every Stark experiment then. This is obviously not the case in the results, so coherent excitons will be ruled out for the discussion.

Generally, the number of different chromophores possibly contributing to holes vary with the burning wave number. While at the red edge of the redmost shoulder there is only one species of molecules, the blue edge overlaps with the red edge of the next absorption band further to the blue. Although the number of overlapping bands increases when tuning the wave number into the absorption band at $16000\,\mathrm{cm}^{-1}$, the hole burning efficiency decreases until it is not possible to burn persistent holes any longer when tuning to a wave number larger than $15900\,\mathrm{cm}^{-1}$. Due to a low Debye-Waller factor of PCB far in the blue, the number of possibly contributing chromophores decreases again in this region.

There are two models that may account for the observed spectral color effects in the dipole moment differences:

- Simultaneous, but independent excitation of energetically degenerate chromophores
- Resonant Förster transfer mechanisms between chromophores within the protein complex

Assuming, that each absorption band can be ascribed to chromophores at different binding sites, burning a hole at any given spectral position will excite degenerate molecules with deviations in the orientations of their dipole moment differences, depending on their location in the protein. The more species of chromophores are involved, the broader the distribution of those orientations effectively is. This is in line with the observation that the hole broadening is largest where the most chromophores are expected to contribute to the hole – in the spectral region between the two redmost bands. Further to the red as well as further to the blue, the number of configurationally different dye molecules is less and accordingly the distribution of the random induced dipole moment differences becomes smaller again. In this picture, the color effect of the hole splitting is simply a transition from one species of chromophores to another: The PCB at around $15300\,\mathrm{cm}^{-1}$ is bound to the protein in such a way, that the dipole moment decreasing effects of the charge transfer states have a lesser impact than in the band at around $15800\,\mathrm{cm}^{-1}$. The steady decrease of the fixed dipole moment differences is just an indicator for the relation of different chromophores involved.

The second model relies on energy transfer between chromophores to explain the effects. Previous measurements showed that resonant as well as non-resonant

energy transfer is very likely to occur within PC [179, 184]. For Stark effect experiments only the resonant energy transfer has to be taken into account, because non-resonant energy transfer will not alter the shape of holes under the Stark effect. In fact, very fast non-resonant energy transfer as proposed by Debreczeny *et al.* even inhibits the creation of persistent holes, which can be the case in the spectral region above $15900\,\mathrm{cm}^{-1}$ where hole burning becomes impossible. Apparently, for the red edge of the redmost absorption band, resonant energy transfer between chromophores does not occur because there is only one species to be excited. The energy transfer gets stronger, when tuning into the band at $15800\,\mathrm{cm}^{-1}$. Accordingly, the hole splitting and therefore the fixed dipole moment difference decreases, because after the resonant energy transfer the hole will consist of chromophores with all sorts of dipole moment orientations so that the anisotropic orientation, a prerequisite for any splitting, tends to smooth out. Of course, the energy transfer probability is highest if the dipole moments of the donor and the acceptor are aligned parallel, but in general an energy transfer is not forbidden even if the dipole moments are aligned perpendicular to each other.

This model is supported by the linewidth experiments – the increase in the quasi-homogeneous linewidth between the bands is a good indication for inner-molecular energy transfer. However, there are no differences between the results for the monomer and the trimer. This shows that resonant energy transfer only occurs within a monomeric unit, even for the trimer. Also the decrease in hole broadening when tuning the wave number from $15550\,\mathrm{cm}^{-1}$ towards $15800\,\mathrm{cm}^{-1}$ is explained with the linewidth model: The polarizability for chromophores in the red edge of the main absorption band is expected to be higher than in the blue edge, so the randomly induced dipole moments which scale with the polarizability decrease in the same fashion. The increase in the broadening for the region between $15300\,\mathrm{cm}^{-1}$ and $15550\,\mathrm{cm}^{-1}$ is again a sign of multiple chromophores contributing to the hole rather than a single one.

Currently, quantumchemical calculations are still in progress to gain further insight into the validity of either model. The difficulty here is to correctly incorporate the charge transfer states into the supermolecular chromophore complex. Recent work has shown that with suitable modeling of the surrounding amino acid residues the overall fixed dipole moments of PCB can be lowered drastically, just like the experimental findings suggest.

8.5 Summary

The biliprotein *c*-phycocyanin (c-PC) in a glycerol/water glass has been investigated for color effects in the homogeneous linewidth and the Stark effect. C-PC was prepared in three configurations: the α-subunit with a single chromophore, the monomer itself with three chromophores and the trimer, a toroidal structure of three combined monomers. The absorption spectra showed a prominent band splitting upon freezing only for the monomer and the trimer sample yielding distinct inhomogeneous absorption bands. Furthermore a shoulder appeared at the red edge of the absorption band, which was assigned to a red-shifted chromophore.

The homogeneous linewidth of the α-subunit showed the same pattern in the color effect that was observed for thionin. Because the chromophore is charged and due to rearrangements in the tertiary protein structure at least partially exposed to the solvent ion-dipole interactions are responsible for the increase in linewidth upon tuning the burning wave number to the blue. In the monomer and the trimer the homogeneous linewidth increases dramatically in the intermediate spectral region between the two redmost absorption bands. This can be explained by the optimized energy transfer between chromophores with overlapping absorption.

Stark effect experiments yielded overall small values for the hole splitting due to the supermolecular complex that the chromophores form with charge transfer states. The ordering of the chromophore environment creates a well defined induced dipole moment difference which counteracts the fixed dipole moment difference. The strong local ordering prevents reasonable estimations of the scaling Lorentz factor, because the fixed and induced dipole moments can not be distinguished in the hole splitting. Two models are in discussion for the observed spectral color effects in the monomer and the trimer: Excitation of degenerate dyes and resonant energy transfer. Both can explain the decrease of the hole splitting with increasing wave number. Furthermore, resonant energy transfer is found to only occur within a protein monomer because the spectral patterns of monomer and trimer do not significantly differ from each other. Theoretical calculations have to be conducted to provide further evidence for the validation of either model.

Parts of this work have been published:

- Christoph Hecht, Peter Hermann, Josef Friedrich, Cheng-Chung Chang, Ta-Chau Chang
  "Thionin in a cyclodextrin nanocavity: Measuring local compressibilities by pressure tuning hole burning spectroscopy"
  Chemical Physics Letters **413**, 335–341 (2005).

- Ta-Chau Chang, Yih-Peh Yang, Kai-Hsiang Huang, Cheng-Chung Chang, Christoph Hecht
  "Investigation of thionin-DNA interaction by satellite hole spectroscopy"
  Optics and Spectroscopy **98** (5), 655–660 (2005).

- Christoph Hecht, Markus Stübner, Josef Friedrich, Ta-Chau Chang
  "Investigation of probe solvent interactions: Color effects in optical line widths"
  Chemical Physics Letters **395**, 21–26 (2004).

- Christoph Hecht, Josef Friedrich, Ta-Chau Chang
  "Interactions of thionin with DNA strands: Intercalation versus external stacking"
  Journal of Physical Chemistry B **108**, 10241–10244 (2004).

The secret to creativity is knowing how to hide your sources.

Albert Einstein

Bibliography

[1] K. A. Sharp and B. Honig, Electrostatic interactions in macromolecules: Theory and applications, *Annual Reviews of Biophysics and Biophysical Chemistry*, 19:301–332, 1990

[2] N. K. Rogers, The modelling of electrostatic interactions in the function of globular proteins, *Annual Review of Biophysics and Biomolecular Structure*, 48:37–66, 1986

[3] C. Sagui and T. A. Darden, Molecular dynamics simulations of biomolecules: Long-range electrostatic effects, *Annual Review of Biophysics and Biomolecular Structure*, 28:155–179, 1999

[4] P. Auffinger and E. Westhof, Simulations of the molecular dynamics of nucleic acids, *Current Opinion in Structural Biology*, 8:227–236, 1998

[5] D. L. Beveridge and G. Ravishanker, Molecular dynamics studies of DNA, *Current Opinion in Structural Biology*, 4:246, 1994

[6] H. Kitano, Computational systems biology, *Nature*, 420:206–210, 2002

[7] F. Wang, W. B. Tan, Y. Zhang, X. Fan, and M. Wang, Luminescent nanomaterials for biological labelling, *Nanotechnology*, 17:1–13, 2006

[8] K. L. Holmes and L. M. Lantz, Protein labeling with fluorescent probes, *Methods in Cell Biology*, 63:185–204, 2001

[9] O. Krichevsky and G. Bonnet, Fluorescence correlation spectroscopy: the technique and its applications, *Reports on Progress in Physics*, 65:251–297, 2002

[10] A. B. Myers, Molecular electronic spectral broadening in liquids and glasses, *Annual Reviews of Physical Chemistry*, 49:267–295, 1998

[11] G. R. Fleming and M. Cho, Chromophore–solvent dynamics, *Annual Reviews of Physical Chemistry*, 47:109–134, 1996

[12] E. G. McRae, Theory of solvent effects on molecular electronic spectra. Frequency shifts, *Journal of Physical Chemistry*, 61:562, 1954

[13] N. S. Bayliss, The effect of electrostatic polarization of the solvent on electronic absorption spectra in solution, *Journal of Chemical Physics*, 18:292–296, 1950

[14] W. E. Moerner (ed.), *Persistent Spectral Hole Burning: Science and Applications*. Springer Verlag, Berlin, 1988

[15] M. Orrit, J. Bernard, and R. I. Personov, High-resolution spectroscopy of organic molecules in solids: From fluorescence line narrowing and hole burning to single molecule spectroscopy, *Journal of Physical Chemistry*, 97:10256–10268, 1993

[16] B. Kharlamov, R. I. Personov, and L. A. Bykovskaya, Stable "gap" in absorption spectra of solid solitons of organic molecules by laser irradiation, *Optics Communications*, 12:191–193, 1974

[17] B. M. Kharlamov, L. A. Bykovskaya, and R. I. Personov, Hole-burning spectra. A new method for obtaining fine structure in absorption spectra of organic molecules, *Chemical Physics Letters*, 50:407–411, 1977

[18] A. A. Gorokhovskiĭ, R. K. Kaarli, and L. A. Rebane, Hole burning in the contour of a pure electronic line in a Shpol'skĭ system, *JETP Letters*, 20:216–218, 1974

[19] J. Friedrich, *Methods in Enzymology*, volume 246. Academic Press, 1995

[20] M. Köhler, J. Friedrich, and J. Fidy, Proteins in electric and pressure fields: basic aspects, *Biochimica et Biophysica Acta – Protein Structure and Molecular Enzymology*, 1386(2):255–288, 1998

[21] S. Reul, W. Richter, and D. Haarer, Spectroscopic studies of the solute–solvent interaction in dye-doped polymers: frequency-dependent pressure shifts, *Chemical Physics Letters*, 180:1–5, 1991

[22] T. Sesselmann, W. Richter, and D. Haarer, Spectroscopic studies of impurity-host interactions in dye-doped polymers: Hydrostatic-pressure effects versus temperature effects, *Physical Review B*, 36:7601–7611, 1987

[23] M. Stübner, J. Friedrich, Y.-P. Yang, and T.-C. Chang, Using external field effects for elucidating specific features in dye-DNA-interactions, *Journal of Luminescence*, 98:153–161, 2002

[24] Y. P. Yang, T.-C. Chang, M. Stübner, and J. Friedrich, Influence of pressure on the spectral properties of dye-DNA supermolecules, *Journal of Physical Chemistry B*, 107:1458–1465, 2003

[25] L. Kador, S. Jahn, D. Haarer, and R. Silbey, Contributions of the electrostatic and the dispersion interaction to the solvent shift in a dye–polymer system, as investigated by hole-burning spectroscopy, *Physical Review B*, 41:12215–12226, 1990

[26] P. Guttmann and P. Ehrlich, Über die Wirkung des Methylenblau bei Malaria, *Berliner Klinische Wochenzeitschrift*, 28:953–956, 1891

[27] M. Stübner, *Lochbrennspektroskopie von Biomolekülen in äußeren Feldern*, PhD Thesis, TU München, 2002

[28] V. A. Zakian, Structure and function of telomeres, *Annual Reviews on Genetics*, 23:579–604, 1989

[29] J. R. Williamson, G-quartet structures in telomeric DNA, *Annual Review of Biophysics & Biomolecular Structure*, 23:703–730, 1994

[30] E. Tuite and J. M. Kelly, The interaction of methylene blue, azure B, and thionine with DNA: Formation of complexes with polynucleotides and mononucleotides as model systems, *Biopolymers*, 35:419–433, 2004

[31] B.-S. Herbert, A. E. Pitts, S. I. Baker, S. E. Hamilton, W. E. Wright, J W. Shay, and D. R. Corey, Inhibition of human telomerase in immortal human cells leads to progressive telomere shortening and cell death, *Proceedings of the National Academy of Sciences*, 96:14276–14281, 1999

[32] M. Z. Levy, R. C. Allsopp, A. B. Futcher, C. W. Greider, and C. B. Harley, Telomere end-replication problem and cell aging, *Journal of Molecular Biology*, 225(4):951–960, 1992

[33] C. B. Harley and B. Villeponteau, Telomeres and telomerase in aging and cancer, *Current Opinion in Genetics & Development*, 5:249–255, 1995

[34] J. Szejtli, Introduction and general overview of cyclodextrin chemistry, *Chemical Reviews*, 98:1743–1753, 1998

[35] J. Gafert and J. Friedrich, Looking into frozen proteins with hole-burning, *Journal of Luminescence*, 64(1–6):45–50, 1995

[36] M. Stübner, E. Schneider, and J. Friedrich, Hole burning Stark-effect studies on aromatic aminoacids: I. Phenylalanine in a glycerol-water glass, *Physical Chemistry Chemical Physics*, 3(24):5369–5372, 2001

[37] M. Stübner, C. Hecht, and J. Friedrich, Hole burning Stark-effect studies on aromatic amino acids: II. A comparative investigation of tyrosine and the BPTI-protein, *Physical Chemistry Chemical Physics*, 4:6080–6085, 2002

[38] M. Stübner, C. Hecht, and J. Friedrich, Labeling proteins via hole burning of their aromatic amino acids: Pressure tuning spectroscopy of BPTI, *Biophysical Journal*, 83:3553–3557, 2002

[39] C. Schnell, C. Scharnagl, and J. Friedrich, Hole burning spectroscopy of ribonuclease A, *Physical Chemistry Chemical Physics*, 8:1315–1320, 2006

[40] W. A. Sidler, Phycobilisome and phycobiliprotein structures, In D. A. Bryant, editor, *The molecular biology of cyanobacteria*. Kluwer Academic Publishers, Dordrecht, The Netherlands, 1994

[41] N. Tandeau de Marsac, Phycobiliproteins and phycobilisomes: the early observations, *Photosynthesis Research*, 76:197–205, 2003

[42] N. Bloembergen, E. M. Purcell, and R. V. Pound, Relaxation effects in nuclear magnetic resonance absorption, *Physical Reviews*, 71:679–712, 1948

[43] C. E. Hamilton, J. L. Kinsey, and R. W. Field, Stimulated emission pumping: New methods in spectroscopy and molecular dynamics, *Annual Reviews of Physical Chemistry*, 37:493–524, 1986

[44] M. Wendling, F. van Mourik, I. H. M. van Stokkum, J. M. Salverda, H. Michel, and R. van Grondelle, Low-intensity pump-probe measurements on the B800 band of *rhodospirillum molischianum*, *Biophysical Journal*, 84:440–449, 2003

[45] S. A. Kovalenko, N. P. Ernsting, and J. Ruthmann, Femtosecond hole-burning spectroscopy of the dye DCM in solution: The transition from the locally excited to a charge-transfer state, *Chemical Physics Letters*, 238:445–454, 1996

[46] A. Szabo, Observation of hole burning and cross relaxation effects in ruby, *Physical Reviews B*, 11:4512–4517, 1975

[47] J. Friedrich, H. Scheer, B. Zickendraht-Wendelstadt, and D. Haarer, High-resolution optical studies on *c*-phycocyanin via photochemical hole burning, *Journal of the American Chemical Society*, 103:1030–1035, 1981

[48] W. Baumann and Z. Nagy, Photoinduced charge transfer as revealed by ground and excited state dipole moments, *Pure & Applied Chemistry*, 65:1729–1732, 1993

[49] S. Völker and J. H. Van der Waals, Laser-induced photochemical isomerization of free-base porphyrin in an *n*-octane crystal, *Molecular Physics*, 32(6):1703–1718, 1976

[50] A. R. Gutierrez, J. Friedrich, and D. Haarer, Multiple photochemical hole burning in organic glasses and polymers – spectroscopy and storage aspects, *IBM Journal of Research and Development*, 26(2):198–208, 1982

[51] I. Willner and B. Willner, Photochemical biomolecular switches: The route to optobioelectronics, In B. L. Feringa, editor, *Molecular Switches*. Wiley-VCH, Weinheim, 2001

[52] T. Masciangioli, S. Devanathan, M. A. Cusanovich, and G. Tollin nd M. A. el Sayed, Probing the primary event in the photocycle of photoactive yellow protein using photochemical hole-burning technique, *Photochemistry Photobiology*, 72:639–644, 2000

[53] J. Pieper, K. D. Irrgang, M. Rätsep, J. Voigt, G. Renger, and G. J. Small, Assignment of the lowest Q_y-state and spectral dynamics of the cp29 chlorophyll *a/b* antenna complex of green plants: A hole-burning study, *Photochemistry Photobiology*, 71:574–581, 2000

[54] U. P. Wild, S. Bernet, B. Kohler, and A. Renn, From supramolecular photochemistry to the molecular computer, *Pure & Applied Chemistry*, 63:1335–1342, 1992

[55] R. Ao, L. Kümmerl, and D. Haarer, Present limits of data storage using dye molecules in solid matrices, *Advanced Materials*, 7:495–499, 2004

[56] J. Friedrich and D. Haarer, Photochemical hole burning: A spectroscopic study of relaxation processes in polymers and glasses, *Angewandte Chemie Int. Ed.*, 23(2):113–140, 1984

[57] J. M. Hayes and G. J. Small, Mechanisms of non-photochemical hole-burning in organic glasses, *Chemical Physics Letters*, 54(3):435–438, 1978

[58] J. M. Hayes and G. J. Small, Non-photochemical hole burning and impurity site relaxation processes in organic glasses, *Chemical Physics*, 27(1):151–157, 1978

[59] D. H. P. Trommsdorff, A. Corval, and L. von Laue, Spectral hole burning: Spontaneous and photoinduced tunneling reactions in low temperature solids, *Pure and Applied Chemistry*, 67:191–198, 1995

[60] H. Riesen, V. È. Bursian, and N. E. Manson, Efficient non-photochemical spectra hole burning in single crystal SrO:CO^{2+}, *Journal of Luminescence*, 85:107–112, 1999

[61] M. Kasha, Characterization of electronic transitions in complex molecules, *Discussions of the Faraday Society*, 9:14–19, 1950

[62] W. Breinl, J. Friedrich, and D. Haarer, Linewidth study of the dye molecule quinizarin in solid glasses, *Physical Review B*, 34:7271–7277, 1986

[63] J. M. Hayes, P. A. Lyle, and G. J. Small, A theory for the temperature dependence of hole-burned spectra, *Journal of Physical Chemistry*, 98:7337–7341, 1994

[64] P. Schellenberg, J. Friedrich, and J. Kikas, Thermal recovery and spectral diffusion of photochemical holes in polymorphic systems, *Journal of Chemical Physics*, 101:9262–9270, 1994

[65] A. A. Gorokhovskiĭ and J. Kikas, Inhomogeneous broadening of local vibrations in spectra of organic molecules in solid matrices, *Optics Communications*, 21:272–274, 1977

[66] K. K. Rebane and R. A. Avarmaa, Sharp line vibronic spectra of chlorophyll and its derivatives in solid solutions, *Chemical Physics*, 68:191–200, 1982

[67] C. C. Chiang, C. Y. Mou, and T.-C. Chang, Photoreaction of neutral 9-aminoacridine in glycerol:water glass characterized by satellite holes and antiholes, *Chemical Physics Letters*, 273:153–158, 1997

[68] P. Geissinger, B. E. Kohler, and J. C. Woehl, Electric field and structure in the myoglobin heme pocket, *Journal of Physical Chemistry*, 99:16527–16529, 1995

[69] J. Gafert, J. Friedrich, and F. Parak, Stark-effect experiments on photochemical holes in chromoproteins: Protoporphyrin IX substituted myoglobin, *Proceedings of the National Academy of Science*, 92:2116–2120, 1995

[70] D. W. Pierce and S. G. Boxer, Stark effect spectroscopy of tryptophan, *Biophysical Journal*, 68:1583–1591, 1995

[71] M. Orrit, J. Bernard, A. Zumbusch, and R. I. Personov, Single molecule spectroscopy: Stark effect of pentacene in *p*-terphenyl, *Chemical Physics Letters*, 196:595–600, 1992

[72] A. J. Meixner, A. Renn, S. E. Bucher, and U. P. Wild, Spectral hole burning in glasses and polymer films: The Stark effect, *Journal of Physical Chemistry*, 90:6777–6785, 1986

[73] G. U. Bublitz and S. G. Boxer, Stark spectroscopy: Applications in chemistry, biology, and materials science, *Annual Review of Physical Chemistry*, 48:213–242, 1997

[74] U. P. Wild, F. Güttler, M. Pirotta, and A. Renn, Single molecule spectroscopy: Stark effect of pentacene in *p*-terphenyl, *Chemical Physics Letters*, 193:451–455, 1992

[75] C. Brunel, P. Tamarat, B. Lounis, J. C. Woehl, and M. Orrit, Stark effect on single molecules of dibenzanthanthrene in a naphthalene crystal and in a *n*-hexadecane Shpol'skĭ matrix, *Journal of Physical Chemistry A*, 103:2429–2434, 1999

[76] H. Wendt and J. Friedrich, Hole burning stark spectroscopy of *j* aggregates, *Chemical Physics*, 210:101–107, 1996

[77] P. Schätz and M. Maier, Calculations of electric field effects on persistent spectral holes in amorphous host-guest systems, *Journal of Chemical Physics*, 87:809–820, 1987

[78] H. Fröhlich, *Theory of Dielectrics*. Clarendon Press, Oxford, 2^{nd} edition, 1986

[79] J. G. Kirkwood, The dielectric polarization of polar liquids, *Journal of Chemical Physics*, 7:911–919, 1939

[80] L. Onsager, Electric moments of molecules in liquids, *Journal of the American Chemical Society*, 58:1486–1493, 1936

[81] H. A. Lorentz, *The Theory of Electrons*. B. G. Teubner, Leipzig, 1909

[82] H. Lesch, C. Hecht, and J. Friedrich, Protein phase diagrams: The physics behind their elliptic shape, *Journal of Chemical Physics*, 121:12671, 2004

[83] B. B. Laird and J. L. Skinner, Microscopic theory of reversible pressure broadening in hole burning spectra of impurities in glasses, *Journal of Chemical Physics*, 90:3274–3281, 1989

[84] J. Israellachvili, *Intermolecular and Surface Forces*. Academic Press, London, 1992

[85] G. Gradl, J. Zollfrank, W. Breinl, and J. Friedrich, Color effect in pressure-tuned hole-burned spectra, *Journal of Chemical Physics*, 94:7619–7624, 1991

[86] B. Plagemann, I. Renge, and A. Renn, Molecular interactions and correlation phenomena between pressure shift and solvent shift: A spectral hole-burning study, *Journal of Physical Chemistry*, 97:6902–6906, 1993

[87] P. Schellenberg, J. Friedrich, and J. Kikas, Spectral hole burning in polymorphic systems: Single site pressure phenomena and glassy behavior, *Journal of Chemical Physics*, 100:5501–5507, 1994

[88] W. Liptay, Dipole moments and polarizabilities of molecules in excited states, In E. C. Lim, editor, *Excited States*. Academic Press, New York, 1992

[89] N. S. Bayliss and E. G. McRae, Solvent effects in organic spectra: Dipole forces and the Franck-Condon principle, *Journal of Physical Chemistry*, 58:1002–1006, 1954

[90] J. Zollfrank and J. Friedrich, Pressure shift and solvent shift: A hole-burning study of resorufin-doped glasses, *Journal of Physical Chemistry*, 96:7889–7895, 1992

[91] A. M. Stoneham, Shapes of inhomogeneously broadened resonance lines in solids, *Reviews of Modern Physics*, 41:82–108, 1969

[92] L. Kador, Stochastic theory of inhomogeneous spectroscopic line shapes reinvestigated, *Journal of Chemical Physics*, 95:5574–5581, 1991

[93] D. P. Kharakoz and A. P. Sarvazyan, Hydrational and intrinsic compressibilities of globular proteins, *Biopolymers*, 33:11–26, 1993

[94] W. Doster, B. Simon, G. Schmidt, and W. Mayr, Compressibility of lysozyme in solution from time-resolved Brillouin difference spectroscopy, *Biopolymers*, 24:1543–1548, 1985

[95] B. Gavish, E. Gratton, and C. J. Hardy, Adiabatic compressibility of globular proteins, *Proceedings of the National Academy of Sciences*, 80:750–754, 1983

[96] H. Lesch, J. Schlichter, J. Friedrich, and J. M. Vanderkooi, Molecular probes: What is the range of their interaction with the environment?, *Biophysical Journal*, 86:467–472, 2004

[97] F. W. Smith and J. Feigon, Quadruplex structure of *oxytricha* telomeric DNA oligonucleotides, *Nature*, 356:164–168, 1992

[98] M. Storf, *Chromophorbindung und Photochemie der α-Untereinheit des Phycoerythrocyanins aus Mastigocladus laminosus*, PhD Thesis, LMU München, 2004

[99] K. C. Weng, C.-C. Chiang, J.-Y. Cheng, S.-Y. Cheng, R. I. Personov, and T.-C. Chang, Investigation of tautomeric structures of thionin by satellite holes: Matrix dependence, *Chemical Physics Letters*, 302:347–354, 1999

[100] IMSL, *Fortran Subroutines for Statistical Analysis*, 1987

[101] R. R. Gupta, *Phenothiazines and 1,4-Benzothiazines: Chemical and Biomedical Aspects*. Elsevier Amsterdam, Oxford, 1988

[102] S. Nagy, G. Argyelan, J. Molnar, M. Kawase, and N. Motohashi, Antitumor activity of phenothiazine-related compounds, *Anticancer Research*, 16(4A):1915–1918, 1996

[103] J. C. V. P. Moura and N. Cordeiro, 3,7-bis(dialkylamino)phenothiazin-5-ium derivatives: Biomedical applications and biological activity, *Current Drug Targets*, 9(2):133–141, 2003

[104] M. Wainwright and R. M. Giddens, Phenothiazinium photosensitisers: Choices in synthesis and application, *Dyes and Pigments*, 57(3):245–257, 2003

[105] M. Wainwright and L. Amaral, Review: The phenothiazinium chromophore and the evolution of antimalarial drugs, *Tropical Medicine & International Health*, 10:501–511, 2005

[106] N. Marek, S. Kunsági-Máté, and K. Szabó, Theoretical considerations of the conformation of thionin-proton complexes, *Journal of Molecular Structure (THEOCHEM)*, 315:187–190, 1994

[107] C. C. Chiang, C. C. Hwang, J. Yu, J. Y. Cheng, C. Y. Mou, S. H. Lin, and T.-C. Chang, Satellite hole investigations of the hole-burning mechanism and vibrational mode coupling of 9-aminoacridine in glycerol-water glasses at different pH values, *Journal of the Chemical Society Faraday Transactions*, 93:1297–1304, 1997

[108] C.-T. Kuo and T.-C. Chang, Satellite hole investigations of energy transfer between two different dyes, *Journal of Chemical Physics*, 106:5947–5950, 1997

[109] J. Y. Cheng, S. H. Lin, and T.-C. Chang, Vibrational investigation of DODC cation for recognition of guanine dimeric hairpin quadruplex studied by satellite holes, *Journal of Physical Chemistry B*, 102:5542–5546, 1998

[110] C.-T. Kuo, C. C. Chiang, J. Yu, K. Peck, and T.-C. Chang, Satellite hole investigation of binding mechanism of dipyrrometheneboron difluorid derivative and oligonucleotide in glycerol-water glass, *Journal of the Chemical Society Faraday Transactions*, 94:1989–1994, 1998

[111] Y. P. Yang, C.-T. Kuo, C. S. Yan, K. C. Lina, W. C. Huang, and T.-C. Chang, Different binding structures of a covalently linked BODIPY-493/503 dye to an oligonucleotide investigated by satellite hole burning spectroscopy, *Physical Chemistry Chemical Physics*, 2:5271–5274, 2000

[112] T.-C. Chang, K. C. Lin, C. C. Chiang, Y. P. Yang, and W. S. Chang, Satellite hole spectroscopy of thrombin–aptamer complexes, *Chembiochem*, 3:197–200, 2000

[113] M. J. Frisch, G. W. Trucks, M. Head-Gordon, P. M. W. Gill, M. W. Wong, J. B. Foresman, B. G. Johnson, H. B. Schlegel, M. A. Robb, E. S. Replogle, R. Gomperts, J. L. Andres, K. Raghavachari, J. S. Binkley, C. Gonzalez, R. L. Martin, D. J. Fox, D. J. Defrees, J. Baker, J. J. P. Stewart, and J. A. Pople.
Gaussian 92, Revision C, 1992.
Gaussian, Inc., Pittsburgh, PA, 1992

[114] A. Waggoner, Covalent labeling of proteins and nucleic acids with fluorophores, *Methods in Enzymology*, 246:362–373, 1995

[115] I. Johnson, Fluorescent probes for living cells, *Journal of Molecular Histology*, 30:123–140, 1998

[116] A. Burghart, H. Kim, M. B. Welch, L. H. Toresen, J. Reibenspies, K. Burgess, F. Bergström, and L. B. Johansson, 3,5-diaryl-4,4-difluoro-4-bora-3,4a-diaza-*s*-indacene (BODIPY) dyes: Synthesis, spectroscopic, electrochemical, and structural properties, *Journal of Organic Chemistry*, 64:7813–7819, 1999

[117] T.-C. Chang, C. T. Kuo, C. C. Chiang, J. Y. Cheng, C. S. Yan, and K. Peck, Investigation of guanine-rich DNA telomeric structure by a covalently linked BODIPY dye, *Physical Chemistry Chemical Physics*, 1:3783–3787, 1999

[118] P. Avouris, A. Campion, and M. A. El-Sayed, Variations in homogeneous fluorescence linewidth and electron-phonon coupling within an inhomogeneous spectral profile, *Journal of Chemical Physics*, 67:3397–3398, 1977

[119] P. Avouris and T. N. Morgan, A tunneling model for the decay of luminescence in inorganic phosphors: The case of Zn_2SiO_4:Mn, *Journal of Chemical Physics*, 74:4347–4355, 1981

[120] I. Renge, Relationship between electron-phonon coupling and intermolecular interaction parameters in dye-doped organic glasses, *Journal of the Optical Society of America B*, 9:719, 1992

[121] C. Hecht, M. Stübner, J. Friedrich, and T.-C. Chang, Investigation of probe–solvent interactions: Color effects in optical line widths, *Chemical Physics Letters*, 395:21–26, 2004

[122] W. Breinl, J. Friedrich, and D. Haarer, Logarithmic decay of photochemically induced two-level systems in an organic glass, *Chemical Physics Letters*, 106:487–490, 1984

[123] M. Berg, C. A. Walsh, L. R. Narasimhan, K. A. Littau, and M. D. Fayer, Dynamics in low temperature glasses: Theory and experiments on optical dephasing, spectral diffusion, and hydrogen tunneling, *Journal of Chemical Physics*, 88:1564–1587, 1988

[124] R. Jankowiak, J. M. Hayes, and G. J. Small, Spectral hole-burning spectroscopy in amorphous molecular solids and proteins, *Chemical Reviews*, 93:1471–1502, 1993

[125] K. Fritsch, J. Friedrich, and B. M. Kharlamov, Nonequilibrium phenomena in spectral diffusion physics of organic glasses, *Journal of Chemical Physics*, 105(5):1798–1806, 1996

[126] W. Götze and M. Sperl, Logarithmic relaxation in glass-forming systems, *Physical Review E*, 66:011405, 2002

[127] P. W. Anderson, B. I. Halperin, and C. M. Varma, Anomalous low-temperature thermal properties of glasses and spin glasses, *Philosophical Magazine*, 25:1, 1972

[128] W. A. Phillips, Tunneling states in amorphous solids, *Journal of Low Temperature Physics*, 7(3–4):351–360, 1972

[129] A. Heuer and R. J. Silbey, Microscopic description of tunneling systems in a structural model glass, *Physical Review Letters*, 70:3911–3914, 1992

[130] P. Neu, D. R. Reichman, and R. J. Silbey, Spectral diffusion on ultralong time scales in low-temperature glasses, *Journal of Chemical Physics*, 56:5250–5260, 1997

[131] L. Amaral, M. Viveiros, and J. E. Kristiansen, Phenothiazines: potential alternatives for the management of antibiotic resistant infections of tuberculosis and malaria in developing countries, *Tropical Medicine & International Health*, 6:1016–1022, 2001

[132] T. Da Ros, G. Spalluto, A. S. Boutorine, R. V. Bensasson, and M. Prato, DNA-photocleavage agents, *Current Pharmaceutical Design*, 7(17):1781–1821, 2001

[133] A. Erdem and M. Ozsoz, Electrochemical DNA biosensors based on DNA-drug interactions, *Electroanalysis*, 14(14):965–974, 2002

[134] P. D. Cook, Medicinal chemistry of antisense oligonucleotides – future opportunities, *Anticancer Drug Design*, 6:585–607, 1991

[135] S. T. Crooke, Therapeutic applications of oligonucleotides, *Nature Biotechnology*, 10:882–886, 1992

[136] G. Ramsay, DNA chips: State-of-the art, *Nature Biotechnology*, 16:40–44, 1998

[137] P. Ehrlich, Chemotherapeutics: Scientific principles, methods, and results, *Lancet*, 2:445–451, 1913

[138] M. I. Simon and H. van Vunakis, The photodynamic reaction of methylene blue with deoxyribonucleic acid, *Journal of Molecular Biology*, 4:488–499, 1962

[139] J. Piette, J. Decuyper, M. P. Merville-Louis, and A. van de Vorst, Biomolecular photoalterations mediated by phenothiazine derivatives, *Biochimie*, 68:835–842, 1986

[140] E. Yashima, T. Tajima, N. Suehiro, M. Akashi, and N. Miyauchi, Study on the interaction of aromatic dyes with nucleic acids by means of UV, CD and NMR spectroscopies, *Nucleic Acids Sympoium Series*, 22:101–102, 1990

[141] E. Tuite and B. Nordén, Sequence-specific interactions of methylene blue with polynucleotides and DNA: A spectroscopic study, *Journal of the American Chemical Society*, 116:1548–1556, 1994

[142] H. M. Berman and P. R. Young, The interaction of intercalating drugs with nucleic acids, *Annual Review of Biophysics & Bioengineering*, 10:87–114, 1981

[143] G. Dougherty and W. J. Pigram, Spectroscopic analysis of drug-nucleic acid interactions, *Critical Reviews in Biochemistry and Molecular Biology*, 12(2):103–132, 1982

[144] D. Řeha, M. Kabeláč, F. Ryjáček, J. Šponer, J. E. Šponer, M. Elstner, S. Suhai, and P. Hobza, Intercalators. 1. Nature of stacking interactions between intercalators (ethidium, daunomycin, ellipticine, and 4',6-diaminide-2-phenylindole) and DNA base pairs. *ab initio* quantum chemical, density functional theory, and empirical potential study, *Chemical Physics Letters*, 124:3366–3376, 2002

[145] D. E. Wemmer and P. B. Dervan, Targeting the minor groove of DNA, *Current Opinion in Structural Biology*, 7:355–361, 1997

[146] Z. Morávek, S. Neidle, and B. Schneider, Protein and drug interactions in the minor groove of DNA, *Nucleic Acids Research*, 30(5):1182–1191, 2002

[147] J. D. Watson and F. H. C. Crick, Molecular structure of nucleic acids: A structure for deoxyribose nucleic acid, *Nature*, 171:737–738, 1953

[148] I. R. Gould and P. A. Kollman, Theoretical investigation of the hydrogen bond strengths in guanine–cytosine and adenine–thymine base pairs, *Journal of the American Chemical Society*, 116:2493–2499, 1994

[149] T. Simonsson, G-quadruplex DNA structures – variations on a theme, *Biological Chemistry*, 382:621–628, 2001

[150] J. M. Kelly, W. J. van der Putten, and D. J. McConnell, Laser flash spectroscopy of methylene blue with nucleic acids, *Photochemistry Photobiology*, 45(2):167–175, 1987

[151] C. OhUigin, D. J. McConnell, J. M. Kelly, and W. J. van der Putten, Methylene blue photosensitised strand cleavage of DNA: effects of dye binding and oxygen, *Nucleic Acids Research*, 15:7411–7427, 1987

[152] R. Lyng, T. Härd, and B. Nordén, Induced CD of DNA intercalators: electric dipole allowed transitions, *Biopolymers*, 26:1327–1345, 1987

[153] A. M. Olovnikov, A theory of marginotomy. The incomplete copying of template margin in enzymic synthesis of polynucleotides and biological significance of the phenomenon, *Journal of Theoretical Biology*, 41:181–190, 1973

[154] M. A. Keniry, E. A. Owen, and R. H. Shafer, The contribution of thymine–thymine interaction to the stability of folded dimeric quadruplexes, *Nucleic Acids Research*, 25:4389–4392, 1997

[155] J.-L. Mergny, A.-T. Phan, and L. Lacroix, Following G-quartet formation by UV-spectroscopy, *FEBS Letters*, 435:74–78, 1998

[156] G. D. Strahan, M. A. Keniry, and R. H. Shafer, NMR structure refinement and dynamics of the K^+-$[d(G_3T_4G_3)]_2$ quadruplex via particle mesh ewald molecular dynamics simulations, *Biophysical Journal*, 75:968–981, 1998

[157] C. W. Greider, Telomeres and senescence: The history, the experiment, the future, *Current Biology*, 8:R178–R181, 1998

[158] J. W. Shay, Y. Zou, E. Hiyama, and W. E. Wright, Telomerase and cancer, *Human Molecular Genetics*, 10:677–685, 2001

[159] M. Famulok and G. Mayer, Aptamers as tools in molecular biology and immunology, *Current Topics in Microbiology and Immunology*, 243:123–136, 1999

[160] E. N. Brody and L. Gold, Aptamers as therapeutic and diagnostic agents, *Reviews in Molecular Biotechnology*, 74:5–13, 2000

[161] L. C. Bock, L. C. Griffin, J. A. Latham, E. H. Vermaas, and J. J. Toole, Selection of single-stranded DNA molecules that bind and inhibit human thrombin, *Nature*, 355:564–566, 1992

[162] C. Hecht, J. Friedrich, and T.-C. Chang, Interactions of thionin with DNA strands: Intercalation versus external stacking, *Journal of Physical Chemistry B*, 108:10241–10244, 2004

[163] J. Friedrich, J. Gafert, J. Zollfrank, J. M. Vanderkooi, and J. Fidy, Spectral hole burning and selection of conformational substates in chromoproteins, *Proceedings of the National Academy of Sciences*, 91:1029–1033, 1994

[164] G. D. Reid, D. J. Whittaker, M. A. Day, C. M. Creely, E. M. Tuite, and J. M. Kelly, Ultrafast electron-transfer reactions between thionine and guanosine bases, *Journal of the American Chemical Society*, 123:6953–6954, 2001

[165] C. Dohno, E. D. A. Stemp, and J. K. Barton, Fast back electron transfer prevents guanine damage by photoexcited thionine bound to DNA, *Journal of the American Chemical Society*, 125(32):9586–9587, 2003

[166] A. Villiers, Sur la transformation de le fécule en dextrine par le ferment buytrique, *Comptes Rendus de l'Académie des Sciences*, 112:435–437, 1891

[167] F. Schardinger, Über thermophile Bacterien aus verschiedenen Speisen und Milch, sowie über einige Umsetzungsproducte darselben in kohlenhydrathaltigen Nährlösungen, darunter krystallisierte Polysaccharide (Dextrine) aus Stärke, *Zeitschrift für Untersuchung der Nahrungs- und Genussmittel, sowie der Gebrauchsgegenstände*, 6:865–880, 1903

[168] E. M. Martin Del Valle, Cyclodextrins and their uses: a review, *Process Biochemistry*, 39:1033–1046, 2002

[169] J. Szejtli, Medicinal applications of cyclodextrins, *Medicinal Research Reviews*, 14(3):353–386, 1994

[170] K. L. Larsen, Large cyclodextrins, *Journal of Inclusion Phenomena and Macrocyclic Chemistry*, 43(1–2):1–13, 2002

[171] K.-H. Frömming and J. Szejtli, *Cyclodextrins in Pharmacy*. Kluwer Academic Publishing, Dordrecht, 1994

[172] C. J. Easton and S. F. Lincoln, *Modified Cyclodextrins: Scaffolds and Templates for Supramolecular Chemistry*. Imperial College Press, River Edge, NJ, 1999

[173] T.-C. Chang, Y. P. Yang, K. H. Huang, C. C. Chang, and C. Hecht, Investigation of thionin–DNA interaction with satellite hole spectroscopy, *Optics & Spectroscopy*, 98:655–660, 2005

[174] Q.-X. Guo, H.-Y. Liu, X.-Q. Ruan, X.-Q. Zheng, Y.-Y. Shi, and Y.-C. Liu, Experimental and theoretical studies on the inclusion complexation of β-cyclodextrin with phenothiazine derivatives, *Journal of Inclusion Phenomena and Macrocyclic Chemistry*, 35:487–496, 1999

[175] C. Hecht, P. Hermann, J. Friedrich, C. C. Chang, and T.-C. Chang, Thionin in a cyclodextrin nanocavity: Measuring local compressibilities by pressure tuning hole burning spectroscopy, *Chemical Physics Letters*, 413:335–341, 2005

[176] M. Glauser, D. A. Bryant, G. Frank, E. Wehrli, S. S. Rusconi, W. Sidler, and H. Zuber, Phycobilisome structure in the cyanobacteria *mastigocladus laminosus* and *anabaena sp.* PCC 7120, *European Journal of Biochemistry*, 205:907–915, 1992

[177] T. Schirmer, W. Bode, R. Huber, W. Sidler, and H. Zuber, X-ray crystallographic structure of the light-harvesting biliprotein *c*-phycocyanin from the thermophilic cyanobacterium *mastigocladus laminosus* and

its resemblance to globin structures, *Journal of Molecular Biology*, 184(2):257–277, 1985

[178] S. Siebzehnrübl, R. Fischer, and H. Scheer, Chromophore assignment in *c*-phycocyanin from *mastigocladus laminosus*, *Zeitschrift für Naturforschung. C. Biosciences*, 42(3):258–262, 1987

[179] K. Sauer and H. Scheer, Excitation transfer in *c*-phycocyanin: Förster transfer rate and exciton calculations based on new crystal structure data for *c*-phycocyanins from *agmenellum quadruplicatum* and *mastigocladus laminosus*, *Biochimica et Biophysica Acta*, 936(2):157–170, 1988

[180] T. Gillbro, A. V. Sharkov, I. V. Kryukov, E. V. Khoroshilov, P. G. Kryukov, R. Fischer, and H. Scheer, Förster energy transfer between neighbouring chromophores in *c*-phycocyanin trimers, *Biochimica et Biophysica Acta. Bioenergetics*, 1140:321–326, 1993

[181] S. A. Pizarro and K. Sauer, Spectroscopic study of the light-harvesting protein *c*-phycocyanin associated with colorless linker peptides, *Photochemistry and Photobiology*, 73:556–563, 2001

[182] M. P. Debreczeny, K. Sauer, J. Zhou, and D. A. Bryant, Comparison of calculated and experimentally resolved rate constants for excitation energy transfer in *c*-phycocyanin. 2. Trimers, *Journal of Physical Chemistry*, 99:8420–8431, 1995

[183] J. Friedrich, H. Scheer, B. Zickendraht-Wendelstadt, and D. Haarer, Energy transfer in phycobiliproteins as studied by photochemical hole burning, *Journal of Luminescence*, 24–25:815–818, 1981

[184] M. P. Debreczeny, K. Sauer, J. Zhou, and D. A. Bryant, Monomeric *c*-phycocyanin at room temperature and 77 K: Resolution of the absorption and fluorescence spectra of the individual chromophores and the energy-transfer rate constants, *Journal of Physical Chemistry*, 97:9852–9862, 1993

[185] B. J. Homoelle and W. F. Beck, Solvent accessibility of the phycocyanobilin chromophore in the α-subunit of *c*-phycocyanin: Implications for a molecular mechanism for inertial protein–matrix solvation dynamics, *Biochemistry*, 36:12970–12975, 1997

[186] H. Scheer, Biliproteine, *Angewandte Chemie*, 93:230–250, 1981

[187] C. Scharnagl and S. F. Fischer, Reversible photochemistry in the α-subunit of phycoerythrocyanin: Characterization of chromophore and protein by molecular dynamics and quantum chemical calculations, *Photochemistry and Photobiology*, 57(1):63–70, 1993

[188] A. V. Sharkov, V. Gulbinas, L. Gottschalk, H. Scheer, and T. Gillbro, Dipole–dipole interaction in phycobiliprotein trimers. Femtosecond dynamics of allophycocyanin excited state absorption, *Brazilian Journal of Physics*, 26:553–559, 1996

Epilogue

I would like to extend my thanks to all the people, who helped to contribute in one way or another to the completion of this work:

Prof. Josef Friedrich – he gave guidance, advise and inspiration, had an open ear for all questions, was always available for discussions and had the invaluable virtue of piecing together the jumbled data to a coherent, stringent and convincing unit of scientific work.
Dipl.-Phys. Peter Herrmann – our collaboration on the cage complexes was one of the most effective I have had the honor to experience so far.
Ellen Schneider – whether literature or sample preparation, she was always helpful, accurate and friendly, even when the circumstances were a bit adverse at times.
Erika Bischofs – for knowing everything about organizational issues there is to know; and for sharing it at any time with a laugh on her lips.
Prof. Ta-Chau Chang, Kai-Hsiang Huang and **Cheng-Chung Chang** – my visits in Taiwan have been most fruitful, refreshing and interesting due to their unexcelled hospitality.
All others at the E14 – Dr. Harald Lesch, Dr. Markus Stübner, Dr. Christoph Schnell, Dipl.-Phys. Alfred Sigl, Armin Forster, Dr. Johannes Wiedersich, Dr. Christina Scharnagl, Dr. Mark Somoza, Tom Zeitzler, Dr. Vladimir Ponkratov, Dipl.-Phys. Christiane Ullrich, Tarekegn Chimdi, Helene Budjarek und Ludwig Hütt have created the pleasant working atmosphere at our institute.

Petra, my wife – although there might have been times where our relationship has severely been put to the test she always supported me, shared my worries with me and lifted up my spirits. Even if she knows the least in physics of all the people here, she somehow contributed the most to this thesis.

This list is by no means complete: To all the friends and helpers – you know who you are.